Lake County Seismic and Liquefaction Hazard Maps
(HUD Grant Year One Products)

Chris H. Cramer, Roy B. Van Arsdale, Taylor Weathers, David Arellano, Shahram Pezeshk, Nima Nazemi, Juan A. Jimenez, Hamed Tohidi, Stephan P. Horton, Luke P. Ogweno

Abstract

A five-year seismic and liquefaction hazard mapping project for five western Tennessee counties began in 2017 under a Disaster Resilience Competition grant from the U.S. Department of Housing and Urban Development to the State of Tennessee. The project supports natural hazard (flood and earthquake) mitigation efforts in these five counties. The seismic hazard maps for Lake County in northwestern most Tennessee were completed in early 2018. Additional geological, geotechnical, and geophysical information has been gathered in Lake Co. to improve the base northern Mississippi Embayment hazard maps of Dhar and Cramer (2018). Information gathered includes additional geological and geotechnical subsurface exploration logs, water table level data collection and measurements, new measurements of shallow and deep shear-wave velocity (Vs) profiles, and the compilation of existing Vs profiles in and around the county. Improvements were made in the 3D geological model, water table model, the geotechnical liquefaction probability curves, and the Vs correlation with lithology model for Lake Co. Resulting improved soil response amplification distributions on a 0.5 km grid were combined with the 2014 U.S. Geological Survey seismic hazard model (Petersen et al., 2014) sources and attenuation models to add the effect of local geology for Lake Co. Resulting products are an improved 3D-geology, geotechnical, seismic hazard, and liquefaction hazard models and maps for Lake Co. Seismic hazard maps at PGA and 1.0 s show a 50% decrease in hazard at short periods and a 10% increase at long periods compared with USGS NSHMP maps.

Introduction

As part of the 2015 Disaster Resilience Competition, the State of Tennessee received funds from the Department of Housing and Urban Development (HUD) for several grants for flood hazard mitigation efforts. The University of Memphis received one of the grants for flood and seismic hazard mapping efforts in five western Tennessee counties (Figure 1) covering a five-year period starting in 2017. The first year seismic hazard mapping effort is for Lake County seismic and liquefaction hazard maps (this report) and an earthquake early warning feasibility study for western Tennessee (Ogweno, Withers, and Cramer, 2019).

The goal for the seismic hazard mapping project is to develop seismic and liquefaction hazard maps for use in flood hazard mitigation efforts in other portions of the HUD grant effort via the University of Memphis. The hazard maps will also be useful for other earthquake hazard mitigation efforts in the five western Tennessee counties.
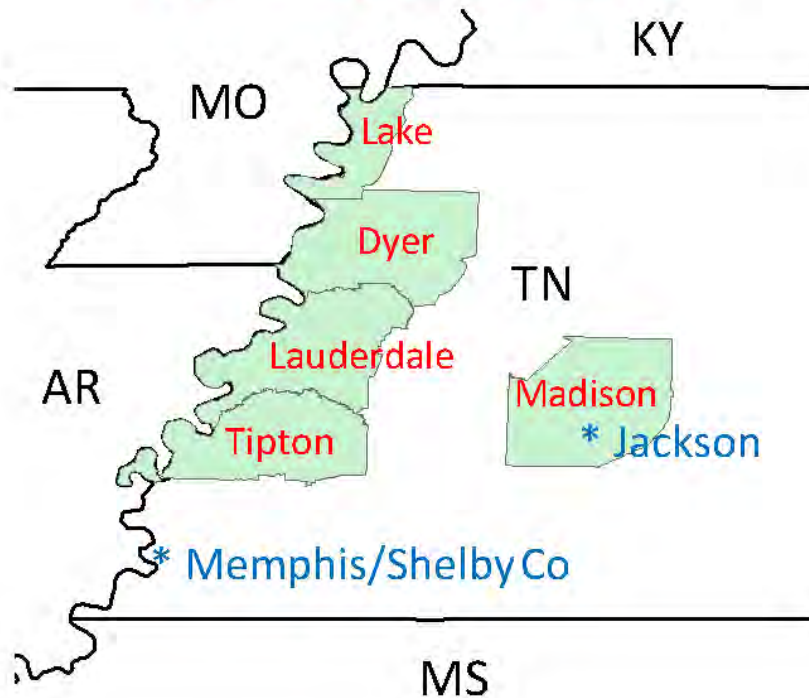
Figure 1: Five western Tennessee counties of the HUD grant supported seismic hazard study. AR – Arkansas, KY – Kentucky, MO – Missouri, MS – Mississippi, and TN – Tennessee.

The major elements to the seismic and liquefaction hazard mapping in this project are (1) geological 3D model development, (2) geotechnical (soil response to ground motions) model development, (3) seismological data gathering, and (4) hazard maps generation. The 3D geological model of sediments above bedrock involves the gathering and interpretation of boring logs, entering geological information into a geographic information system (GIS), and developing maps of the depth to the tops of key geological sediment layers. The accompanying geotechnical model involves the gathering of geotechnical information (sediment properties and water table levels) from boring logs, and modeling liquefaction potential of the shallow sediments. Seismological data gathering includes collecting published sediment velocity profiles with depth, making new measurements of sediment velocity with depth in the study area, and estimating the depth to the water table at seismic measurement sites. The final step is to integrate the geological, geotechnical, and seismological data into a county wide hazard model and maps that included the effects of local geology (sediments).

Geological Model

Geologic Methodology

Data Collection

Lithological logs from Lake County, and within a 4-km buffer zone, were collected from the Tennessee Department of Environmental Conservation (TDEC), the Tennessee Department of Transportation (TDOT), the United States Army Corps of Engineers (USACE), and the Center for Applied Earth Science and Engineering Research (CAESER). The purpose of the buffer zone was to produce more accurate maps of Lake County by removing mapping edge effects. Lithologic logs from the North American Coal Company, archived in CAESER, are lignite exploration logs. Thirty-four of these logs are in Lake County and 43 are in the buffer zone counties. The lignite exploration logs record lithological information for depths up to 300 ft. (91.4 m) and some are accompanied by geophysical logs. The geophysical logs contain gamma ray and resistivity measurements, which may help identify lithology. Additional lithologic logs include 116 boring logs along the levees (USACE), 10 boring logs for bridges, railroads, and highways (TDOT), 4 boring logs of municipal water wells, 129 boring logs for irrigation and residential wells (TDEC), and 11 petroleum exploration well logs housed in CAESER. The boring depths vary, but typically are 30 – 200 ft. (9 – 61 m) for USACE borings, between 30 – 100 ft. (9 – 30 m) for TDOT, between 60 – 120 ft. (18 – 37 m) for TDEC residential and irrigation wells while municipal well depths range between 700 – 800 ft. (213 – 244 m), and 1800-3000 ft. (549 – 914 m) for the petroleum exploration wells (Weathers, 2019).

Depths to stratigraphic tops from seismic reflection data were included from publications by Purser and Van Arsdale (1998), Van Arsdale et al. (1998), Csontos and Van Arsdale (2008), Guo et al. (2014), and Greenwood et al. (2016). When depth estimates of stratigraphic tops were not in a publication, conversion from two-way travel time to depth was conducted using published interval velocities (Table 1). Depths of subsurface reflectors (stratigraphic tops) were then converted into elevation relative to sea level.

Table 1: Interval velocities of the Holocene, Paleogene, and Cretaceous sections and depth conversion equation (from Guo et al., 2014; Guo, personal communication, 2018).

Stratigraphic Unit(s)	RMS Velocity Function (km/s)
Holocene	1.7
Paleogene	2
Cretaceous	2.7
TWT - Depth Conversion Equation	
Depth = (TWT (s) / 2) * RMS Velocity Function (km/s)	

Data Interpretation and Entry

Stratigraphic picks were made from interpreted logs and published seismic reflection data. Within the Quaternary Mississippi River floodplain section, maps were made at 5 ft. (~ 1.5 m) depth intervals. Tops of the Eocene, Memphis Sand, Flour Island, Fort Pillow Sand, Old Breastworks, Porters Creek Clay, Clayton, Late Cretaceous, and Paleozoic strata were picked (Appendix A) but structure contour maps were only made of the tops of the Eocene, Late Cretaceous, and Paleozoic strata.

All data including top of unit elevations and unit thickness were compiled into a single master Excel 2016 spreadsheet and into separate spreadsheets for each individual geologic unit (Appendix A). Units of measure used in this study include both feet (ft.) and meters (m) because most of the drilling records are in feet. The latitude and longitude of each boring was copied from the drilling log to the spreadsheets and were then converted into Decimal Degrees and Universal Transverse Mercator (UTM) to construct geometrically accurate 3-D projections of subsurface geology. Surface elevations of the boring and seismic line shot points were extracted from a LiDAR-sourced digital elevation model (DEM). The DEMs were created in Global Mapper 18.2 and were exported as ASCII files into ArcMap 10.3.1. The reason for using Global Mapper 18.2 was because Global Mapper can read LAS.zip (ZLAS) files, which are LiDAR point cloud files obtained from the USGS Digital Elevation Database. Ground surface elevations were extracted using ArcMap 10.3.1 Spatial Analyst tools (Extraction – Extract Values to Points) and Data Management tools (Conversion – Table to Excel).

Surface Geologic Map and Three-Dimensional Lake County Quaternary Geologic Model

A geologic map of the surface sediments in Lake County was constructed from the interpretation of 336 lithologic logs. Sediment types were assigned a number in Excel 2016 (Table 2). These values were assigned to lithologies, described in well logs, based on grain size starting with gravel as value '0' to clay as value '6'. Eocene sediments were assigned a value of '7'. A spreadsheet containing the lithology data was imported into ArcMap 10.3.1 for map interpolation. The Natural Neighbor interpolation method from Spatial Analyst tools was chosen for the Mississippi River Quaternary alluvium mapping because this algorithm best honored the assigned numerical values for lithological classification. The interpolation assigned raster values to the pixels between well locations based upon the weight and distance between data points. This process created a raster of values with decimal ranges between the initially assigned values. The Raster Calculator tool was then applied to multiply all pixel values by 100 to make whole number values, which would then be used for the conversion of raster values to integer. Raster values were then converted to integer values using the Raster to Integer conversion tool to remove the decimal points. The Raster to Polygon tool was used to provide for more precise classification around data points (Pryne, 2012). Due to the range of values produced for the polygons, in this case from 0 to 700, and the uncertainties between points, manual adjustments of the polygon classifications were needed to refine the lithological maps. The time needed to perform this manual operation was greatly reduced by introducing the data points from the spreadsheet as a shapefile and by opening individual depth layer attribute

Table 2: Values assigned to lithologies for the 3-D Holocene model.

Lithology	Value
Sandy Gravel	0
Sand	1
Silty/ Clayey Sand	2
Loam	3
Silt	4
Clay/Silt	5
Clay	6
Eocene	7

tables to validate assigned lithologies, both pre-interpolation and post-interpolation, so that the most accurate polygon maps could be created.

A 3-D model of the uppermost 300 ft. (91.4 m) was developed to show the detailed Quaternary alluvium beneath Lake County. Five foot (1.5 m) thick lithologic layers were constructed from lithologic logs in the manner just discussed. The model consists of 5 ft. (1.5 m) vertical intervals that show the lateral distribution of the alluvial sediments in each 5 ft. (1.5 m) layer (Pryne et al., 2013). The polygonal surfaces were then imported into ArcScene 10.3.1 and were stacked by their layer depth in 5 ft. layers from the ground surface to 300 feet deep. Surfaces were then extruded, 0 ft. for the surface layer and - 5 ft. for all other sediment layers to account for spatial gaps between layers so that the model was continuous. Layers can be deactivated and reactivated so that each 5 ft. (1.5 m) layer within the Mississippi River alluvium of Lake County can be examined in the three-dimensional model (Appendices B and C).

Structure Contour Maps

Structure contour maps were made of the tops of the Quaternary alluvial sand, Quaternary alluvial sandy gravel, Eocene, Late Cretaceous, and Paleozoic sections. Un-faulted structure contour maps were created in ArcMap 10.3.1 using the Natural Neighbor interpolation method (Pryne, 2012), which allows for smooth, geological reasonable, contouring and for the removal of 'bullseye' artifacts seen in other interpolation methods. Faulted structure contour maps were then made of these surfaces using the Spline with Barriers interpolation method, which

allows for the introduction of faults and abrupt surface changes into the interpolation and for the smoothing of contours to produce a geologically reasonable, interpolated surface.

The first step was to import the stratigraphic top data from the Excel 2016 spreadsheets (Appendix A) into ArcMap 10.3.1 as individual tables of each geologic unit. These tables were exported as shapefiles (.shp) so that they could be displayed as point features by using their XY coordinates. The coordinate system in which XY coordinates were projected is WGS 1984 UTM Zone 16N. Natural Neighbor (Spatial Analyst -> Interpolation -> Natural Neighbor) was used to produce the un-faulted contour maps. Cubic Convolution was selected for the resampling method because it retains the high detail of the raster at large scale. The classified symbology was selected, and the classification method was set to defined contour intervals, which for the top of the Quaternary Mississippi River floodplain sand facies is 5 m, Quaternary Mississippi River floodplain sand and gravel facies 5 m, Eocene 5 m, Cretaceous 10 m, and Paleozoic 10 m. Shapefiles (polylines) were constructed to represent published mapped faults within Lake County. This required georeferencing figures from publications and to overlay them with 25 – 50% transparency on top of the DEMs. This ensured that the faults were located accurately. The shapefiles of each fault were then merged into a single feature class. This is necessary because the interpolators only allow for a single feature class to act as barriers. The Spline with Barriers method was then selected from the 3D Analyst tools to produce the interpolated, faulted surface.

Isopach Maps

Isopach (sediment thickness) maps were made of the Quaternary Mississippi River floodplain and clay/silt, sand, and sand/gravel dominant facies within the Mississippi River alluvium. Isopach maps were also made of the Paleogene section and the Late Cretaceous section using the Natural Neighbor algorithm in ArcMap 10.3.1. These maps also provide information about the Mississippi River alluvial aquifer that would be useful in selecting locations for agricultural water wells.

Cross Sections

Cross sections were made from stacked structure contour maps using ArcMap. This software creates cross sections based on manually entered parameters such as the search distance of borings from a cross section line and vertical exaggeration. Cross sections illustrate the Quaternary, Paleogene, Cretaceous, and top of the Paleozoic.

Three-Dimensional Geologic Model from the Quaternary Land Surface to top of Paleozoic

A separate 3-D geological model was made that includes the surface Mississippi River alluvium to the top of the Paleozoic. The Spline with Barriers method was chosen for this portion of the research to allow for the addition of faults in the structure contour maps. In the Spline with Barriers method, surfaces (e.g. top of the Paleozoic) are divided into separate fault-bounded grids and contoured. This algorithm also provides interpolated amounts of vertical

displacement along the fault break-lines. Faulted structure contour maps of the tops of the Quaternary, Eocene, Late Cretaceous, and Paleozoic sections were imported into ArcScene 10.3.1 and were stacked to the elevations of each geological unit's surface raster. The model illustrates the subsurface geology and structure of Lake County in pseudo three-dimensional space (Appendix D).

Geology of Lake County, Tennessee

Stratigraphy

Lake County, Tennessee, is located on the eastern margin of the Mississippi River floodplain (Figure 2) and the surface elevation of the county is between 243 ft. (74 m) and 325 ft. (99m) above sea level (Figure 3). Surface geology of Lake County consists of unconsolidated clay, silt, and sand deposited by the Mississippi River within the last ~ 4,000 years (Figure 4). The Quaternary Mississippi River floodplain alluvium, in general, consists from top to bottom of silt and clay, sand, and sandy gravel. The Mississippi River floodplain sediments that underlie Lake County have been further divided into 5 ft. (1.5 m) thick layers (Figure 5). Each 5 ft (1.5 m) layer, and its 3-D animation are presented in Appendices B and C.

Immediately below the Quaternary Mississippi River floodplain sediments are ~ 30 million years old Eocene sediments consisting of sand, silt, clay, and minor lignite that are more consolidated than the overlying floodplain sediments. Regionally, the Eocene stratigraphy has been subdivided from top down into the Jackson, Cockfield, Cook Mountain, Memphis Sand, Flour Island, Fort Pillow, and Old Breastworks formations (Figure 6). All of these formations reflect shallow coastal marine and fluvial sediments. Of particular regional importance, the Memphis Sand is a thick ancient river floodplain sand deposit that is the primary aquifer of western Tennessee and adjoining states.

Underlying the Eocene sediments are Paleocene sediments of the Porters Creek and Clayton formations (Figure 6). Beneath the Paleocene sediments are the ~ 80 million years old Late Cretaceous sediments, which in descending order consist of the Owl Creek, McNary Sand, Demopolis, and Coffee formations (Figure 6). These sediments also reflect near-shore marine sand, silt, and clay sediments with the Demopolis also having calcareous (sea shell) shallow marine sediment.

Underlying the Late Cretaceous sediments is the Paleozoic bedrock strata (Figure 6). The uppermost portion of the Paleozoic strata consists of the early Ordovician (~ 480 million years old) Knox Megagroup, which consists of dolomite.
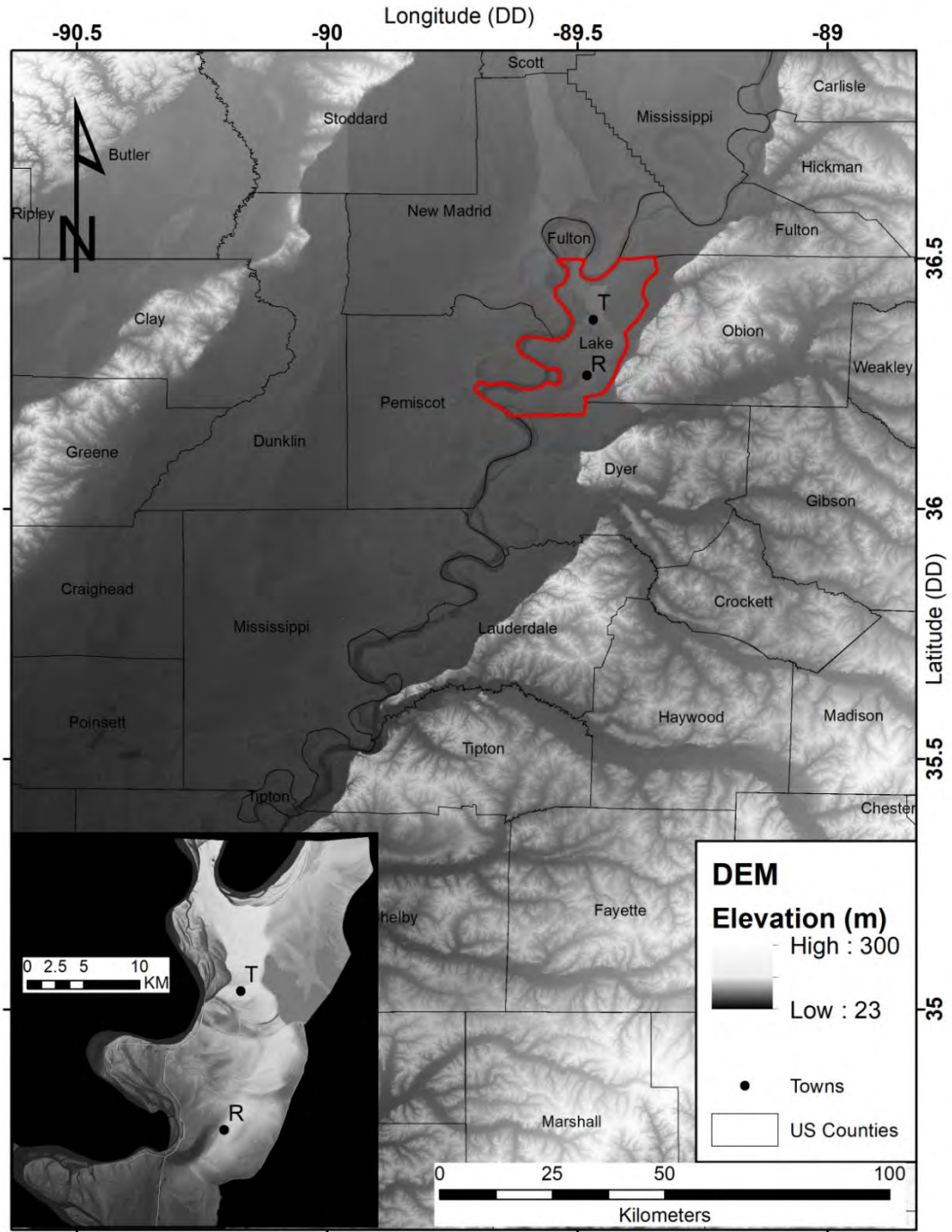
Figure 2: Digital Elevation Map (DEM) of West Tennessee and a portion of the central Mississippi River valley. States shown in bold include: Arkansas (AR), Kentucky (KY), Mississippi (MS), Missouri (MO), and Tennessee (TN). Several counties are labeled. Cities represented by white dots include: Memphis, TN (M), Blytheville, AR (B), Dyersburg, TN (D), and Jackson, TN (J). The red line locates Lake County, TN and a more detailed DEM of Lake County is provided in the inset box. On the Lake County inset map are the towns (black dots) of Tiptonville (T) and Ridgely (R).
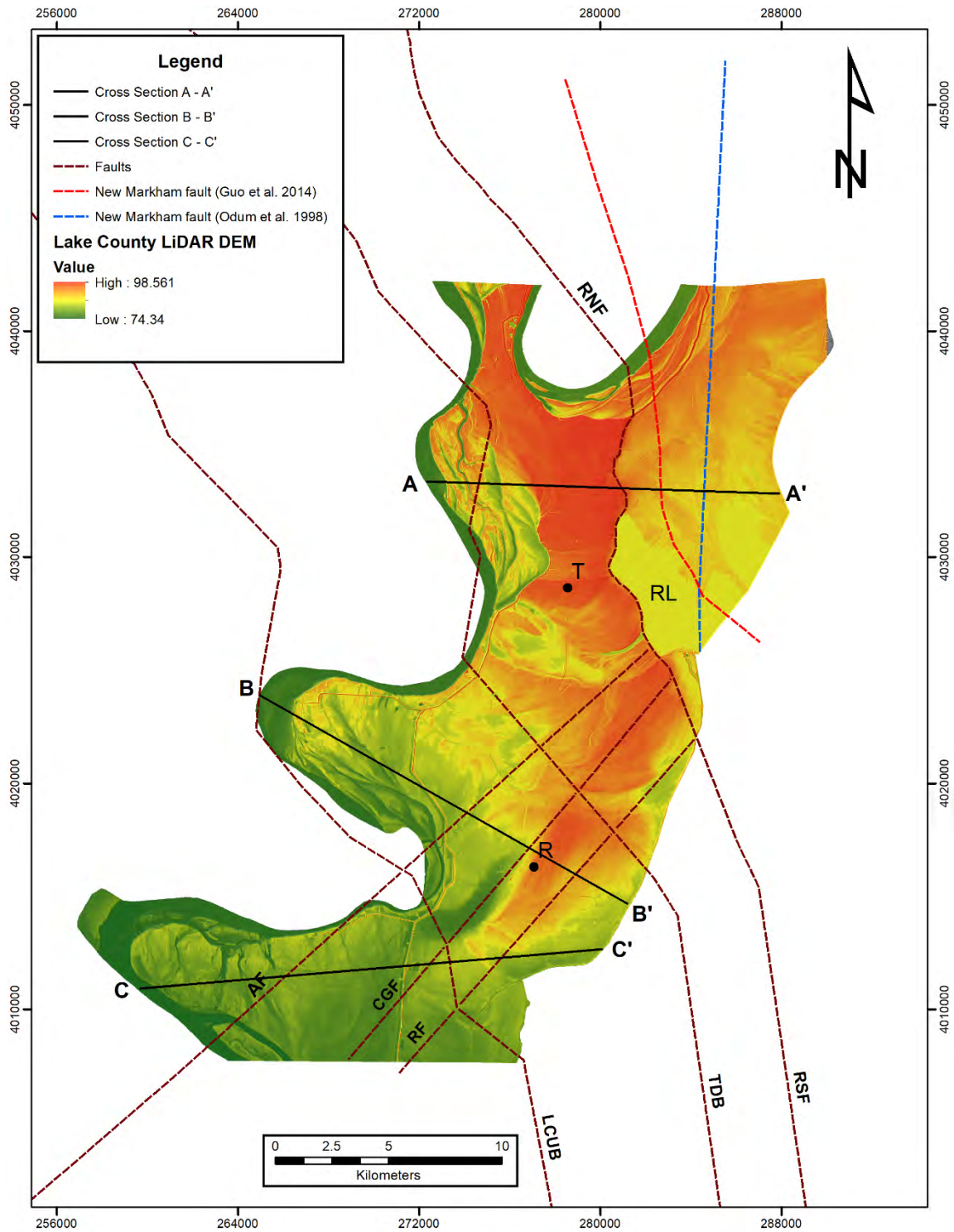
Figure 3: Digital Elevation Model (DEM) of Lake County. R = Ridgely, T = Tiptonville, RL = Reelfoot Lake, RNF = Reelfoot North fault, RSF = Reelfoot South fault, TDB = Tiptonville dome backthrust, LCUB = Lake County uplift backthrust, RF = Ridgely fault, CGF = Cottonwood Grove fault, AF = Axial fault.
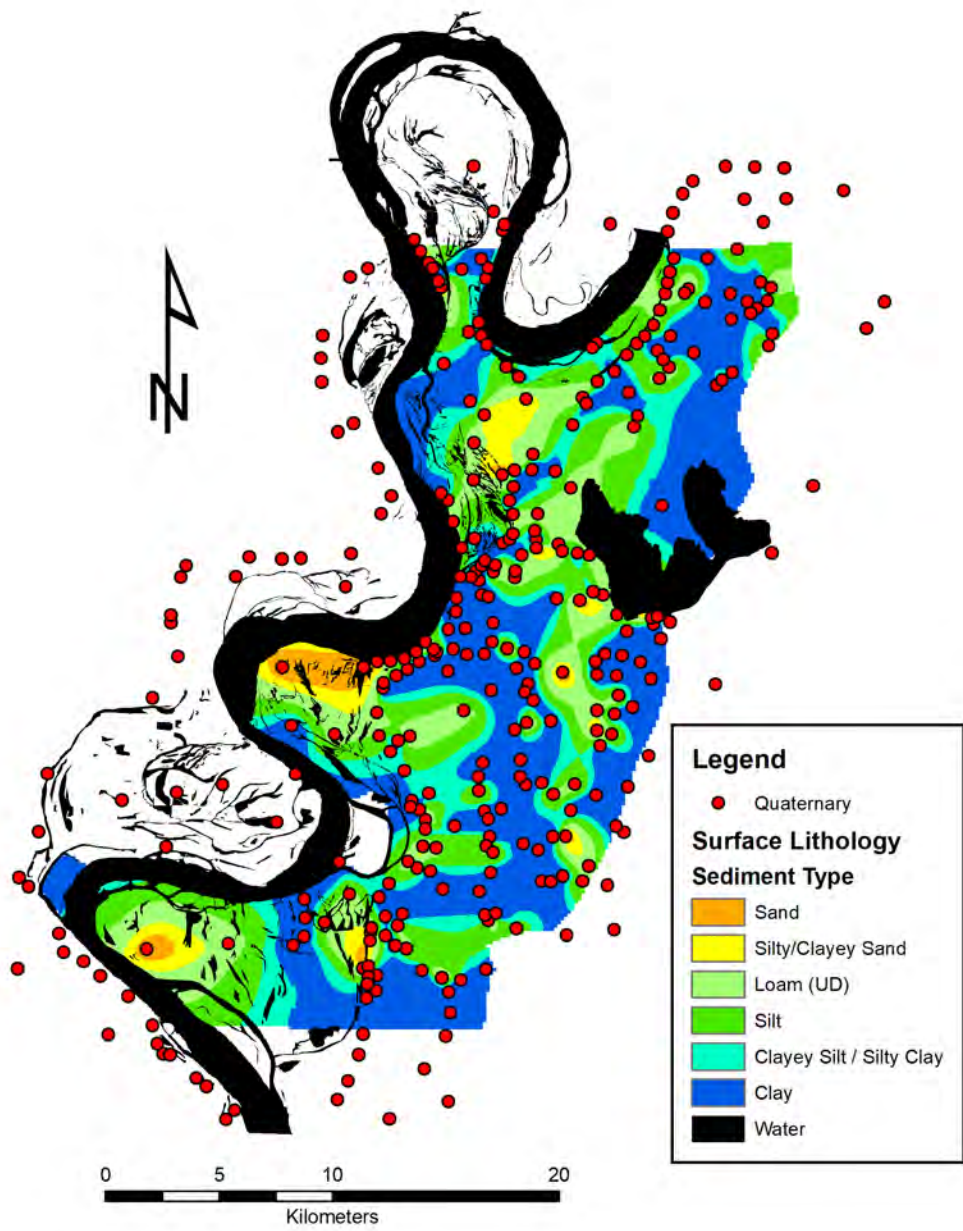
Figure 4: Surface sediments of Lake County, Tennessee. Red dots are drill hole locations used in this map construction.
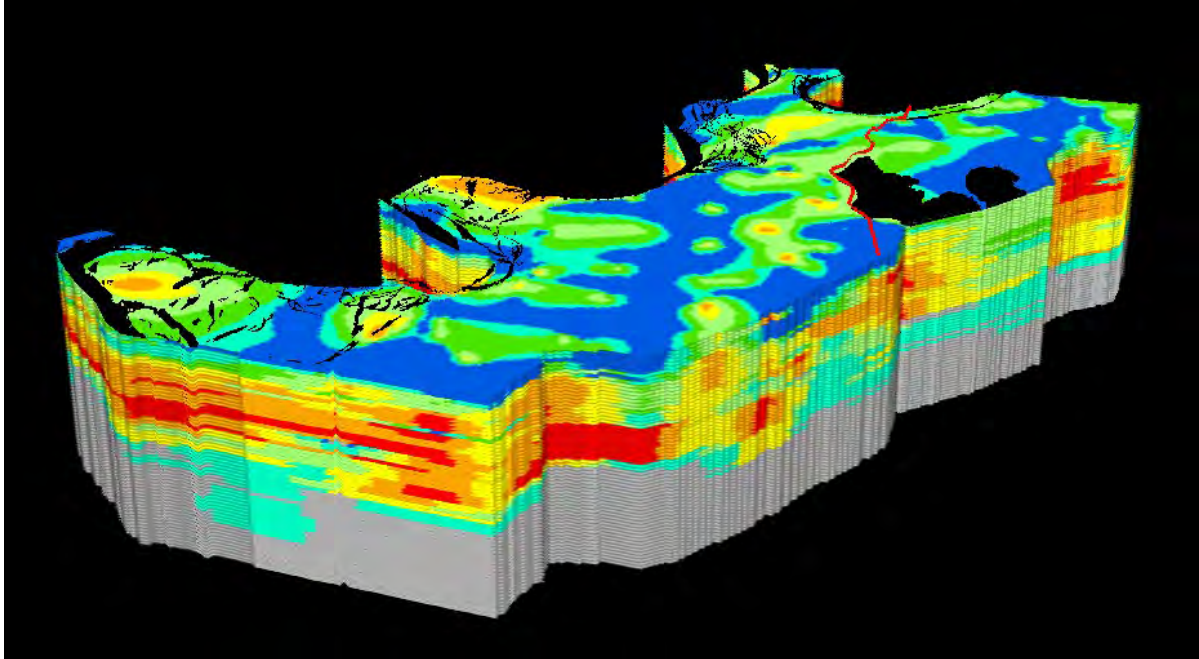
Figure 5: Quaternary Mississippi River floodplain sediments in 5 foot (2 m) thick layers. Red = sandy gravel, orange = sand, yellow = silty/clayey sand, light green = loam, dark green = silt, light blue = clayey silt/silty clay, dark blue = clay. The pseudo 3-dimentional animation of this figure is available in Appendix B. Individual 5 ft. (1.5 m) layers are shown in Appendix C.

ERA	PER.	GROUP	FORMATION	LITHOLOGY
CENOZOIC	QUAT.		ALLUVIUM, GRAVEL & LOESS	
	NEO.		UPLAND COMPLEX	
	PALEOGENE	EMBAYMENT MEGAGROUP	JACKSON	
		CLAIBORNE	COCKFIELD	
			COOK MTN.	
			MEMPHIS SAND	
		WILCOX	FLOUR ISLAND	
			FT. PILLOW	
			OLD BRSTWRKS.	
		MIDWAY	PORTER'S CREEK	
MESOZOIC	LATE CRETACEOUS		CLAYTON	
			OWL CREEK	
			McNAIRY SAND	
			DEMOPOLIS	
			COFFEE	
PALEOZOIC	EARLY ORDOVICIAN	KNOX MEGAGROUP		
	LATE CAMBRIAN			
	MIDDLE CAMBRIAN	POTSDAM MEGAGROUP	ELVINS	
	EARLY CAMBRIAN		BONNETERRE	
			LAMOTTE	
LATE pЄ			PRECAMBRIAN METAMORPHIC BASEMENT	

GENERALIZED STRATIGRAPHIC COLUMN OF WESTERN TENNESSEE

- SAND
- CLAYEY SAND
- CALCAREOUS SAND
- CALCAREOUS CLAY
- DOLOMITIC CLAY
- SILTY CLAY
- SHALE
- SANDY SHALE
- SAND & GRAVEL
- LIMESTONE
- SHALY LIMESTONE
- OOLITIC LIMESTONE
- DOLOMITE
- CHERTY DOLOMITE
- METAMORPHIC IGNEOUS ROCK
- UNCONFORMITY

Figure 6: Generalized stratigraphic column of West Tennessee (modified from Parrish and Van Arsdale, 2004 and Ward, 2016). Quat. = Quaternary and Plio. = Pliocene.

Isopach Maps of Lake County

Isopach maps were made of the thickness of the strata that underlies Lake County. The entire Quaternary Mississippi River floodplain alluvium isopach reveals that the Quaternary section varies in thickness from 95 ft. (29 m) to 312 ft. (95 m) (Figure 7A). Within the Quaternary section the near-surface silt and clay facies varies in thickness from 0.7 ft. (0.2 m) to 180 ft. (55 m) (Figure 7B), the underlying sand facies 7 ft. (2 m) to 131 ft. (40 m) (Figure 7C), and the basal sandy gravel facies 7 ft. (2 m) to 180 ft. (55 m) (Figure 7D). The thickness of the Paleogene (Eocene plus Paleocene) strata varies from 1181 ft. (360 m) to 1874 ft. (571 m) (Figure 8) and the thickness of the Late Cretaceous strata is 115 ft. (35 m) to 656 ft. (200 m) (Figure 9). The base of the Paleozoic was not mapped and so we do not have an isopach map of the Paleozoic section.

Geologic Structure of Lake County

Numerous faults, some with ongoing seismicity, have been previously mapped beneath and adjacent to Lake County, Tennessee (Figures 3 and 10). This portion of the United States is undergoing horizontal compression oriented at about N60°E, probably from plate tectonic forces (Figure 10A). As a consequence of this stress field (plate force) the northeast-trending Axial, Cottonwood Grove, and Ridgely faults are undergoing right-lateral transpressive faulting resulting in horizontal and vertical movement and the northwest oriented faults (e.g. Reelfoot fault) are undergoing compression resulting in vertical uplift.

Northwest-trending structures that pass beneath Lake County include the Tiptonville dome, which is bounded on the northeast by the Reelfoot fault and on the southwest by a back thrust (Tiptonville dome back thrust), the Lake County Uplift, which is also bounded on the northeast by the Reelfoot fault and on the southwest by a back thrust (Lake County Uplift back thrust) (Figures 3 and 10). The faults that bound the Tiptonville dome and Lake County uplift are reverse faults with vertical displacement. The northeast-trending structures include Ridgely Ridge horst (an uplifted block) and its bounding Ridgely Ridge and Cottonwood Grove faults (Figs. 3 and 10). The Axial fault is the northwest-bounding fault of an unnamed graben (down-dropped block). These northeast-trending faults are vertical strike-slip faults with horizontal and vertical offset.

Structure Contour Maps

In this research we have mapped the elevations of tops of strata and illustrate their subsurface relief with structure contour maps. A structure contour map is similar to a topographic map in that it illustrates the buried topography on the top of selected strata (e.g. top of the Eocene). The values given in these maps are with respect to sea level and so many values are negative.

The near-surface structure contour maps depict tops of sediment layers within the Quaternary Mississippi River floodplain alluvium. The top of the Quaternary Mississippi River floodplain

sand facies (Figure 11) reveals elevations that range from 180 ft. (55 m) to 312 ft. (95 m) and the top of the underlying Mississippi River sandy gravel facies ranges in elevation from 131 ft. (40 m) to 295 ft. (90 m) (Figure 12). Elevations of the top of the Eocene vary from 213 ft. (65 m) to -16 ft. (-5 m) (Figure 13). The Late Cretaceous top varies in elevation from -280 ft. (-390 m) to -1969 ft. (-600 m) (Figure 14) and the elevation of the top of the Paleozoic Knox ranges in elevation from -1542 ft. (-470 m) to -2438 ft. (-743 m) (Figure 15).

The structure contour maps reveal that the mapped strata tops are vertically displaced, we believe, by faulting. Vertical displacement occurred after deposition of the stratigraphy that underlies Lake County, therefore the tops of the Paleozoic, Late Cretaceous, Eocene, and perhaps the sandy gravel and sand alluvial facies within the Quaternary strata have been vertically displaced (Figures. 11B-15B). Horizontal displacement has not been determined on any faults because that determination cannot be obtained with our data. The amount of vertical displacement varies with the fault and varies with depth. For example, the Reelfoot fault has 230 ft. (70 m) of vertical displacement on the top of the Paleozoic, 197 ft. (60 m) on the top of the Cretaceous, and 49 ft. (15 m) on the top of the Eocene (Van Arsdale et al., 1998). These variable displacements suggest that the Reelfoot fault has been reactivated over the last ~ 80 million years and the ongoing seismicity reveals that the Reelfoot and Axial faults are still active. Figure 3 illustrates where the faults will break the ground surface in the event of major fault movement (coincident with an earthquake with a magnitude greater than 7 on that fault) and the permanent vertical land displacement that will probably occur across the faults is illustrated in Figures 16-18.

Our faulted structure contour maps illustrate fault displacement from the top of the Paleozoic through the top of the Mississippi River floodplain sand facies that is probably younger than 10 ka (Figures 11B - 15B). Thus, the Reelfoot, Tiptonville dome back thrust, Lake County uplift back thrust, Ridgely, Cottonwood Grove, and Axial faults are capable of generating earthquakes (Figure 3). The Reelfoot fault has late Holocene displacement as is reflected in its surface monocline (Kelson et al., 1996). Based on our current research, it is recommended that shallow S-wave seismic reflection profiles be acquired across the Tiptonville dome back thrust, Lake County uplift back thrust, Ridgely, Cottonwood Grove, and Axial faults to confirm the Quaternary displacement that is shown in Figure 11B. If near-surface displacement is confirmed in the seismic reflection profiles, then optimum locations along the reflection lines could be selected for the drilling of shallow bore holes. Drilling through the alluvium will allow the acquisition of subsurface sediment samples for radiometric dating (Ward et al., 2017; Woolery et al., 2018). Radiometrically dated stratigraphic units (seismic reflectors) will allow for the determination of any Quaternary displacement histories on the faults, the magnitude of those displacements, and an earthquake recurrence interval determination for a comprehensive seismic hazard assessment of Lake County.

Cross-Sections

Six cross sections were made across Lake County (Figure 3). Two cross sections were made for each cross-section line; one un-faulted and one faulted. Cross-Section A-A' (Figure 16) crosses

faults TDB, RF, and NMF. Fault TDB is not evident in Figure 16 (upper), but once the fault is introduced in Figure 16 (lower) the Tiptonville dome (TD) becomes readily identifiable. The Reelfoot fault is evident and displaces each unit from the Paleozoic into the base of the Quaternary. Reelfoot Lake is underlain by a graben bounded by the Reelfoot fault and the New Markham fault.

Cross-Section B-B' (Figure 17) crosses faults LCUB, AF, CGF, and RF. Fault LCUB is not evident in this cross section. The Axial fault is not apparent in Figure 17 (upper) though the Cretaceous thickens at this location but is evident in Figure 17 (lower) with up-to-the-west displacement on the tops of the Paleozoic and the Cretaceous. The Cottonwood Grove and Ridgely faults are evident as the west-bounding and east-bounding faults of Ridgely ridge, respectively. There are also two grabens adjacent to Ridgely ridge. All three faults in Cross-Section B-B' appear to displace the base of the Quaternary.

Cross-Section C-C' (Figure 18) crosses the AF, CGF, and RF. Ridgely ridge and its bounding faults are evident in these cross sections, but displacement appears to diminish between Cross-Section B-B' and Cross-Section C-C'. There appear to be previously unidentified faults west and east of Ridgely ridge that displace the tops of the Paleozoic and the Cretaceous, but not the top of the Eocene.
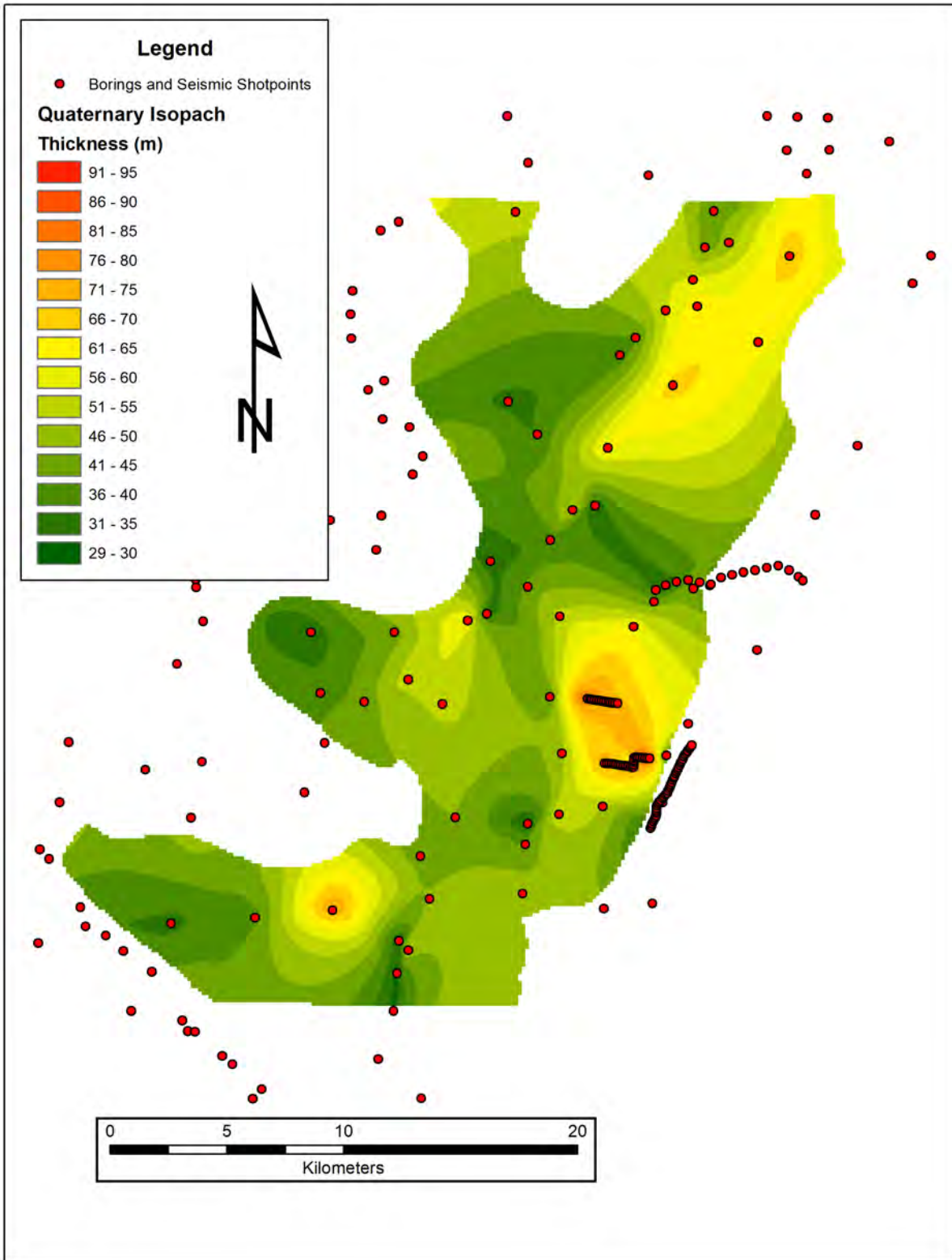
Figure 7A: Isopach map of the Quaternary Mississippi River floodplain alluvium underlying Lake County, Tennessee. Dots are borings used to make the map. Contour interval is 5 m.
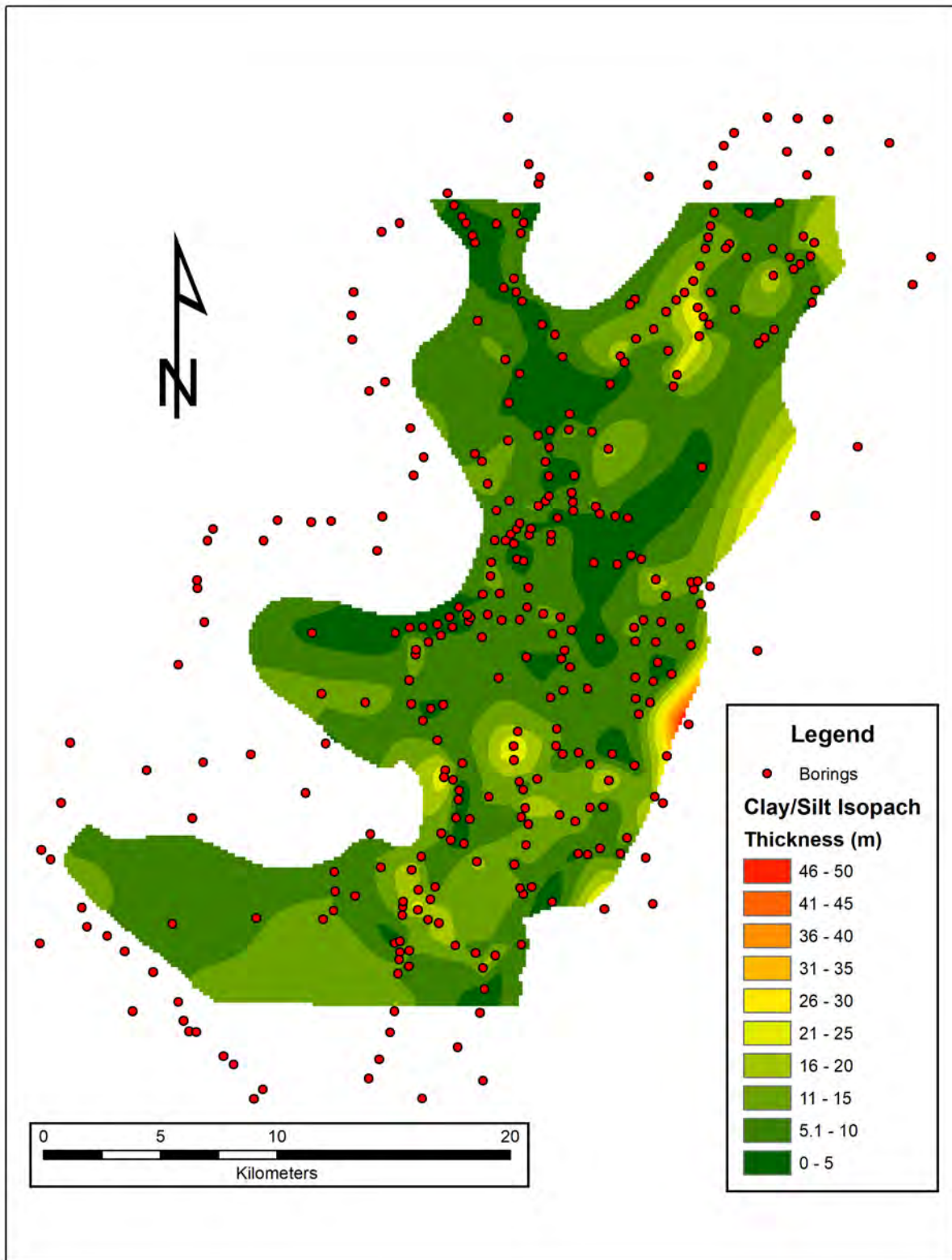
Figure 7B: Isopach map of the clay and silt facies in the uppermost Quaternary Mississippi River alluvium. Dots are borings used to make the map. Contour interval is 5 m.
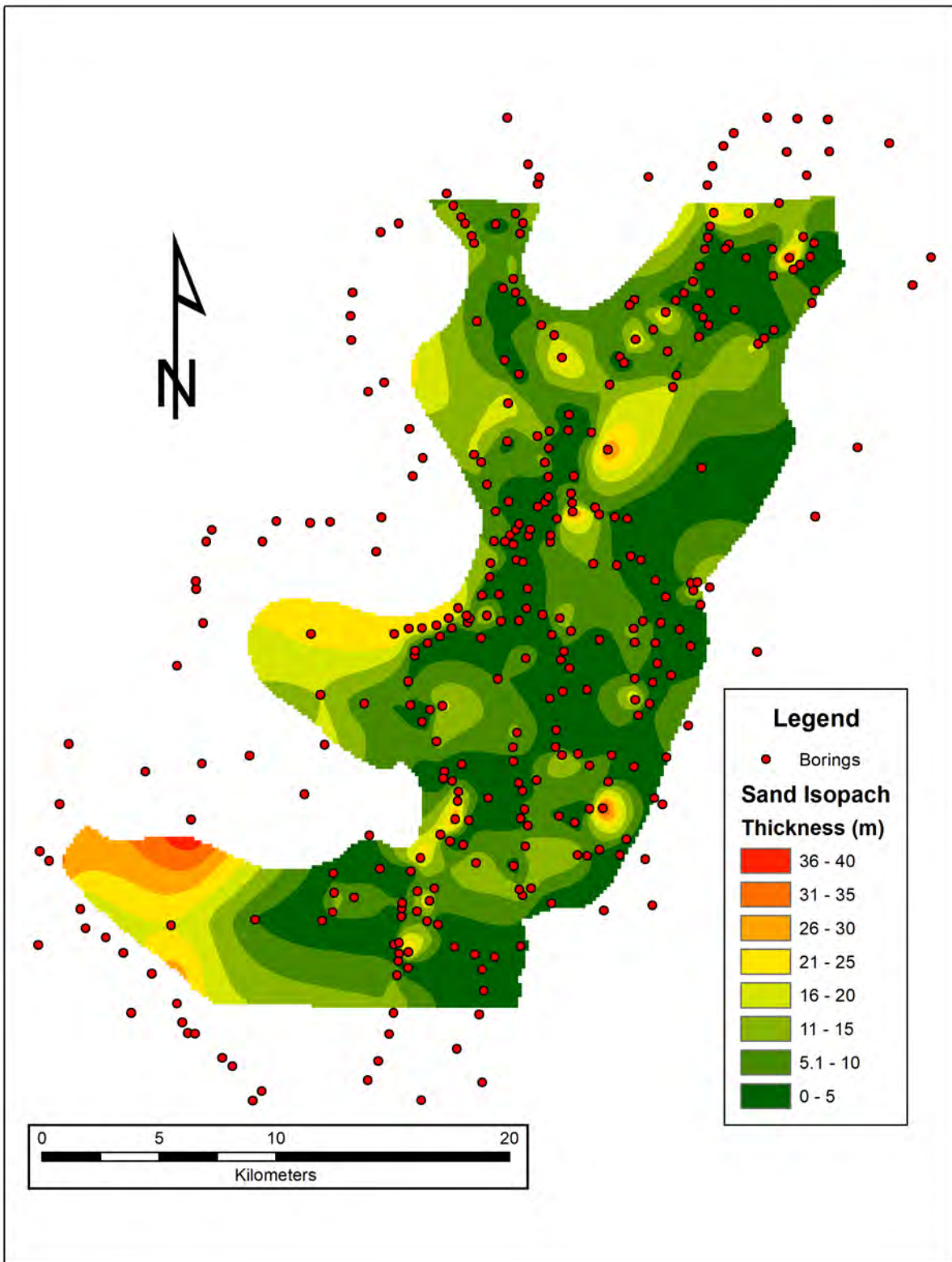
Figure 7C: Isopach map of sand facies at intermediate depth within the Quaternary Mississippi River alluvium. Dots are borings used to make the map. Contour interval is 5 m.
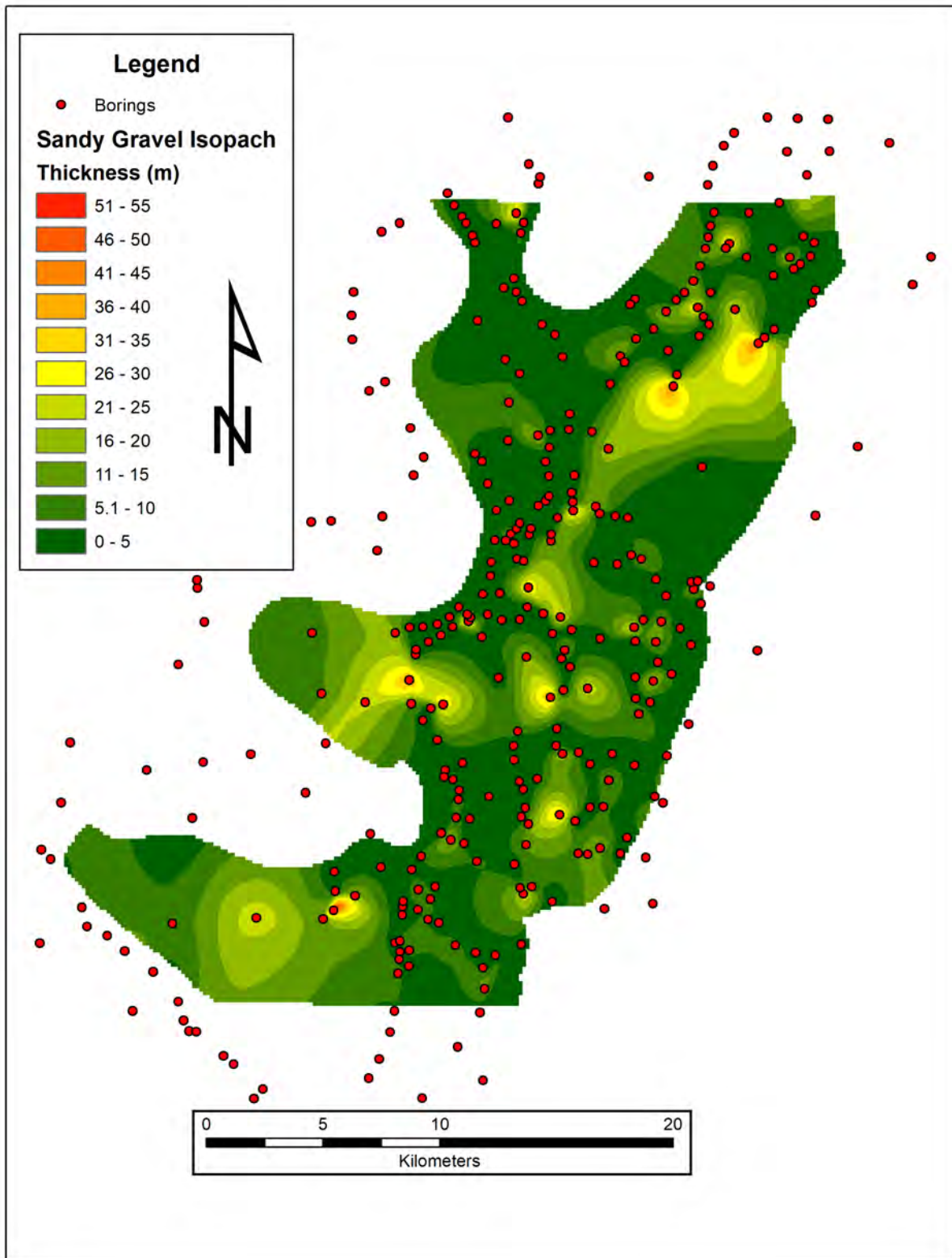
Figure 7D: Isopach map of the basal sandy gravel facies within the Quaternary Mississippi River alluvium. Dots are borings used to make the map. Contour interval is 5 m.
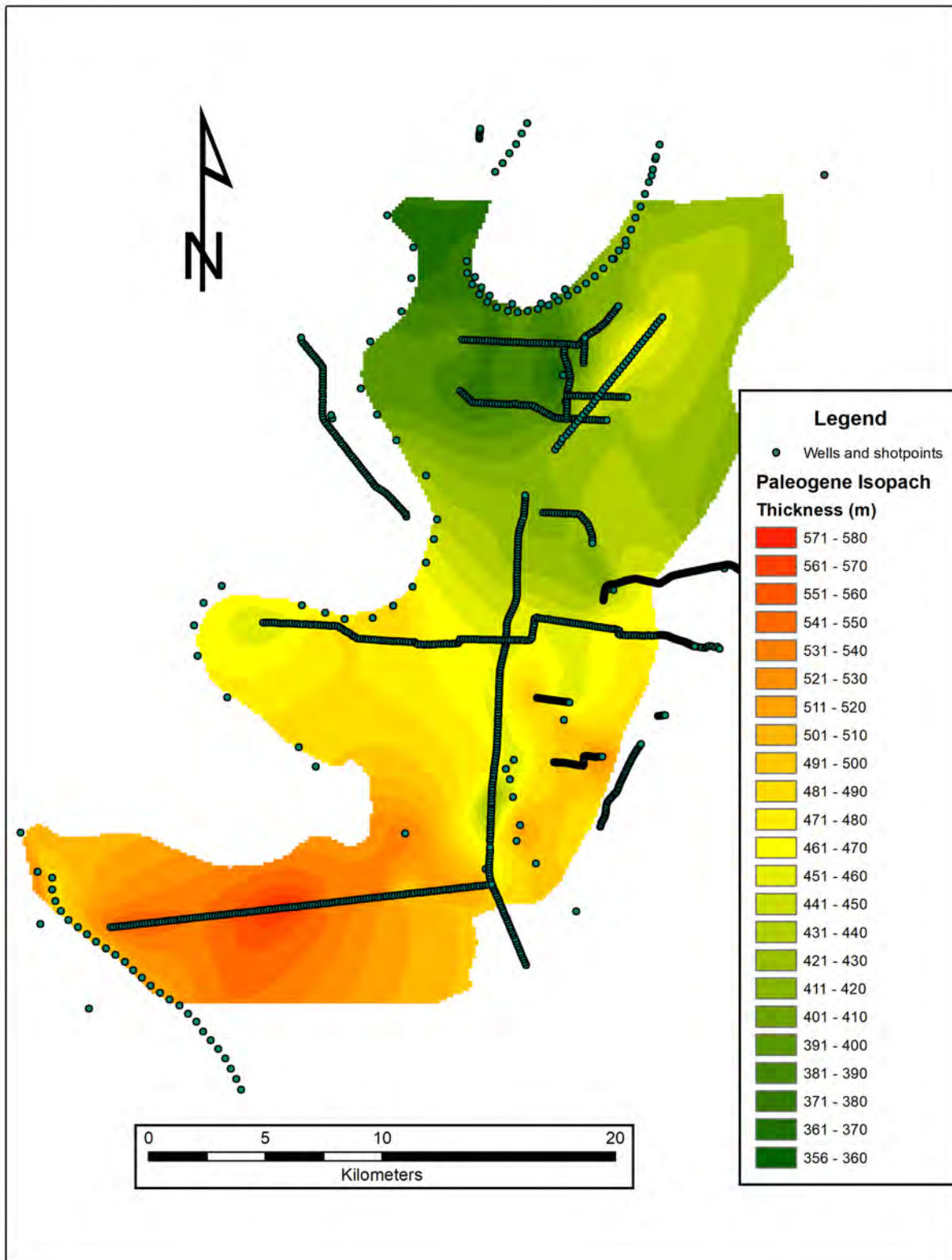
Figure 8: Isopach map of the thickness of the Paleogene strata. Dots are borings and seismic reflection data used to make the map. Contour interval is 10 m.
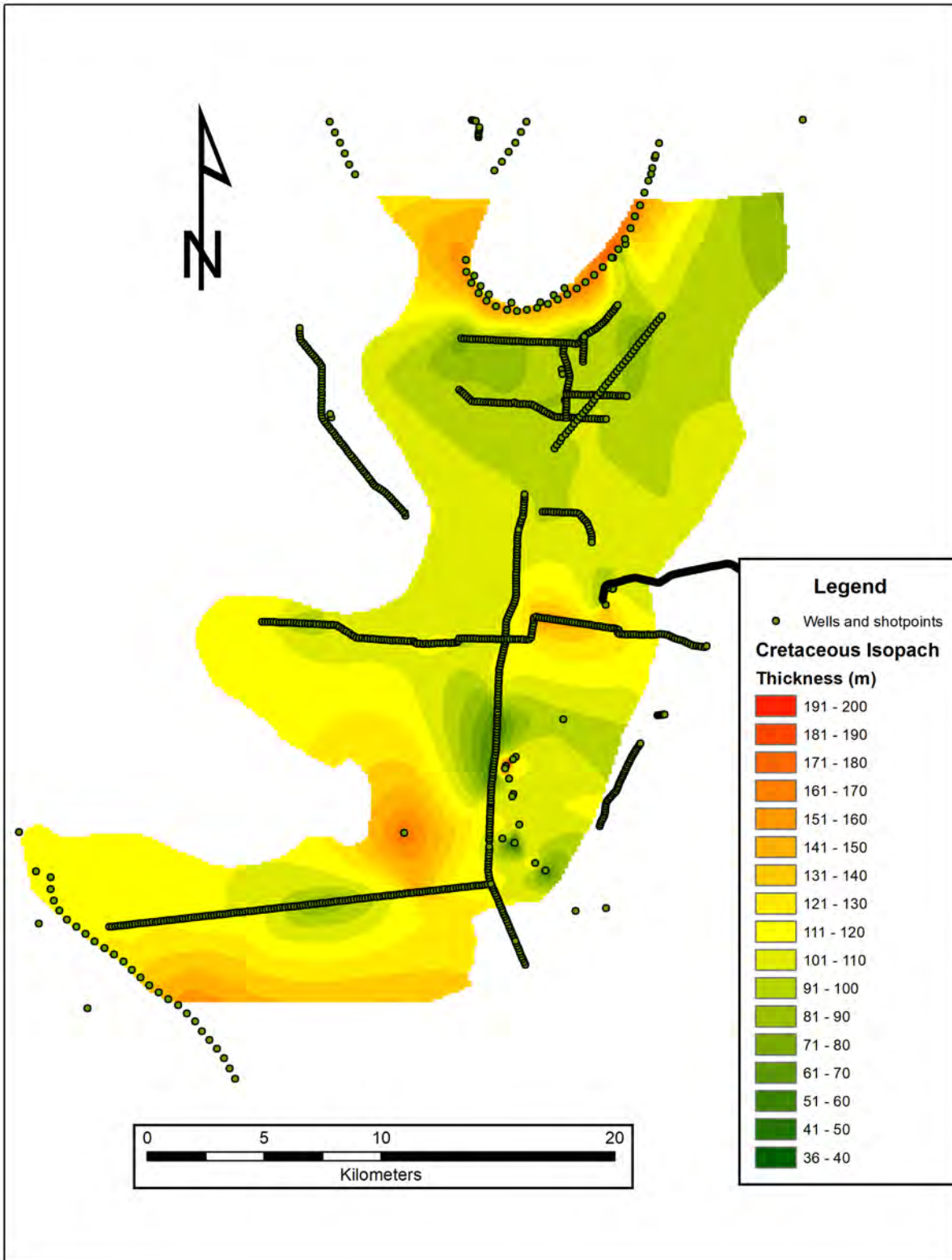
Figure 9: Isopach map of the thickness of the Late Cretaceous strata. Dots are borings and seismic reflection data used to make the map. Contour interval is 10 m.
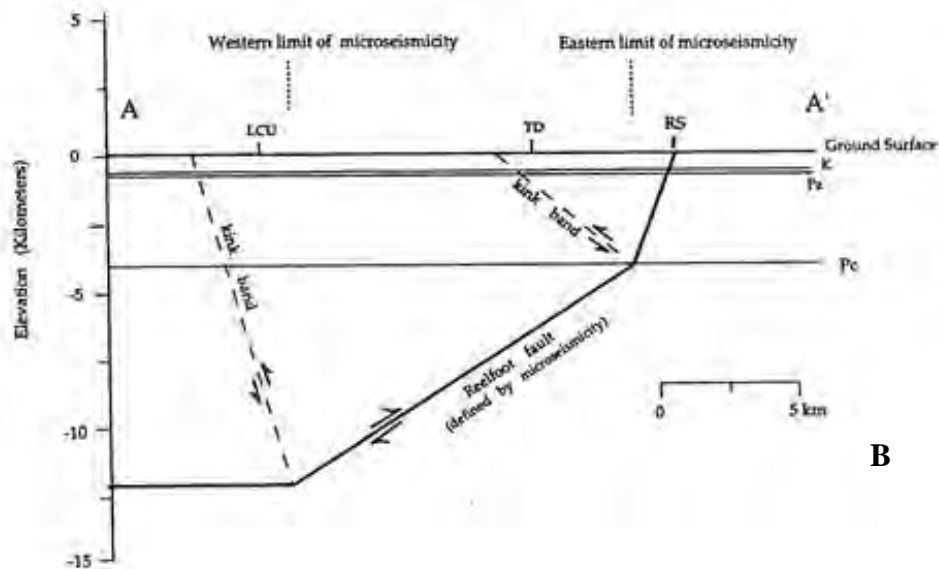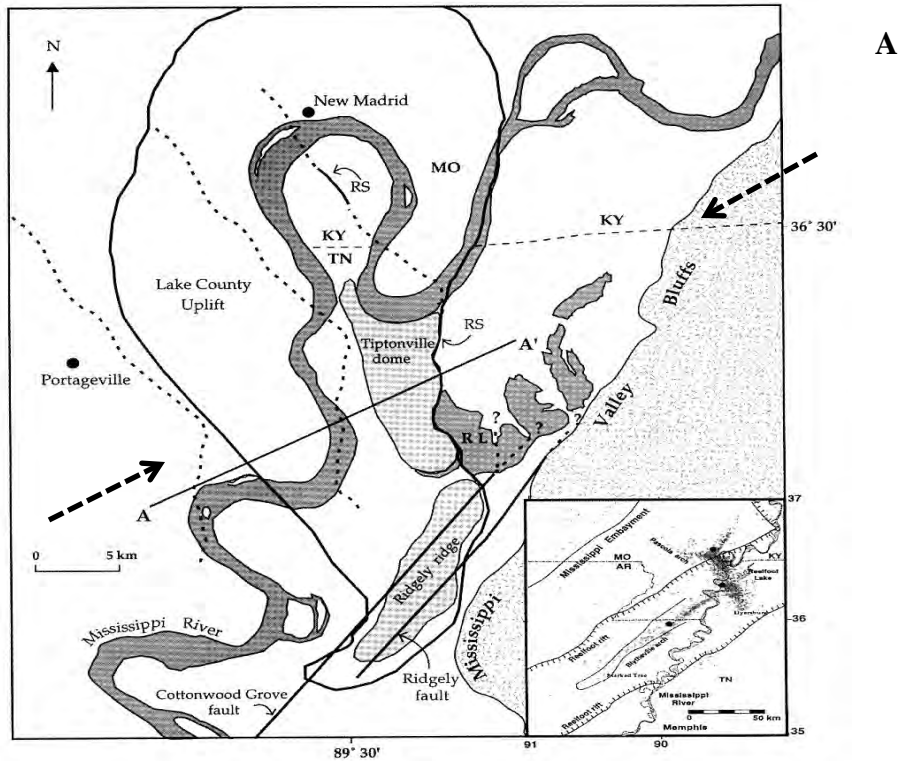
Figure 10: A) The Lake County uplift and vicinity. Solid line marks boundary of the Lake County uplift, and dotted lines are proposed kink bands (back thrusts). Dashed arrows illustrate horizontal principal stress. B) Cross section of the Reelfoot fault using the fault-bend fold model. K = top of Late Cretaceous; Pz = top of Paleozoic; Pc = top of Precambrian; LCU = Lake County uplift western margin; TD = Tiptonville dome western margin; RS = Reelfoot scarp (fault), which is the eastern margin of the Lake County uplift and Tiptonville dome (from Purser and Van Arsdale, 1998).
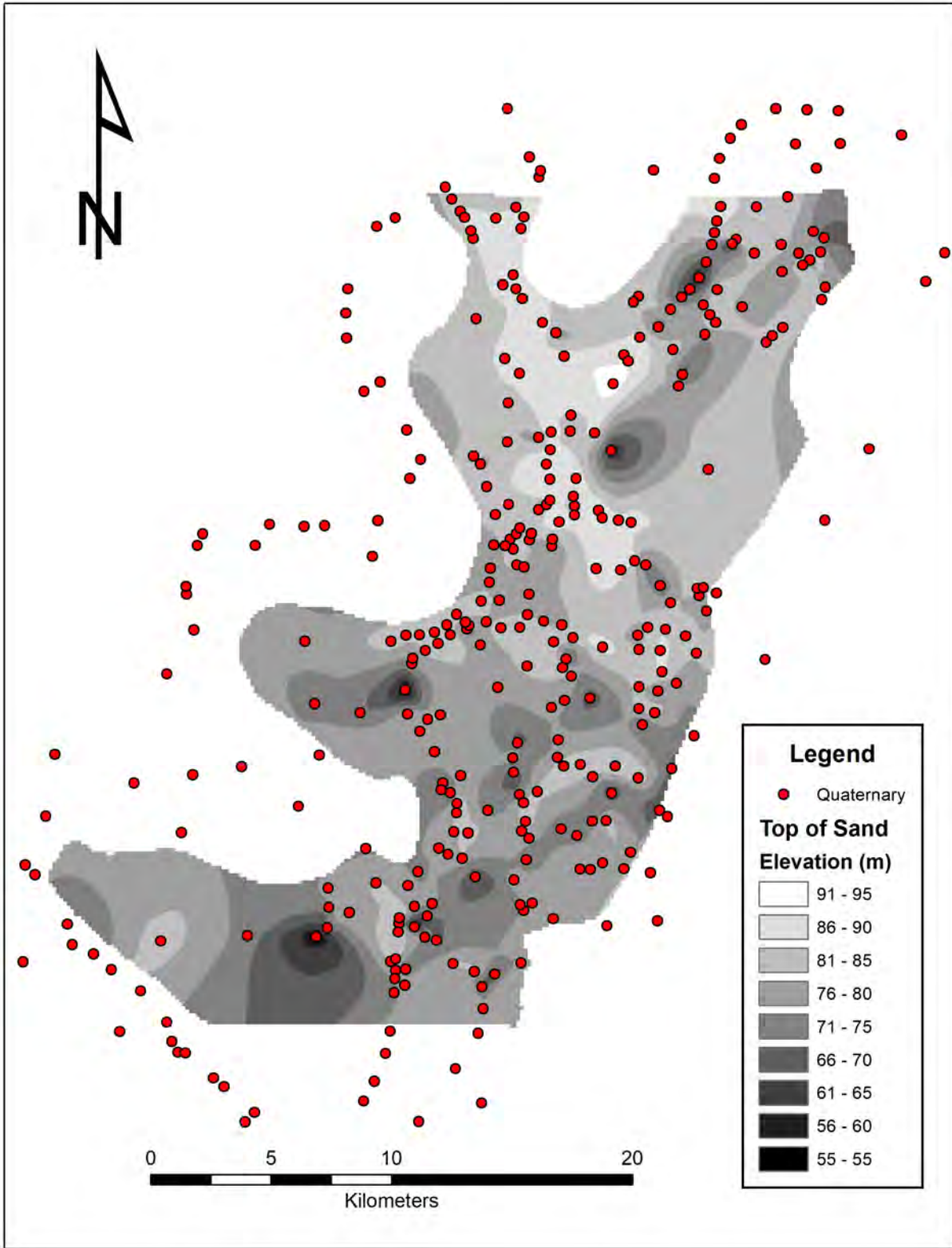
Figure 11A: Structure contour map of the top of Quaternary Mississippi River floodplain sand facies. Contour interval is 5 m.
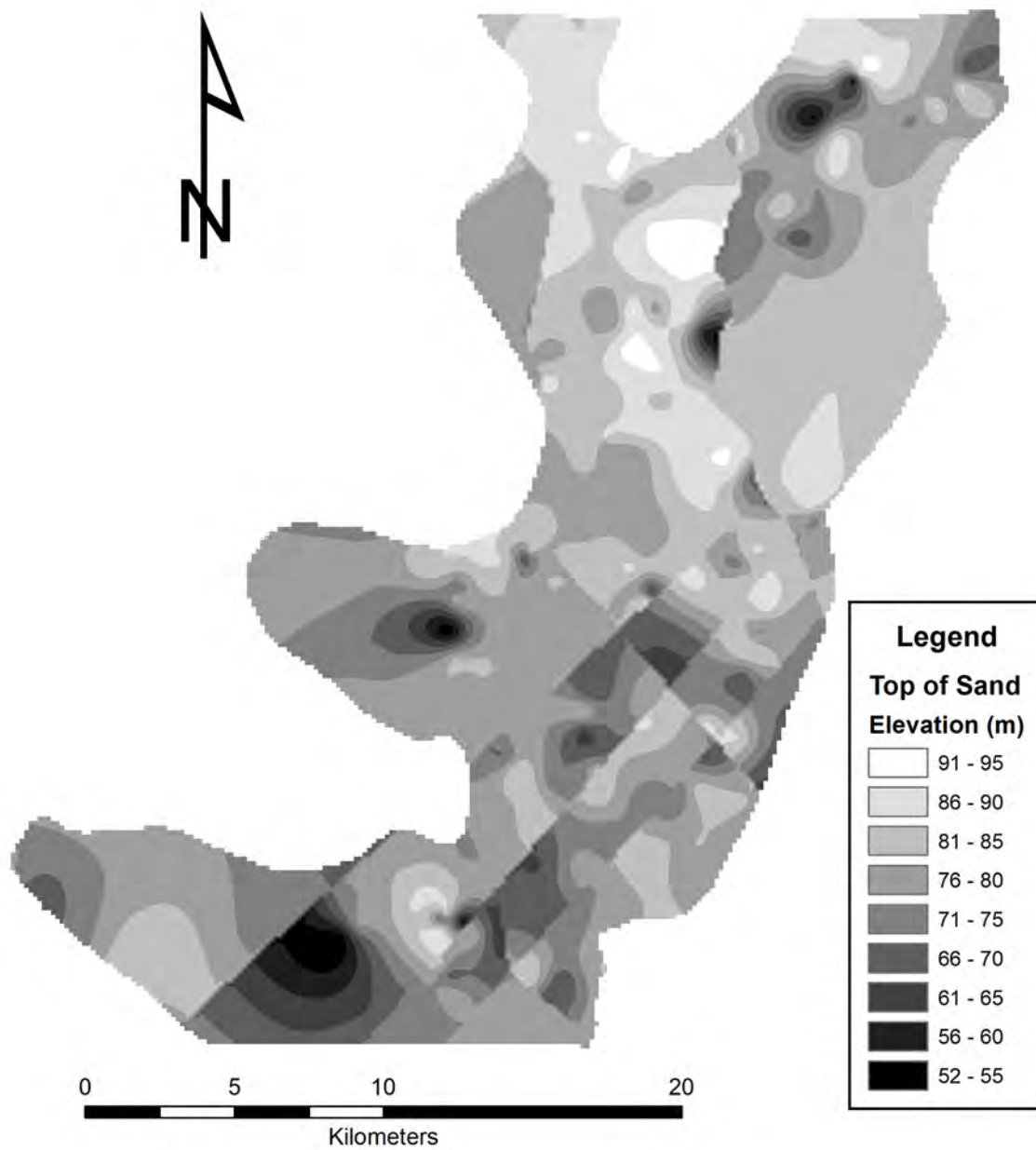
Figure 11B: Structure contour map of the faulted top of Quaternary Mississippi River floodplain sand facies. Contour interval is 5 m.
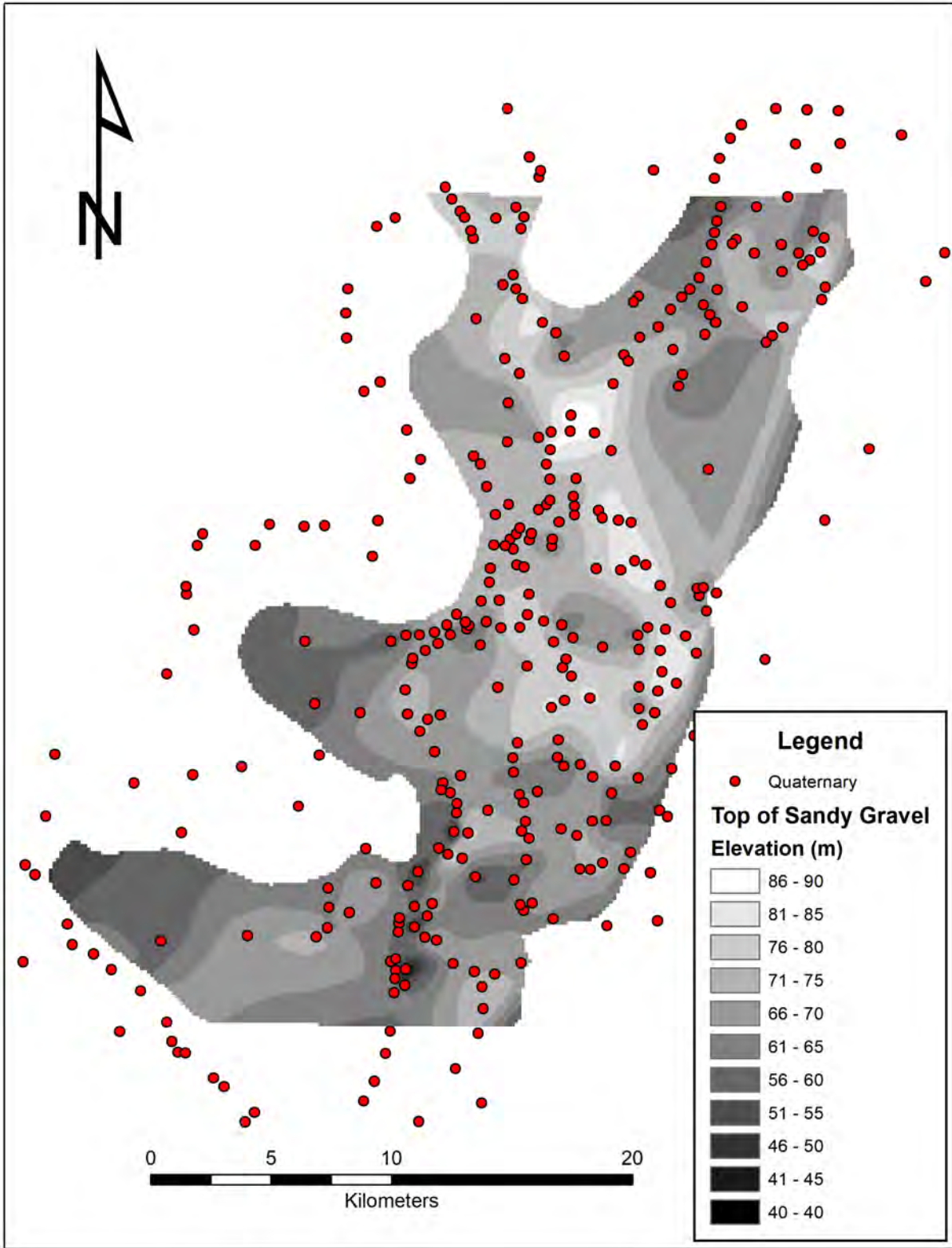
Figure 12A: Structure contour map of the top of Quaternary Mississippi River floodplain sandy gravel facies. Contour interval is 5 m.
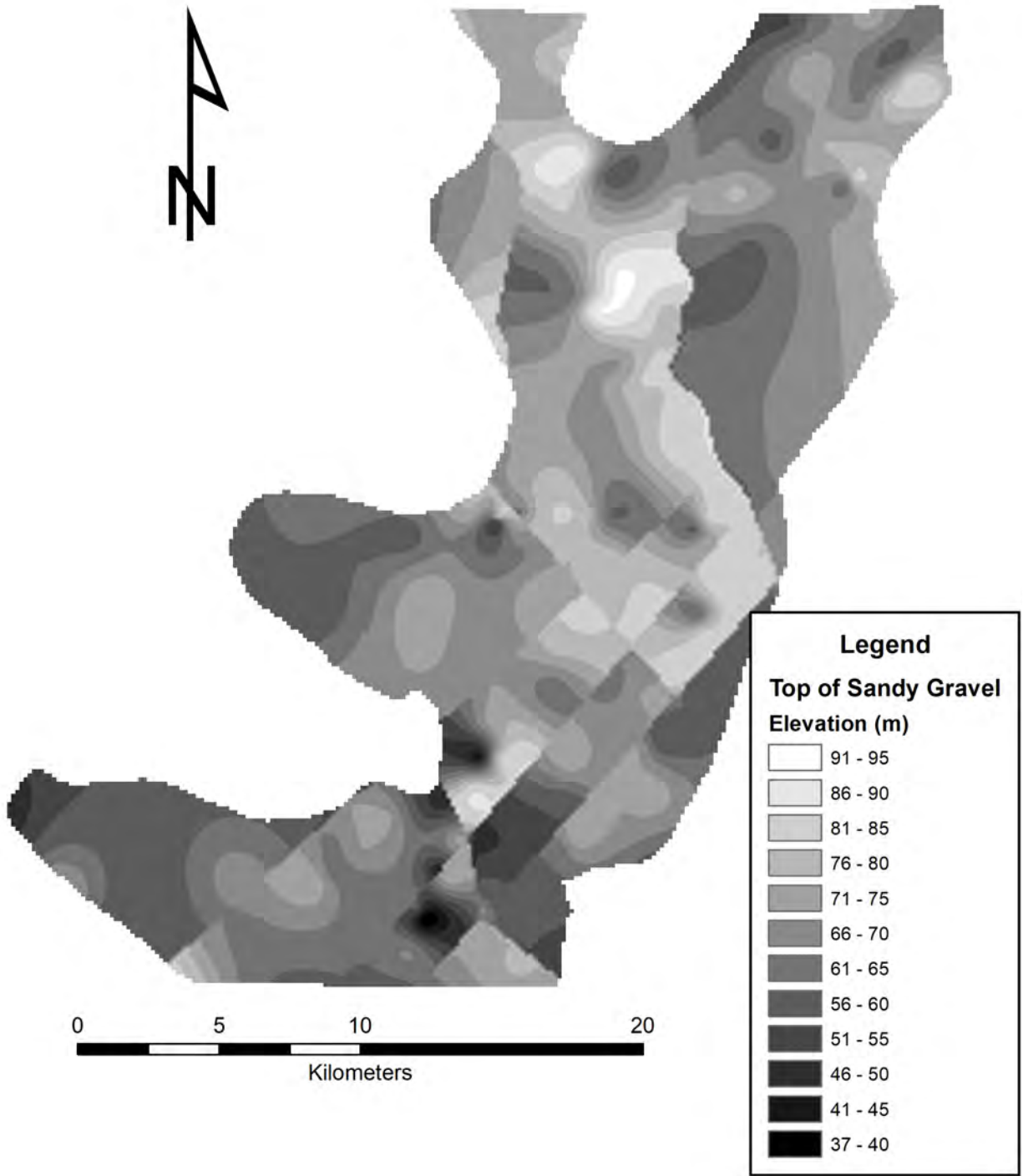
Figure 12B: Structure contour map of the faulted top of Quaternary Mississippi River floodplain sandy gravel facies. Contour interval is 5 m.
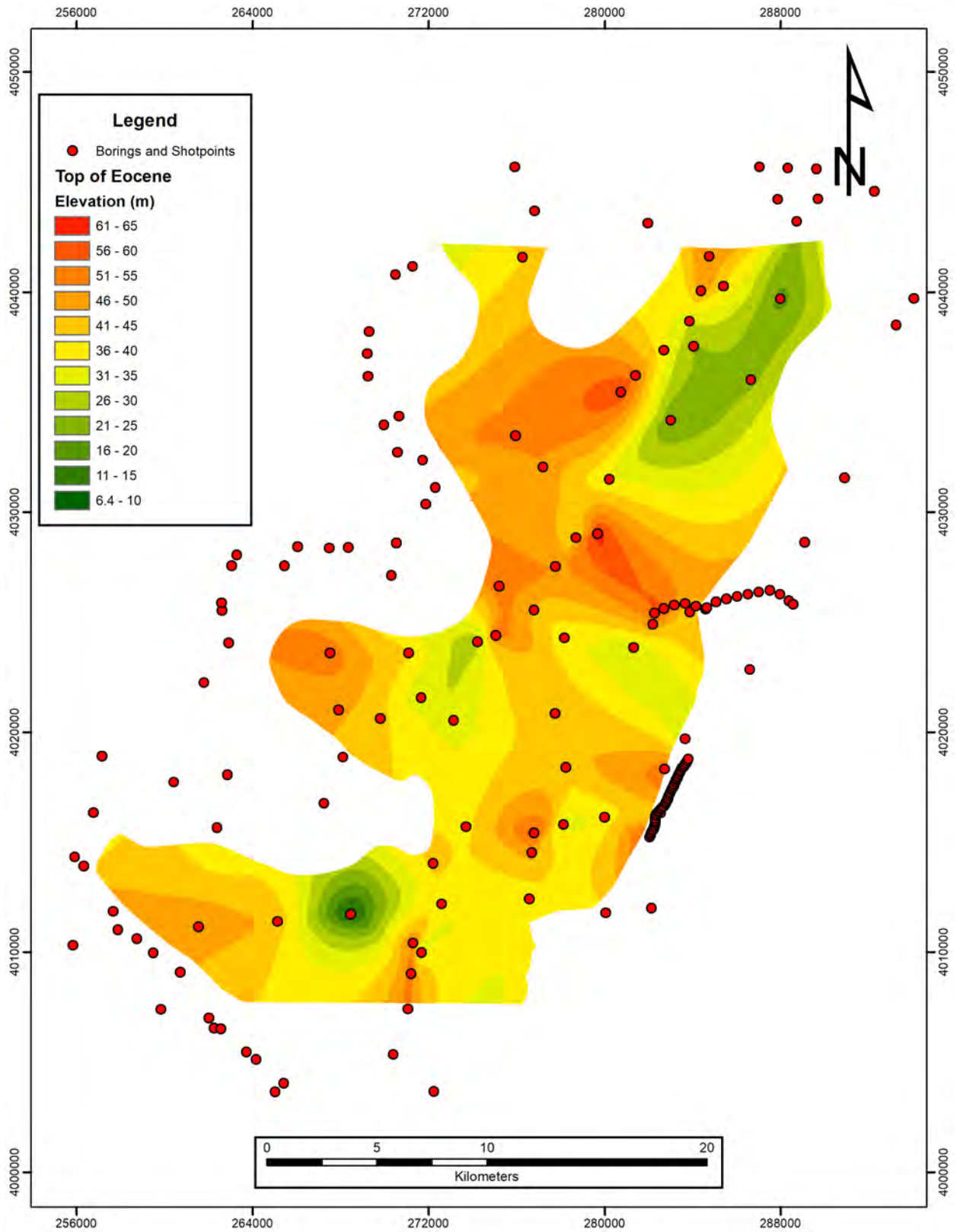
Figure 13A: Structure contour map of the top of the Eocene with borings (dots) used to make the map. Contour interval is 5 m.
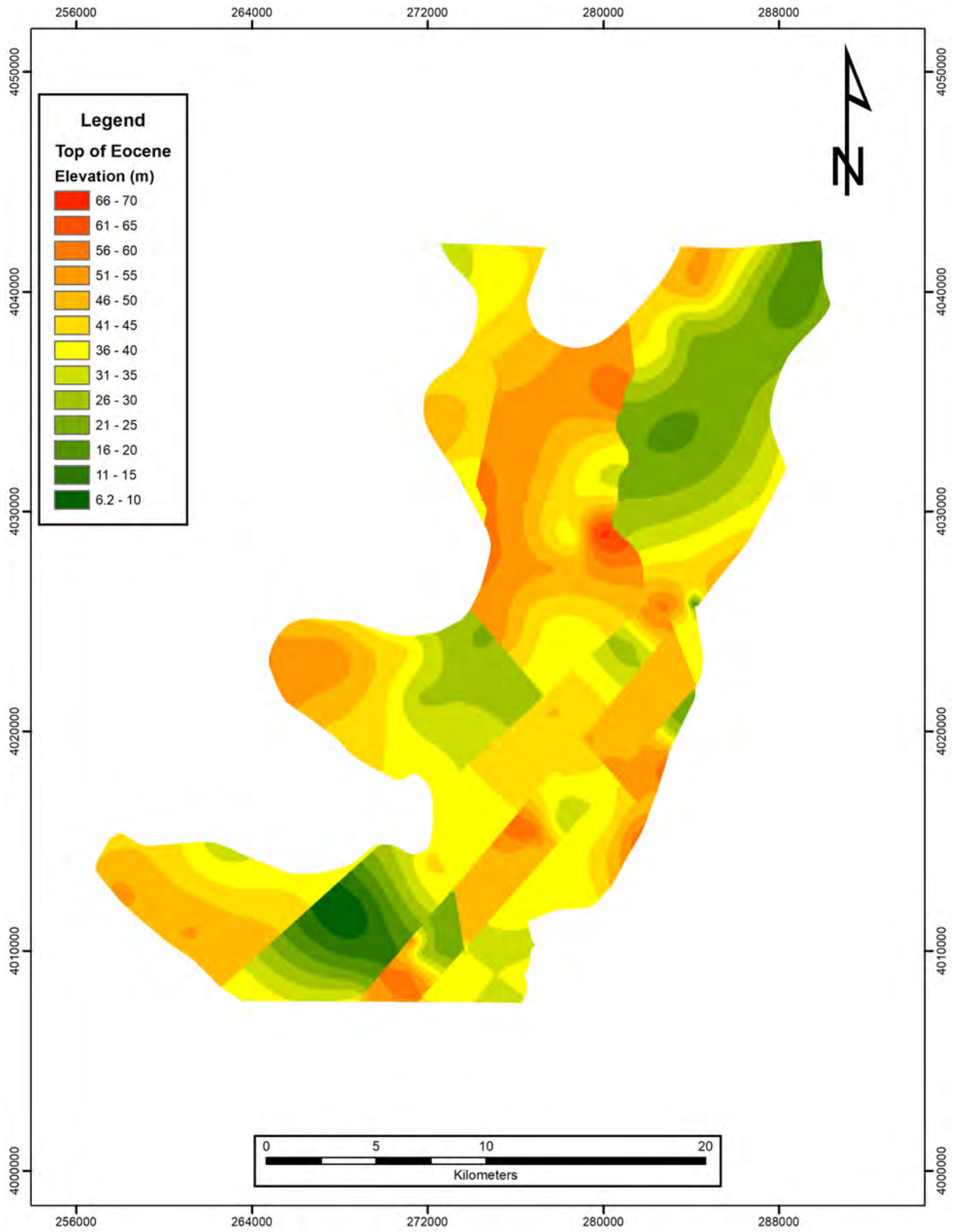
Figure 13B: Structure contour map of the faulted top of the Eocene. Contour interval is 5 m.
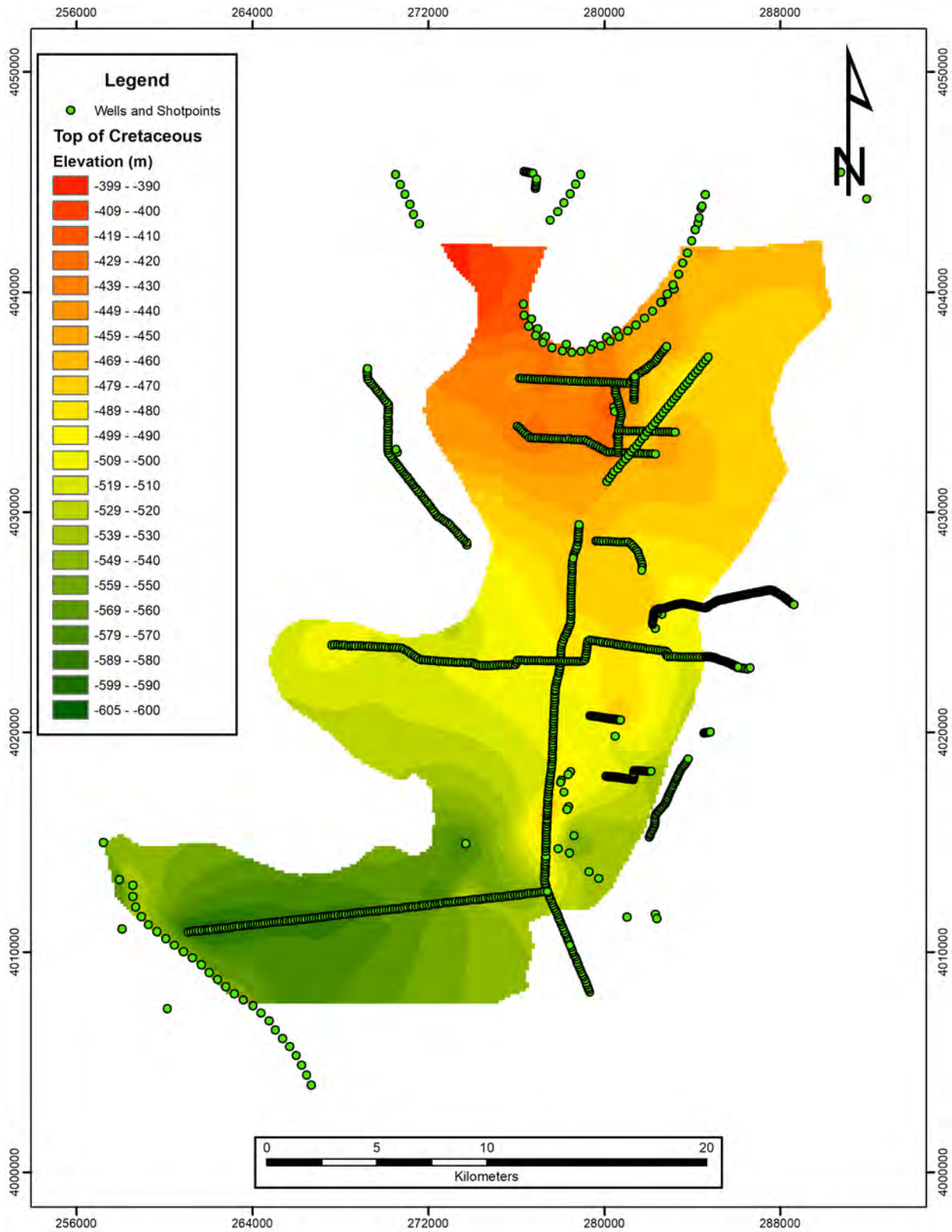
Figure 14A: Structure contour map of the top of the Late Cretaceous strata with borings and seismic reflection data (dots) used to make the map. Contour interval is 10 m.
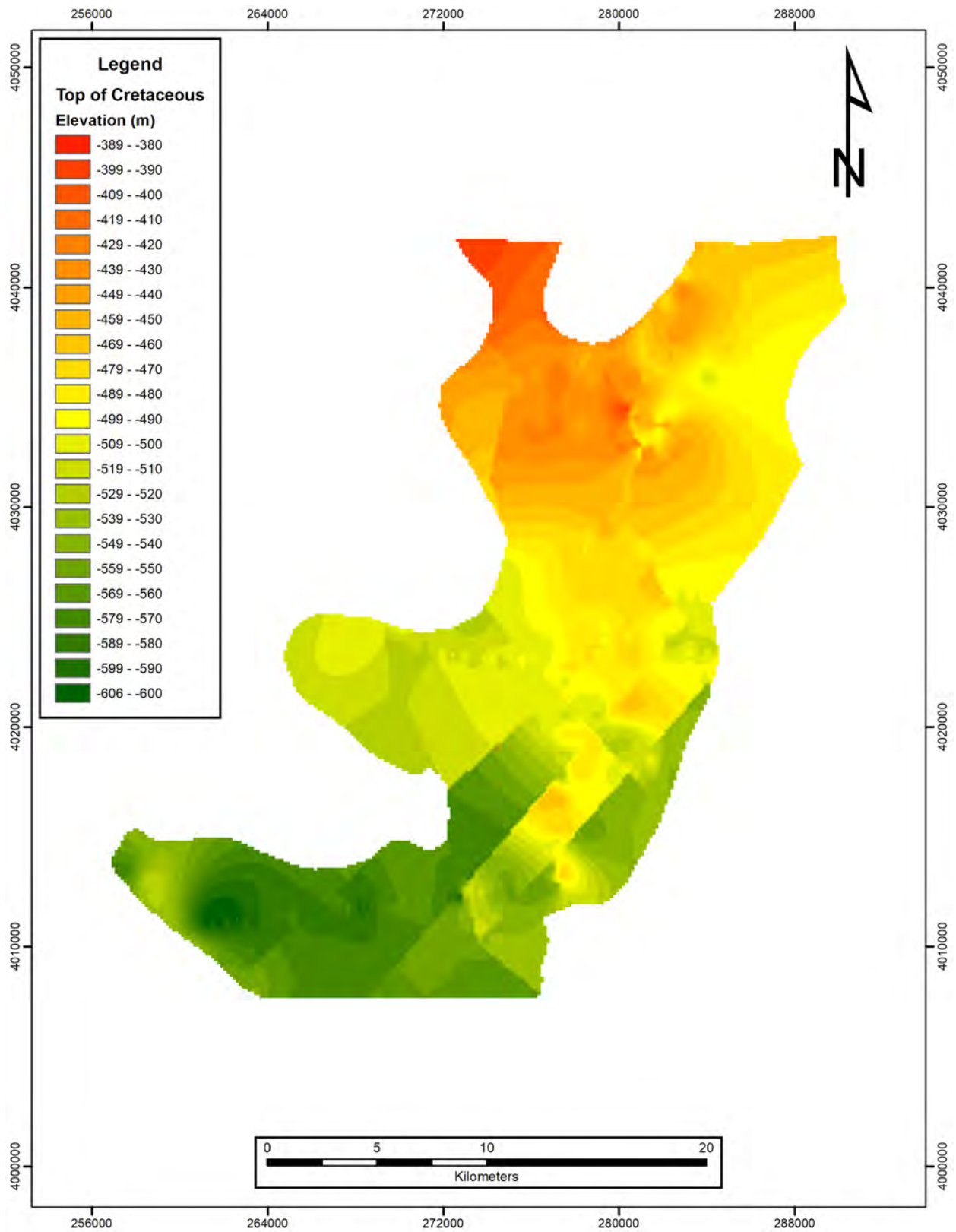
Figure 14B: Structure contour map of the faulted top of the Late Cretaceous strata. Contour interval is 10 m.
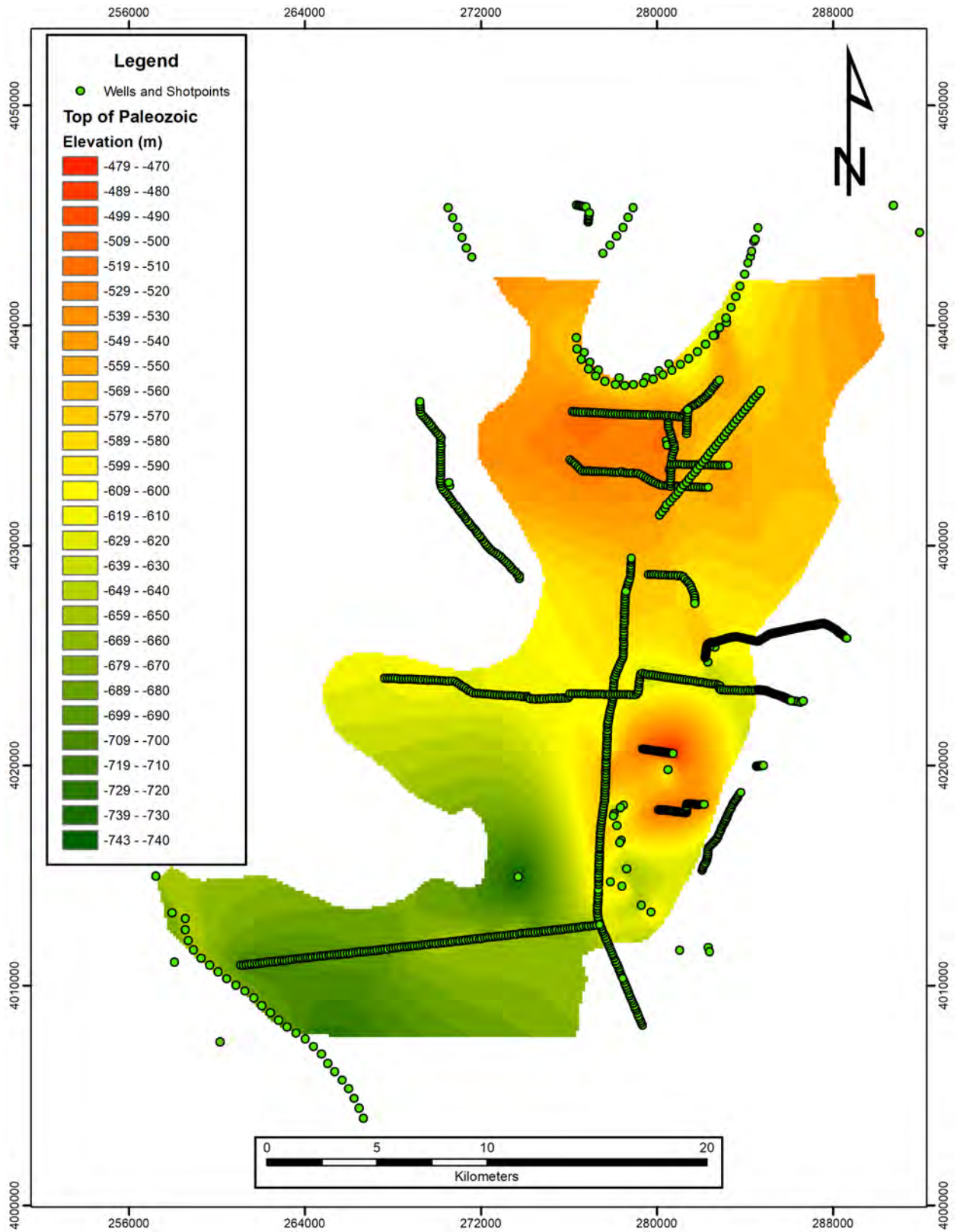
Figure 15A: Structure contour map of the top of the Paleozoic strata with borings and seismic reflection data (dots) used to make the map. Contour interval is 10 m.
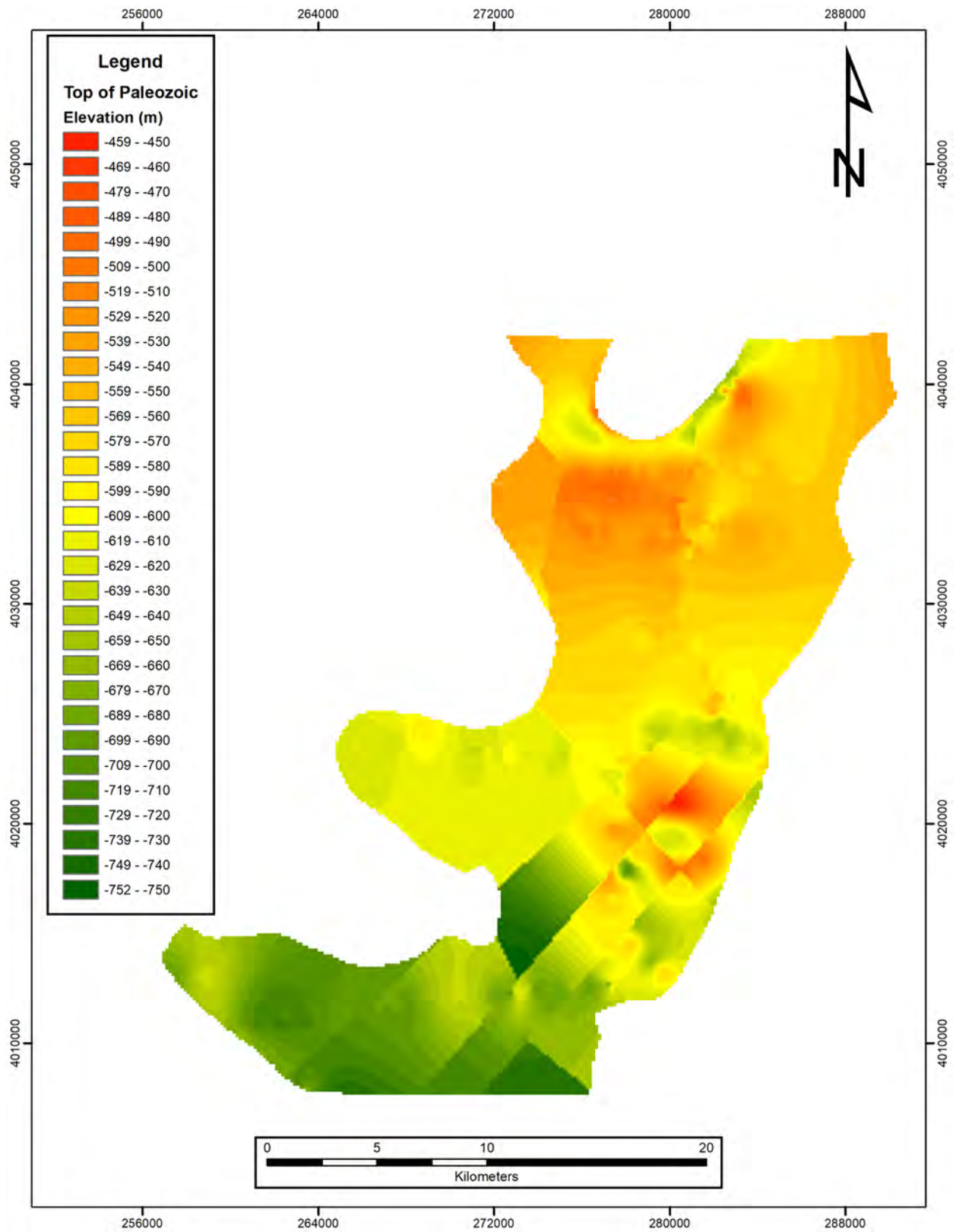
Figure 15B: Structure contour map of the faulted top of the Paleozoic. Contour interval is 10 m.
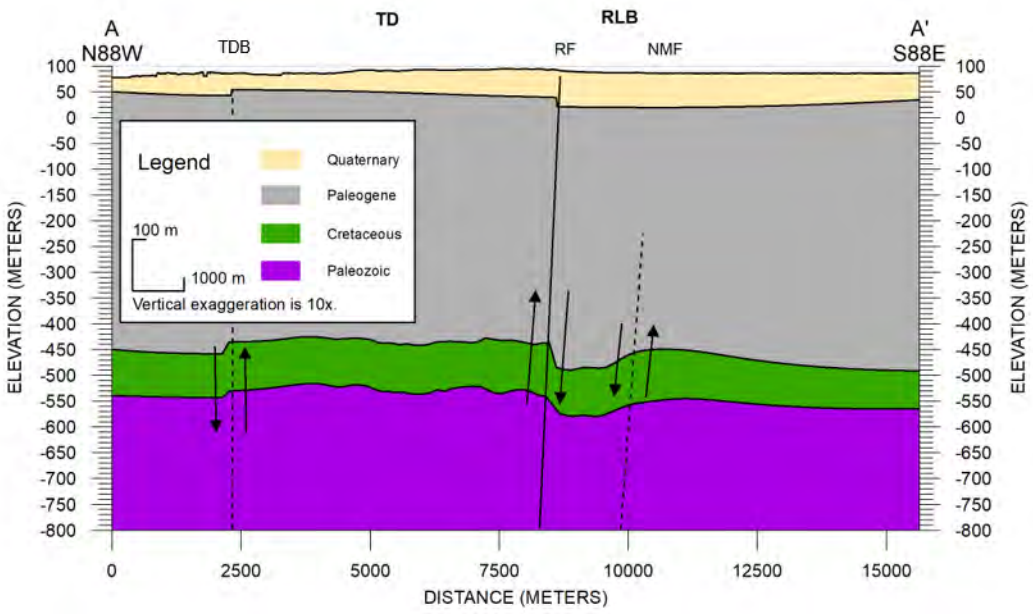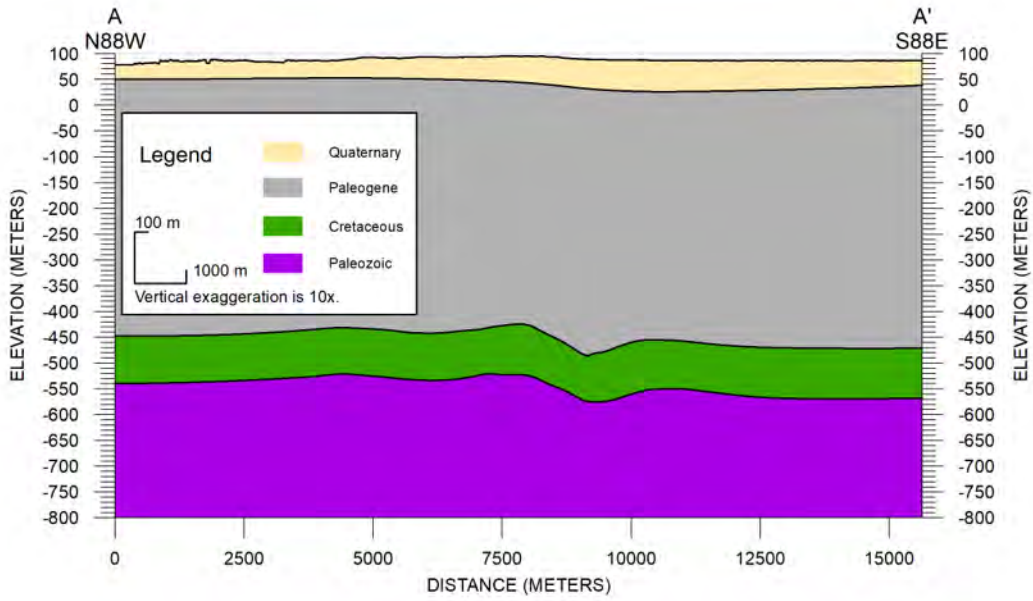
Figure 16: Geologic cross section A-A' located in Figure 3. Upper is un-faulted and lower is faulted. TD - Tiptonville dome; RLB – Reelfoot Lake basin. Vertical exaggeration = 10.
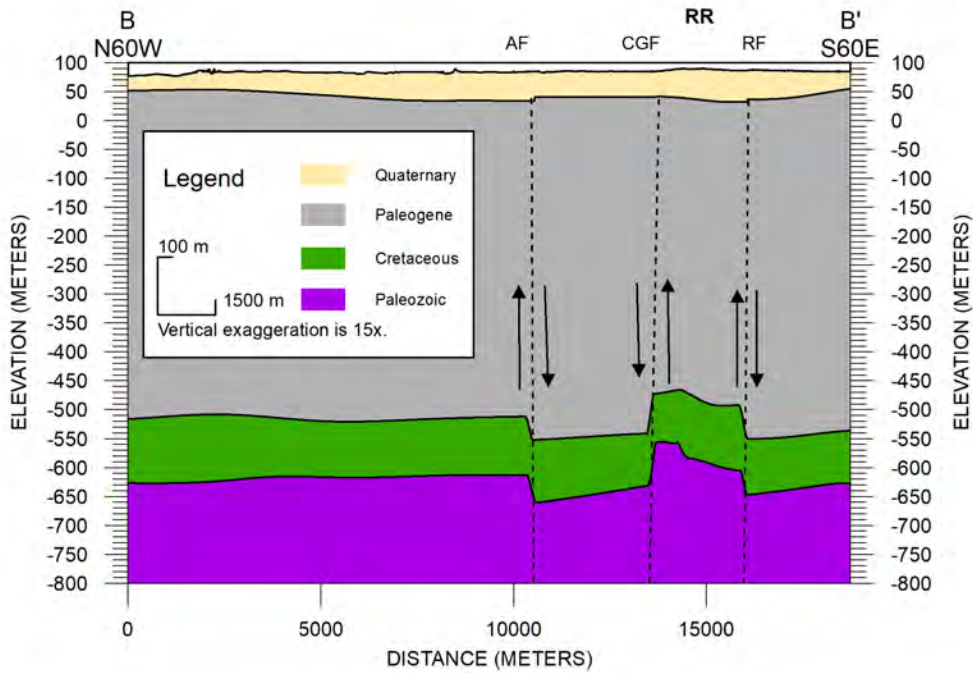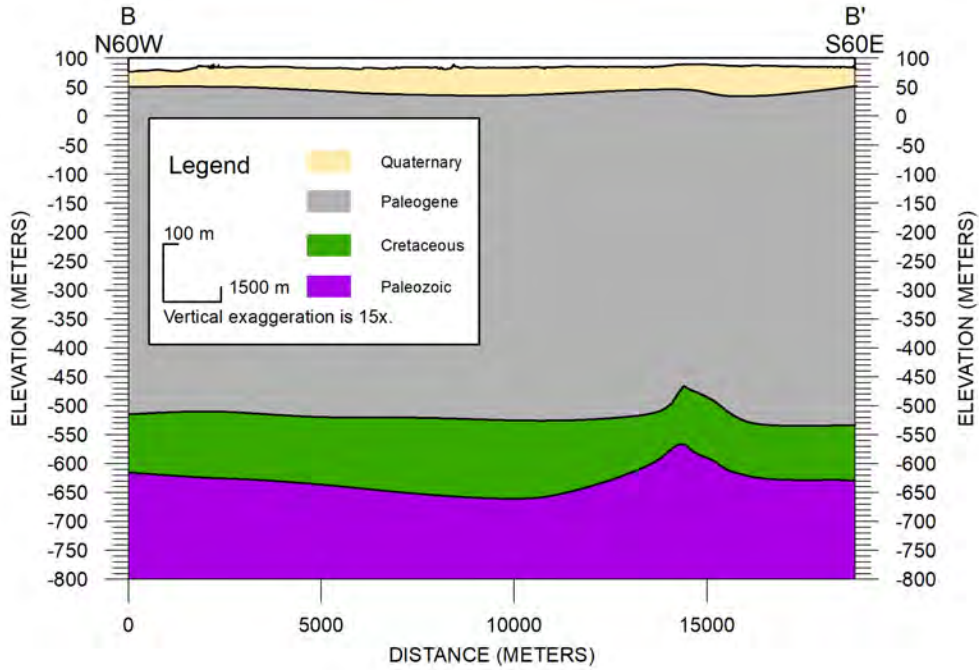
Figure 17: Geologic cross section B-B' located in Figure 3. Upper is un-faulted and lower is faulted. RR – Ridgely ridge. Vertical exaggeration = 16X.
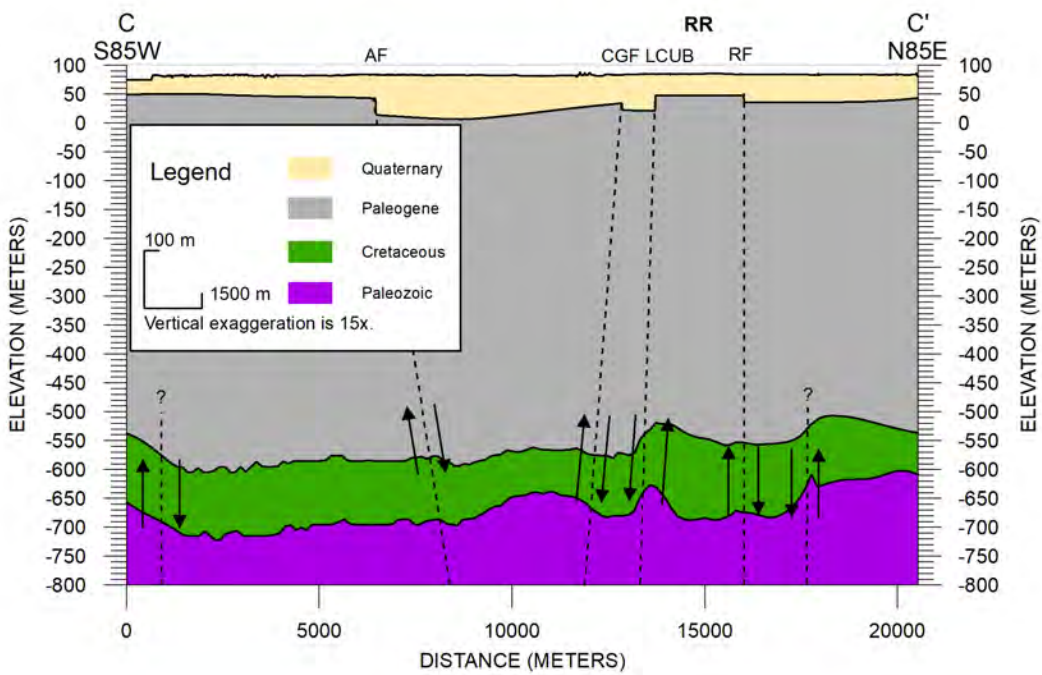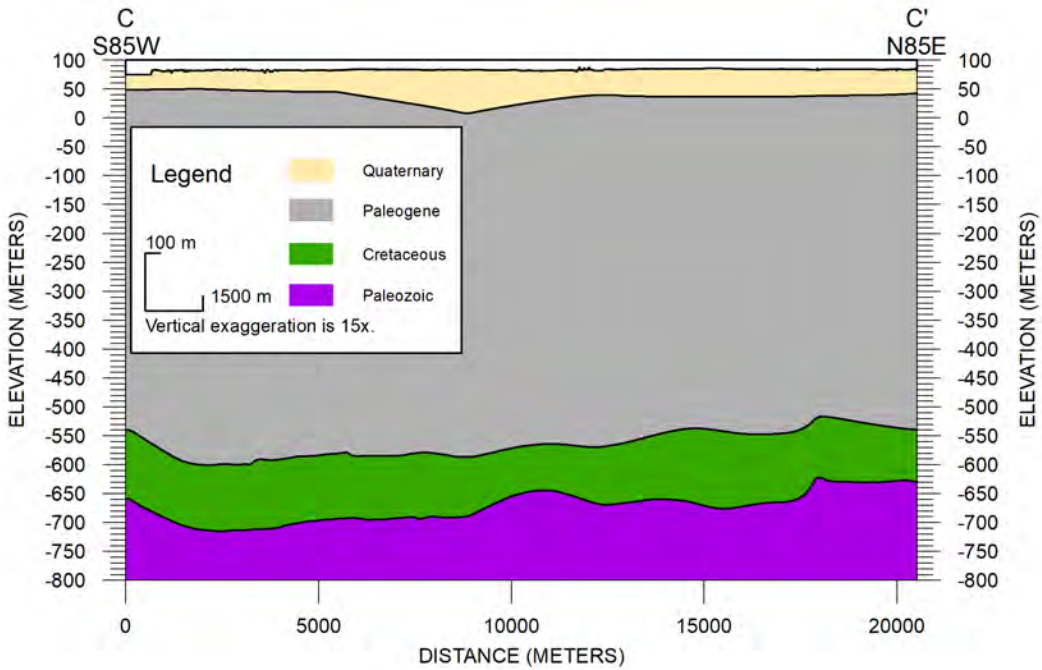
Figure 18: Geologic cross section located in Figure 3. Upper is un-faulted and lower is faulted. RR – Ridgely ridge. Vertical exaggeration = 15.

Geotechnical Model

Introduction

A summary of the geotechnical engineering analysis performed to develop liquefaction probability curves for Lake County is presented in this section. Background information on the subsurface data collection procedures is initially presented followed by a summary of the methodologies used to generate liquefaction probability curves.

Data Collection

Subsurface data that was collected within Lake County consisted of Standard Penetration Test (SPT) resistance or "N-value", shear wave velocity (Vs), Cone Penetration Test (CPT), and groundwater level data. A summary of the procedures used to collect these data is presented next.

<u>SPT data</u>

Soil boring logs that included soil classifications based on the Unified Soil Classification System (USCS) and SPT-N values were obtained from the Memphis District of the U.S. Army Corps of Engineers (USACE), Tennessee Department of Transportation (TDOT), Tennessee Department of Economic & Community Development (TNECD), Construction Materials Laboratory, Inc., and Joel B. Spaulding & Company, Inc. Table 3 shows the total number of soil boring logs that were received from each organization and Figure 18 shows the general locations of all 2,075 soil borings that were obtained.

Table 3: Summary of a total number of borings

Organization	Number of Boring Logs
USACE	2004
Joel B. Spaulding & Company, Inc.	4
Construction Materials Laboratory, Inc.	42
TDOT	10
TNECD	15
Total	2075

The initial soil boring selection screening criteria can be summarized as:
- Borings must extend to a depth of 20 m (66 ft) or greater.
- The borings must include SPT-N values.
- The boring locations must have latitude and longitude coordinates.

The above screening criteria is similar to the screening criteria used in developing the liquefaction probability curves incorporated in the Seismic Hazard Maps for Memphis and

Shelby County (Cramer et al. 2018; Cramer et al. 2015) except that a minimum 66ft (20 m) depth was used instead of 49 ft (15 m) because, as will be described in the Methodologies Used to Develop Liquefaction Probability Curves section, a minimum depth of 66 ft (20 m) of soil data is required to determine the liquefaction probability index.

Figure 19: Geotechnical boring locations.

As shown in Figure 19 and as indicated in Table 4, 859 of the 2,075 borings are located inside Lake County. Additionally, only 189 of the 859 borings within Lake County had some SPT N-values. Unfortunately, a majority of these 189 borings did not meet the minimum desired depth of 66 ft (20 m) nor the borings have N-values at a majority of intervals through the full minimum desired 66 ft (20 m) depth. The procedure to develop liquefaction probability curves requires that N-values be available for a majority of the minimum desired 66 ft (20 m) depth. Only 33 of the 189 soil borings within Lake County had N-values for a majority of the minimum desired 66 ft (20 m) depth. These 33 borings, locations of which are shown in Figure 20, were used in the liquefaction analyses.
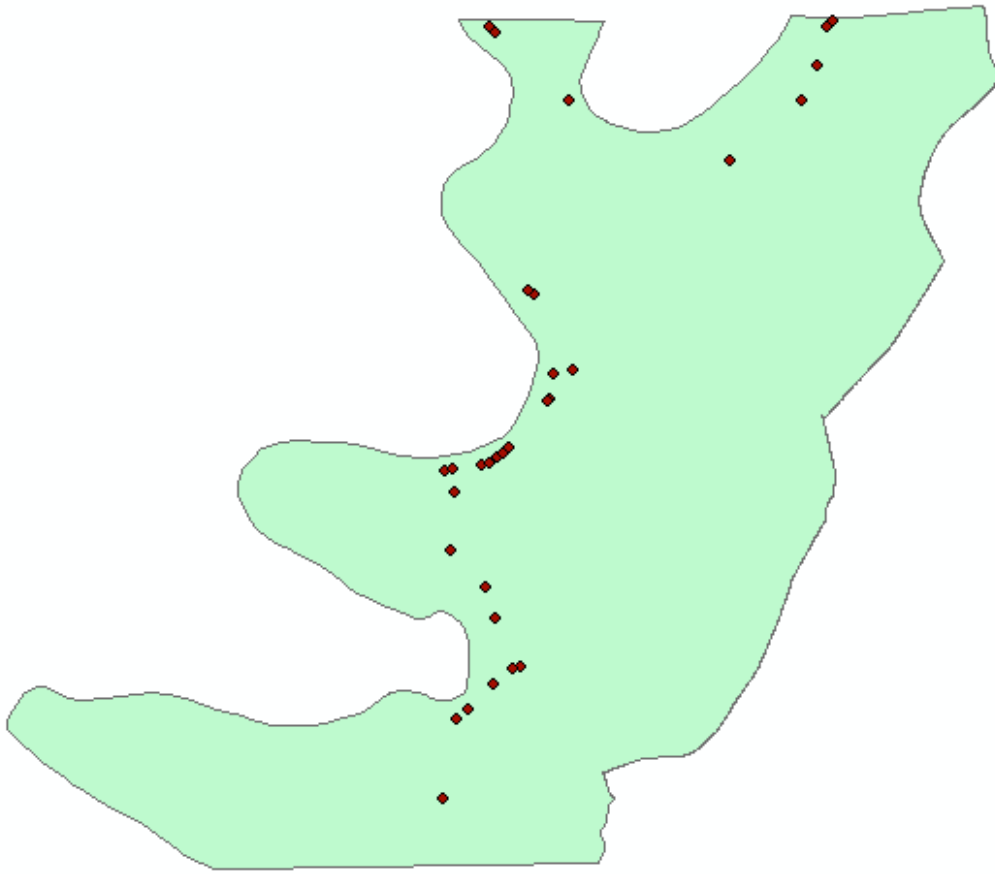
Figure 20: Locations of SPT borings.

Table 4: Summary of the soil borings location and frequency of SPT N-values

Organization	Total Borings	Outside-County	Inside-County	Inside County but No N-values provided	Inside County with some N-values provided	Inside County with many N-values provided & min. 60 ft deep
USACE	2004	1203	801	670	131	33
Construction Materials Laboratory, Inc.	42	9	33	0	33	0
Joel Spaulding & Company, Inc.	4	4	0	0	0	0
TDOT	10	0	10	0	10	0
TNECD	15	0	15	0	15	0
Total	2075	1216	859	670	189	33

Shear Wave Velocity Data

A total of 26 shear wave velocity or Vs profiles were obtained from various studies as shown in Table 5 and Figure 21. Among the 26 Vs profiles, four of those did not have a specific location but all others were located inside Lake County or within a buffer zone defined herein as within 4km (2.5 miles) of the County line. Only one profile (HUD-8) was discarded due to lack of enough data to a depth to 20 m (66 ft.). Thus, a total of 25 Vs profiles were used in the liquefaction analysis.

Table 5: Summary of shear wave velocity profiles

Shear Wave Velocity Data	Total Profiles	Profiles Used in Analysis
HUD	14	13
Finprostats (Cramer 2018)	1	1
Rosenblad (Rosenblad 2007)	2	2
Wynnburg (Pezeshk et al. 1998)	1	1
GaTech (Mayne 2005)	2	2
CUSSO (Woolery et al. 2016)	2	2
OBN (Holzer et al. 2011)	4	4
TOTAL	26	25
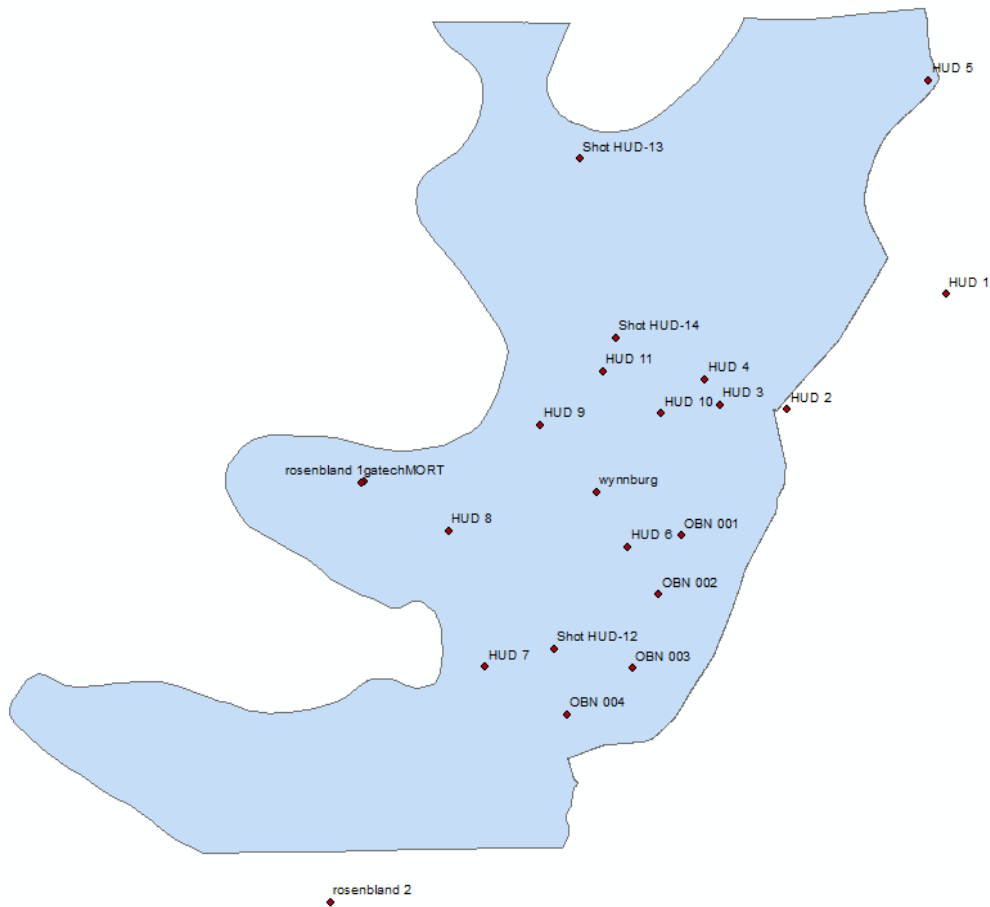
Figure 21: Location of shear wave velocity profiles.

CPT Data

CPT data was available at the USGS website (https://earthquake.usgs.gov/research/cpt/data). The total number of CPT borings within Lake County was only five, which is not sufficient to develop liquefaction probability curves. Thus, liquefaction probability curves were not developed based on CPT data.

Groundwater Data

Holzer et al. (2011) did a study to develop liquefaction probability curves (LPCs) for 14 surficial geologic deposits within the U.S. Holzer's study presented LPCs for three different types of surficial geological deposits in the Mississippi embayment area that included floodplain point bar, abandoned channel, and flood basin. Holzer et al. developed LPCs for each surficial

geologic deposit and for groundwater levels of 1.5 and 5 m. Thus, each geologic deposit was represented by two LPCs, one for each groundwater level, and Holzer et al. developed a total of six LPCs for the three different types of surficial geological deposits located in the Mississippi embayment area. As will be discussed in the Methodologies Used to Develop Liquefaction Probability Curves section, a preliminary LPC for Lake County was developed based on the average of the six LPCs that represents an average groundwater level of 3.25 m, which is the average of groundwater levels 1.5 m and 5 m.

We obtained supplemental groundwater level data from the United States Geological Survey (USGS) groundwater data website (https://maps.waterdata.usgs.gov). Groundwater level data within Lake County was provided by USGS for 15 water wells inside Lake County as shown in Figure 22. Seven of these wells are active, meaning that water levels are currently obtained, and eight are inactive. A total of 30 water level records with readings obtained between 1984 and March 2018 were available at the USGS website. (see Table 6).
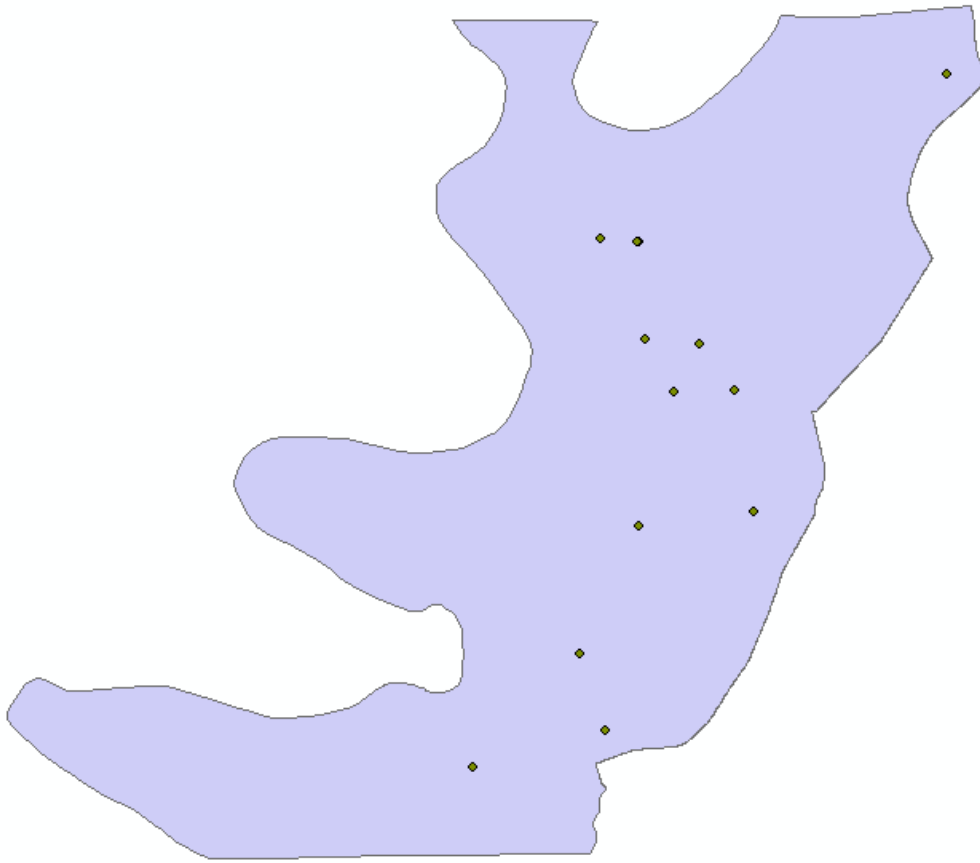
Figure 22: USGS wells within Lake County.

Table 6: Summary for period of record periodic water levels of wells inside the Lake County.

Well NO.	Period of Reading	Level (ft)	Level (m)
G042	7/23/1984	22	6.70
E003	10/7/1985	13.52	4.12
E003	3/14/2007	10.94	3.33
E021	10/7/1985	20.82	6.34
E021	3/14/2007	22.53	6.86
H-5 REELFOOT	7/17/1986	3.62	1.10
H-6	7/23/1986	5.4	1.64
H-7	7/23/1986	5.5	1.67
G040	8/13/1987	29	8.83
G040	5/13/2009	27.55	8.39
G040	6/28/2011	28.62	8.72
G040	5/17/2013	29.58	9.01
G040	6/9/2015	28.61	8.72
G040	4/11/2017	29.17	8.89
C002	Jun-16	4.7	1.43
B002	Jun-16	5.79	1.76
B002	4/3/2018	3.7	1.12
G044	Jun-16	15.4	4.69
G044	4/3/2018	16.15	4.92
E034	Jun-16	5.39	1.64
E034	4/3/2018	3.95	1.20
E035	Jun-16	8	2.43
E035	4/3/2018	6.97	2.12
E036	Jun-16	4.23	1.28
E036	4/3/2018	3.28	0.99
G043	Jun-16	20.38	6.21
G043	3/1/2018	23.76	7.24
G043	4/3/2018	22.47	6.84
G045	3/1/2018	22.03	6.71
G045	4/3/2018	20.77	6.33

We have determined an approximate average water level for Lake County based on the records of these 15 wells using three different methods:

- Based on the average of readings in each year. Because the wells had readings in different years, we classified the well readings based on the year of reading and got an average of all readings in a specific year. The overall average was calculated based on the average of each specific year and used as a single GWL in the analysis.
- Based on the average of all readings. In this method, the average of all 30 readings was computed and used as a single groundwater level in the analysis.

- Based on the average of readings of each well. Some of the wells had multiple readings in different years, in this method, the average of all readings of each well was calculated and used as a single groundwater level for each well. The overall average groundwater level was computed based on the single average level of each well.

Table 7 shows the results of the three methods.

Table 7: Groundwater level estimation using USGS data.

Water level based on the average of each year (meter)	6.5
Water level based on the average of all readings (meter)	4.7
Water level based on the average of each well (meter)	3.7

We also reviewed various USGS reports that were suggested by representatives of the USGS Lower Mississippi Gulf Water Science Center (Schrader 2013; Clark et al. 2011; Waldron et al. 2011; Hosman et al. 1968). However, these reports did not provide specific groundwater level data in Lake County.

Additional groundwater level data of Lake County was provided by a groundwater elevation contour map developed by Schrader (2007). Schrader used the groundwater flow model of the northern Mississippi embayment which was developed by the U.S. Geological Survey Office of Ground-Water Resources Program as part of the Mississippi Embayment Regional Aquifer Study (MERAS). The groundwater elevation contour map covers approximately 70,000 square miles and includes Alabama, Arkansas, Illinois, Kentucky, Louisiana, Mississippi, Missouri, and Tennessee. The map is based on data from 748 water level measurements obtained in spring 2007 from 309 wells in Arkansas, 7 wells in Kentucky, 116 wells in Louisiana, 150 wells in Mississippi, 6 wells in Missouri, and 160 wells in Tennessee. Figure 22 shows the groundwater elevation contour lines, which are based on the National Geodetic Vertical Datum (NGVD) of 1929, that extend through Lake County. As shown in Figure 23, the groundwater levels in Lake County are predominantly between elevations 260 and 280 ft, a difference of 20 ft.

Figure 23: USGS groundwater level contour map (Schrader 2007).

Using the USGS wells coordinates, we located the wells on the USGS contour map and the wells groundwater contour elevations are in agreement with the well groundwater data shown in Table 7.

Figure 24 shows the groundwater level contour map we generated from the Schrader (2007) map. We utilized ArcMap to project the groundwater elevation contour map on a shapefile boundary of Lake County and the two contour lines of 260 ft. and 280 ft. were digitized and located on the Lake County shapefile. Using ArcGIS, the groundwater elevation contour map for the entire County was generated. Then we located the summarized SPT boring logs and shear wave velocity profiles on the groundwater contour map shown in Figure 24 and using the ArcMap interpolation tool, groundwater level was interpolated for all borings and profiles. Because the SPT and V database did not have ground surface elevations at each boring and profile locations, ground surface elevation was estimated using Light Detection and Ranging (LiDAR) map which we received from the geology team in ArcGIS format. The SPT borings and Vs profiles were located on LiDAR map and the ground surface elevations were interpolated for all borings and profiles. The groundwater depth of each profile was computed by subtracting the groundwater elevation from the ground surface elevation.

Figure 24: Groundwater level contour map for Lake County (red points represent soil borings and green points represent shear wave velocity profile locations).

Methodologies Used to Develop Liquefaction Probability Curves

We used the same general procedure to develop LPCs that Rix and Romero-Hudock (2006) and Cramer et al. (2015, 2018) used to develop liquefaction probability curves for each primary surficial geologic unit in Shelby County, TN. The procedure consists of (i) calculating the factor of safety (FS) against liquefaction at a given depth in the soil profile of each soil boring using the simplified procedure (Seed and Idriss, 1971); (ii) calculating liquefaction potential index (LPI) of each soil boring location using the Iwasaki et al. (1978, 1982) method; (iii) developing liquefaction probability curves (LPCs) for the probability of exceeding LPI of 5 and 15 for each primary surficial geologic unit. We utilized this three-step procedure to develop the LPCs for Lake County.

We developed liquefaction probability curves (LPCs) for the Lake County area based on the liquefaction probability curves for the Mississippi embayment from Holzer's study (2011), SPT-N values, and shear wave velocity (Vs) profiles. A summary of these three methods is subsequently provided and a comparison of LPCs obtained from these three methods is made.

<u>Preliminary Liquefaction Probability Curves Based on Holzer's Study</u>

Holzer developed LPCs for 14 different types of surficial geologic units based on the results of 927 CPT data profiles. However, the study only included LPCs for each of three surficial geologic units (point bar, abandoned channel, and flood basin) based on 150 CPT profiles within the Mississippi embayment and we only utilized Mississippi embayment LPCs to estimate an LPC for Lake County because Lake County is within the Mississippi embayment. For each geologic unit, Holzer developed an LPC for each of two different groundwater levels of 1.5 and 5 meters for LPI>5. Thus, Holzer developed six LPCs for the Mississippi embayment and these LPCs are shown in Figure 25.
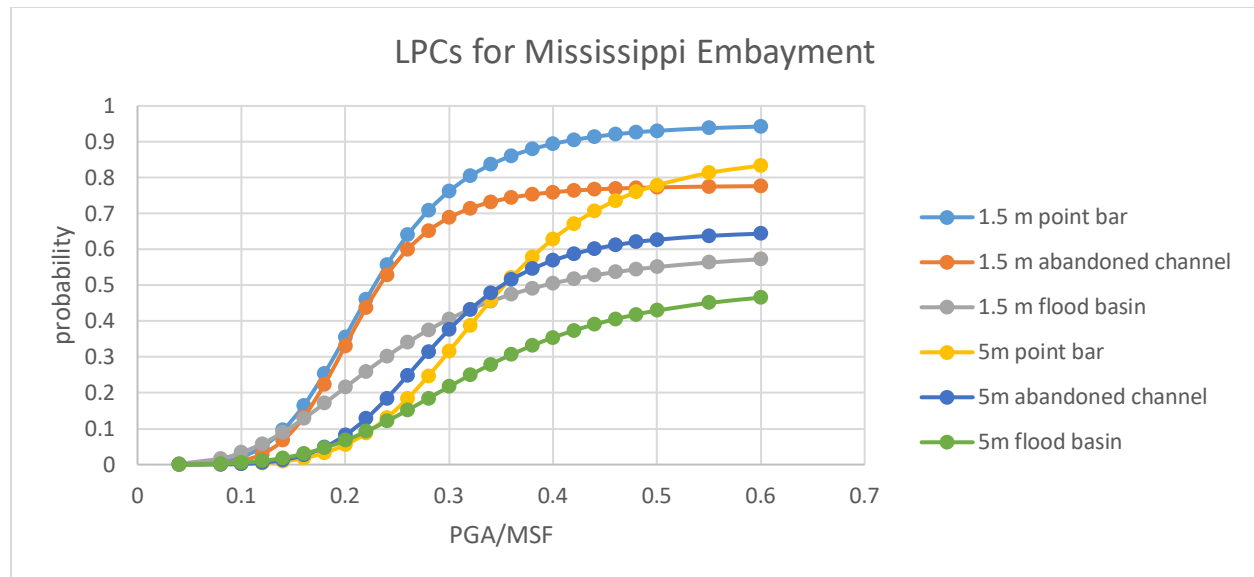
Figure 25: LPCs for LPI>15 for Mississippi embayment from Holzer's study (2011).

Lake County is adjacent to the Mississippi River and may have all three surficial geologic units that Holzer considered in the development of the Mississippi embayment LPCs. The project team required LPC curve data by March 2018 to develop the liquefaction hazard maps by the May 2018 due date. However, since the actual project started about three months after the planned start date, the geotechnical data collection including groundwater level data was not yet completed to develop LPCs by the March deadline. Therefore, an LPC curve based on the average of all six curves shown in Figure 25 that includes all three surficial geologic units and both groundwater levels of 1.5 and 5 m was developed based on the average of all six curves. The resulting average LPC curve is shown in Figure 26 and is representative of an average groundwater level of 3.25 m, which is the average of the 1.5 m and 5 m levels Holzer

considered. This LPC is also referred to has the preliminary LPC curve herein and is the curve used to develop the liquefaction hazard maps.

**Preliminary LPC based on Holzer's Study for GW=3.25m**
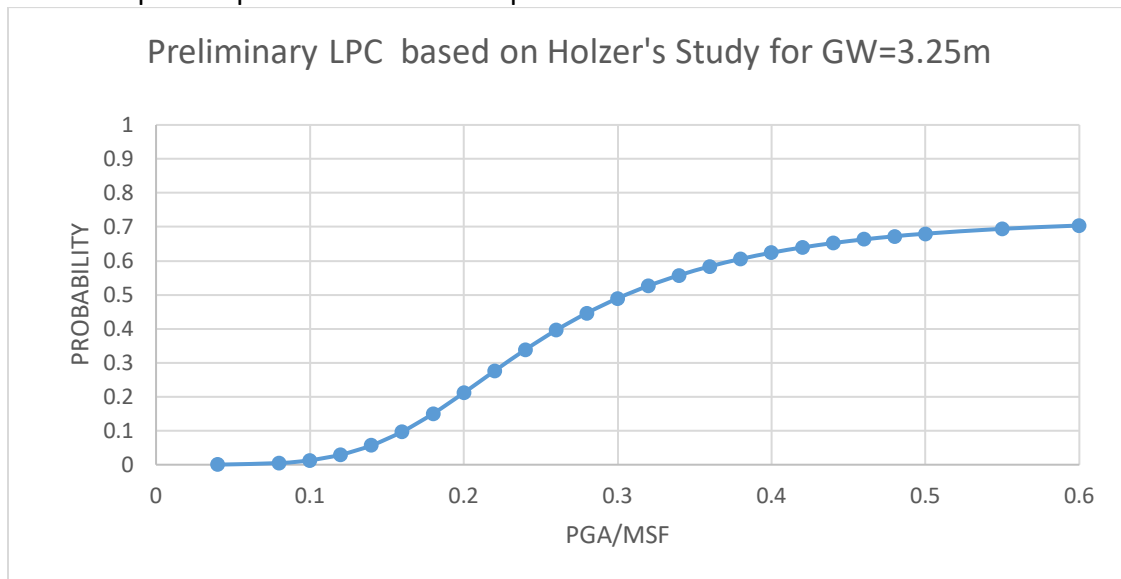
Figure 26: Liquefaction Probability Curve from Holzer's Study.

<u>Liquefaction Probability Curves Based on the Standard Penetration Test (SPT)</u>

As noted in the Data Collection section, only 33 soil borings of the 2,075 collected had N-values for a majority of the minimum desired depth of 66 ft. In an attempt to utilize more of the 2,075 boring logs collected, we developed a statistical model using regression analysis on 33 SPT borings inside Lake County with many N-values in which the SPT N-value was considered as a dependent variable and fines content and soil layer depth were entered as independent variables. Equation 1 provides the obtained logarithmic relationship from the regression analysis. The R-squared of 0.5 was obtained, which indicate that the regression equation does not provide a strong correlation between N value and the fine content/depth. Thus, Equation 1 was not utilized to complete other SPT borings to a minimum depth of 66ft. Therefore, only the 33 soil borings indicated in Table 2 as being inside County with many N-values provided to a minimum depth of 66 ft were used in developing LPCs for Lake County.

$$\log N = 1.33 + (0.00388 DEPTH) - (0.00935 FC) \qquad (1)$$

Missing N-values for any depth at a given boring location was estimated by using the same N-value for a given N-value above or below the depth of the missing N-value if the overlying and underlying soil had the same soil classification. If the soil layers above and below the layer with the missing N-value did not have the same classification or did not have an N-value in a given boring, the N-value was extracted from another boring that had the same classification and the same depth as the classification and depth of the missing N-value.

We used the same general procedure to develop LPCs based on SPT N-vales that Rix and Romero-Hudock (2006) and Cramer et al. (2015, 2018) used to develop LPCs for Shelby County,

TN. Therefore, only the changes made to the Shelby County map procedure are summarized herein.

We conducted a comprehensive literature search of the history of the simplified liquefaction prediction method (Boulanger and Idriss 2014; Idriss and Boulanger 2008; Boulanger and Idriss 2007; Idriss 1999; NCEER/NSF 1998; Andrus and Stokoe 1997; NCEER 1996; Arango 1996; Kayen et al. 1992; Golesorkhi 1989; Liao and Whitman 1986; Seed et al. 1985; Seed et al. 1984; Seed and Idriss 1982; Iwasaki et al. 1982; Iwasaki et al. 1978; Seed and Idriss 1971; Seed and Idriss 1967), which is the procedure used for the Shelby County maps, as well as current suggested changes to the simplified liquefaction prediction method (Boulanger and Idriss 2014; Idriss and Boulanger 2008; Boulanger and Idriss 2007; Idriss 1999) including the recent State of the Art and Practice in the Assessment of Earthquake-Induced Soil Liquefaction and Its Consequences (The National Academies Press 2016). A summary of the changes we made to the Shelby County simplified liquefaction prediction method based on the findings of the literature is presented next.

The stress reduction coefficient (r_d) of Idriss (1999), provided by Equations 2 through 4, was used instead of the Liao and Whitman (1986) r_d because the effect of earthquake magnitude was not considered in Liao and Whitman equations, so we used the revised relationships presented by Idriss (1999) since it considers the effect of M_w on r_d and it was developed based on the original simplified method of Seed and Idriss (1971).

$$r_d = \exp\left(\alpha(z) + \beta(z)M_W\right) \tag{2}$$

$$\alpha(z) = -1.012 - 1.12\sin(\frac{z}{11.7} + 5.133) \tag{3}$$

$$\beta(z) = 0.106 + 0.118\sin(\frac{z}{11.3)} + 5.142) \tag{4}$$

The magnitude scaling factor (*MSF)* of Idriss (1999) provided by Equations 5 through 6 was used instead of the one used in the Shelby County maps (Equation 7) because according to the State of the Art and Practice in the Assessment of Earthquake Induced Soil Liquefaction and Its Consequences by The National Academies Press (2016), it is recommended that only the specific adjustment factors used to develop a specific liquefaction potential relationship be used for that relationship, so we utilized the revised MSF relationship by Idriss (1999), and this relationship was developed based on the original simplified method of Seed and Idriss (1971) (Equations 5 and 6).

$$MSF = 6.9\exp\left(\frac{-M_W}{4}\right) - 0.06, M_W > 5.2 \tag{5}$$

$$MSF = 1.82, M_W \leq 5.2 \qquad\qquad (6)$$

$$MSF = 10^{2.24}/M_W^{2.56} \qquad\qquad (7)$$

Using MATLAB, we have written a code to calculate the liquefaction potential index (LPI) at each soil boring location. After the determination of LPI at each boring location, the distribution of LPI was determined based on estimated groundwater levels at each boring location. The LPI was determined at each soil boring location for a_{max} of 0.1, 0.2, 0.3, 0.4, and 0.5g and earthquake magnitude (M_w) of 6, 6.5, 7, 7.5, and 8. The distribution of LPI was determined for each of the 25 possible combinations of a_{max} and M_w using the same procedure that Rix and Romero-Hudock (2006) and Cramer et al. (2015, 2018) used to determine the distribution of LPI for Shelby County. Additionally, we utilized the same procedure used by Rix and Romero-Hudock (2006) and Cramer et al. (2015, 2018) to calculate the probability of exceeding LPI values of 5 and 15, which are the lower bounds of "moderate" and "major" liquefaction, respectively, based on the results of Iwasaki et al. (1978,1982) and Toprak and Holzer (2003). Figures 26 and 27 show the LPCs for P[LPI>5] and P[LPI>15], respectively.
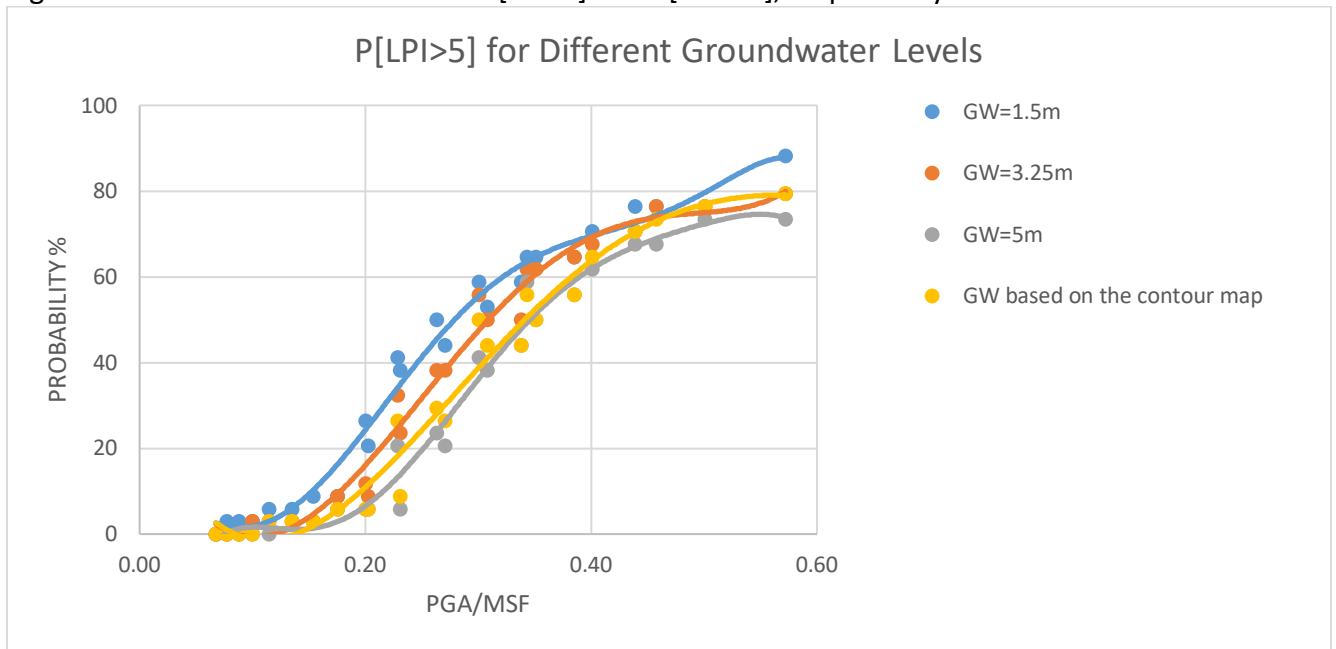
Figure 27: LPCs from SPT data for LPI>5.
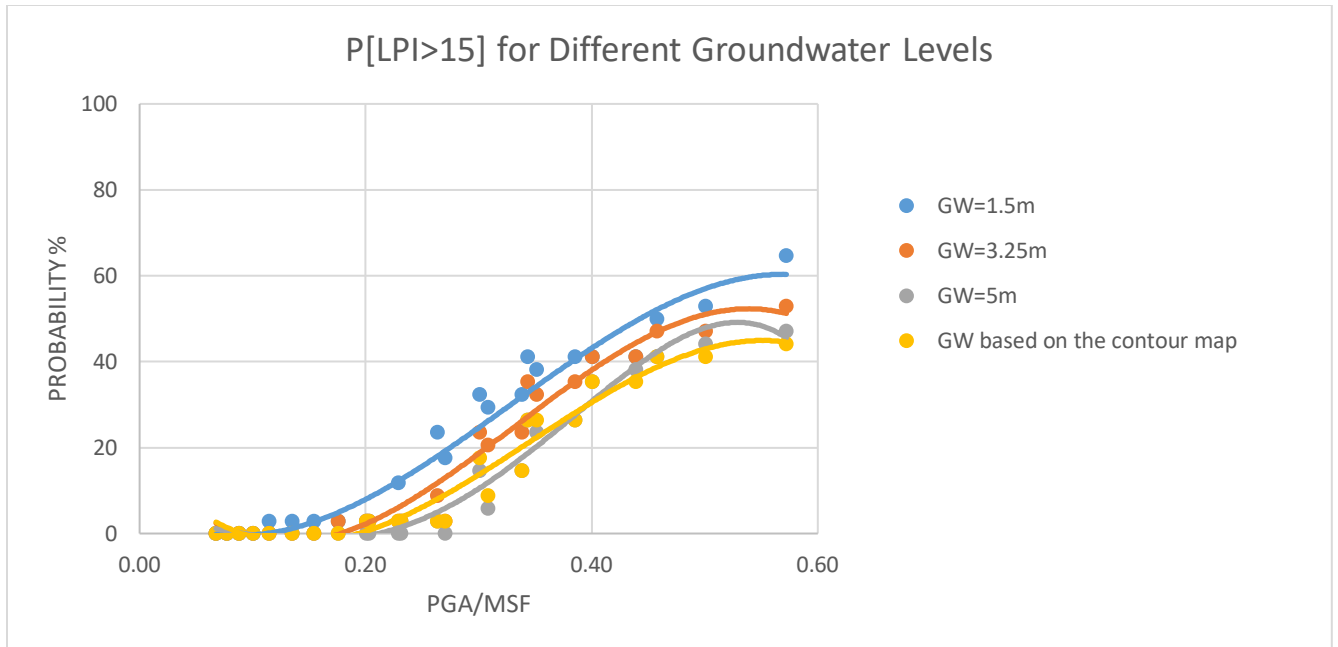
Figure 28: LPCs from SPT data for LPI>15.

As shown in Figures 27 and 28, one LPC curve was determined for each groundwater level we considered in the analysis. The groundwater levels of 1.5 m and 5 m was analyzed because these are the groundwater levels Holzer (2011) used in his study of the Mississippi embayment area and to compare with Holzer's LPCs in Figure 25. The groundwater level of 3.25 m represents the average of Holzer's groundwater levels of 1.5 m and 5 m to compare with the LPC we estimated in Figure 26. In Figures 27 and 28, GW represents the LPC obtained using the GWL contour map in Figure 24.

The LPCs for groundwater levels of 1.5, 3.25, and 5 m in Figures 27 and 28 indicate a higher probability of exceeding an LPI of 5 or 15 with a decrease in groundwater level depth, which is in agreement with the Shelby County maps (Cramer et al. 2015, 2018). The LPC shown in Figure 27 for P[LPI>5] and for groundwater levels obtained from the contour map of Figure 24 is between the 3.25 m and 5 m LPCs because the average groundwater depth at the boring locations is 4.3 m except at higher PGA/MSF ratios of about 0.45 where the LPC obtained from the contour map exceeds the LPC at groundwater level of 3.25 m.

The LPC shown in Figure 28 for P[LPI>15] and for groundwater levels obtained from the contour map of Figure 24 is also between the 3.25 m and 5 m LPCs because the average groundwater depth at the boring locations is 4.3 m except at higher PGA/MSF ratios of about 0.40 where the LPC obtained from the contour map is less than the LPC at groundwater level of 5 m. The groundwater levels obtained from the contour map of Figure 24 may be a better representation of groundwater levels within Lake County than the assumptions of 1.5, 3.25, and 5 m. Therefore, the LPC based groundwater levels obtained from the contour map is recommended for use in future hazard maps. The LPC curve at groundwater level used at 3.25

m utilized in the initial Lake County Hazard maps will yield a slightly larger probability of LPI exceedance and is thus slightly more conservative.

Liquefaction Probability Curves Based on the Shear Wave Velocity (Vs)

Another method used to develop LPCs for Lake County was using Vs profile data. As described in the Shear Wave Velocity Data section, we incorporated 25 Vs profiles in the liquefaction analysis.

To compute the factor of safety against liquefaction, we used the simplified method relationship of Seed and Idriss (1971) to determine the factor of safety (FS) with depth within the Vs profile location that is provided by Equation 8:

$$FS = \frac{CRR_{7.5}}{CSR} MSF \tag{8}$$

where,
CRR7.5 = Cyclic resistance ratio for a magnitude (Mw)=7.5 earthquake,
CSR = Cyclic stress ratio, and
MSF = Magnitude scaling factor that corrects the analysis for earthquake magnitudes other than 7.5. Used the revised relationship by Idriss (1999), (Equations 5 and 6).

CRR represents the capacity of the soil to resist liquefaction and CSR represents the earthquake-induced dynamic stress exerted on the soil. In the above equation, liquefaction is expected if the factor of safety is less than 1, i.e., at depths where the earthquake-induced dynamic stress exceeds the resistance of the soil against liquefaction.

Andrus and Stokoe (1999) utilized data from more than 20 earthquakes and 70 Vs measurement profiles and developed a relationship for evaluating CRR based on Vs data provided by Equation 9:

$$CRR_{7.5} = \left\{ \left(a \frac{V_{s1}}{100} \right)^2 + b \left(\frac{1}{c - V_{s1}} - \frac{1}{c} \right) \right\} \tag{9}$$

where,
a, b, c=curve fitting parameters
- a=0.022
- b=2.8
- C=200-215 m/s, depending on fines content (FC). The following values of C were assumed:
  - C=215 m/s   FC≤ 5%
  - C=215-0.5(FC-5) m/s   5%< FC < 35%
  - C=200 m/s   FC≥ 35%

$V_{s1} = V_s \left(\frac{P_a}{\sigma'_v} \right)^{0.25}$ (Sykora 1987; Robertson et al. 1992) is the shear wave velocity corrected for effective overburden stress (σ'_v) effects and P_a is atmospheric pressure, which is 100 kPa.

Vs profile data that we obtained did not include results from soil boring logs that would provide Unified Soil Classification System (USCS) classifications of subsurface soil layers that are needed to estimate FC of soil layers within the Vs profile. An estimate of FC is required to estimate C. Andrus (1999) recommends that FC ≤ 5% be assumed to obtain C, i.e., C=215 m/s. We utilized the 3-D geology map shown in Figure 29 to identify potential clayey soil layers at each Vs profile location to consider those layers as non-liquefiable soil layers and the factor of safety for clayey layers was forced to one.
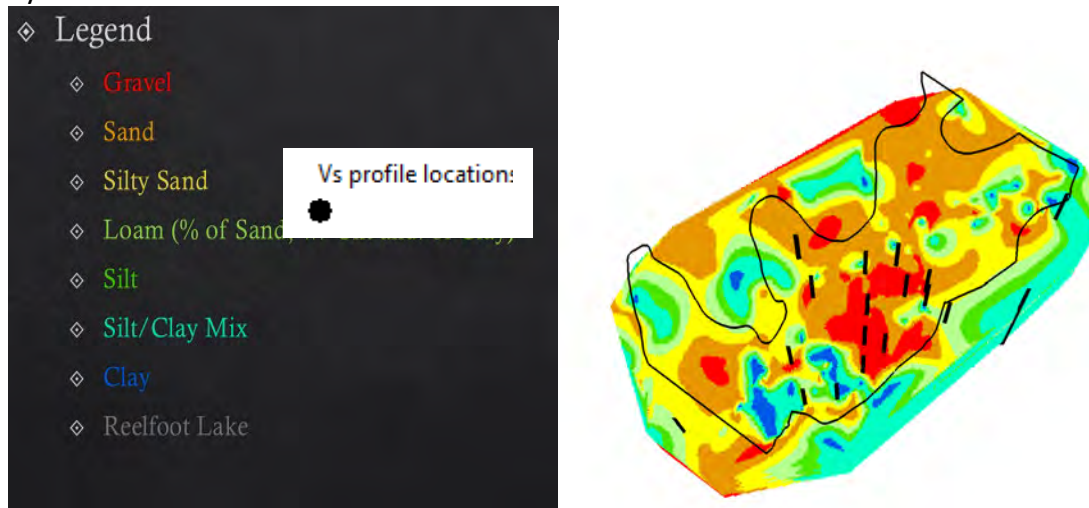
Figure 29: 3-D geology map with Vs profile locations.

Unit weights of the soil layers at the Vs profile locations was also not available with the Vs profile data we obtained. Soil unit weights are needed to estimate σ'_v. Table 8 provides a summary of empirical relationships available to estimate soil unit weight using Vs. The relationship provided by Mayne (2001) was used to estimate unit weights of the soils with depth using Vs profiles we obtained.

Table 8: Empirical relationships to compute the unit weight of soil (Moon and Ku 2016).

Empirical relationships	References
$\gamma_t \ (kN/m^3) = 30.4 \cdot PI^{-0.174}$	Mayne & Peuchen (2013)
$\gamma_t \ (kN/m^3) = 6.87(V_s \ m/s)^{0.227}/(\sigma'_{vo} \ kPa)^{0.057}$	Burns & Mayne (1996)
$\gamma_t \ (kN/m^3) = 8.32log(V_s \ m/s) - 1.61log(z \ m)$	Mayne (2001)
$\gamma_t \ (kN/m^3) = 4.17ln(V_{s1} \ m/s) - 4.03$	Mayne (2007a)

To calculate the cyclic resistance ratio of shear wave velocity profiles, we used the simplified method (Seed and Idriss, 1971), and for the stress reduction factor, we used the revised equation by Idriss (1999).

CSR was obtained using the Seed and Idriss (1971) relationship provided by Equation 10, r_d was estimated using Equations 2 through 4.

$$CSR = \frac{\tau_{av}}{\sigma'_{v0}} = 0.65(\frac{a_{max}}{g})(\frac{\sigma_{v0}}{\sigma'_{v0}})r_d \qquad (10)$$

$CRR_{7.5}$, CSR, and FS were estimated for each 0.5m depth interval up to a depth of 20m at each Vs profile location. Then the same procedure described in the Liquefaction Probability Curves Based on Standard Penetration Test (SPT) section of this report was used to obtain LPCs at groundwater levels of 1.5, 3.25, and 5 m as well as with the groundwater level contour map of Figure 24. Figures 30 and 31 show the LPCs for P[LPI>5] and P[LPI>15], respectively.

As shown in Figures 30 and 31, one LPC curve was determined for each groundwater level we considered in the analysis. The groundwater levels of 1.5 m and 5 m was analyzed because these are the groundwater levels Holzer (2011) used in his study of the Mississippi embayment area and to compare with Holzer's LPCs in Figure 25. The groundwater level of 5 m represents the average of Holzer's groundwater levels of 1.5 m and 5 m and we used this LPC to compare with the LPC we estimated in Figure 26. In Figures 30 and 31, GW based on the contour map represents the LPC obtained using the GWL contour map in Figure 24.
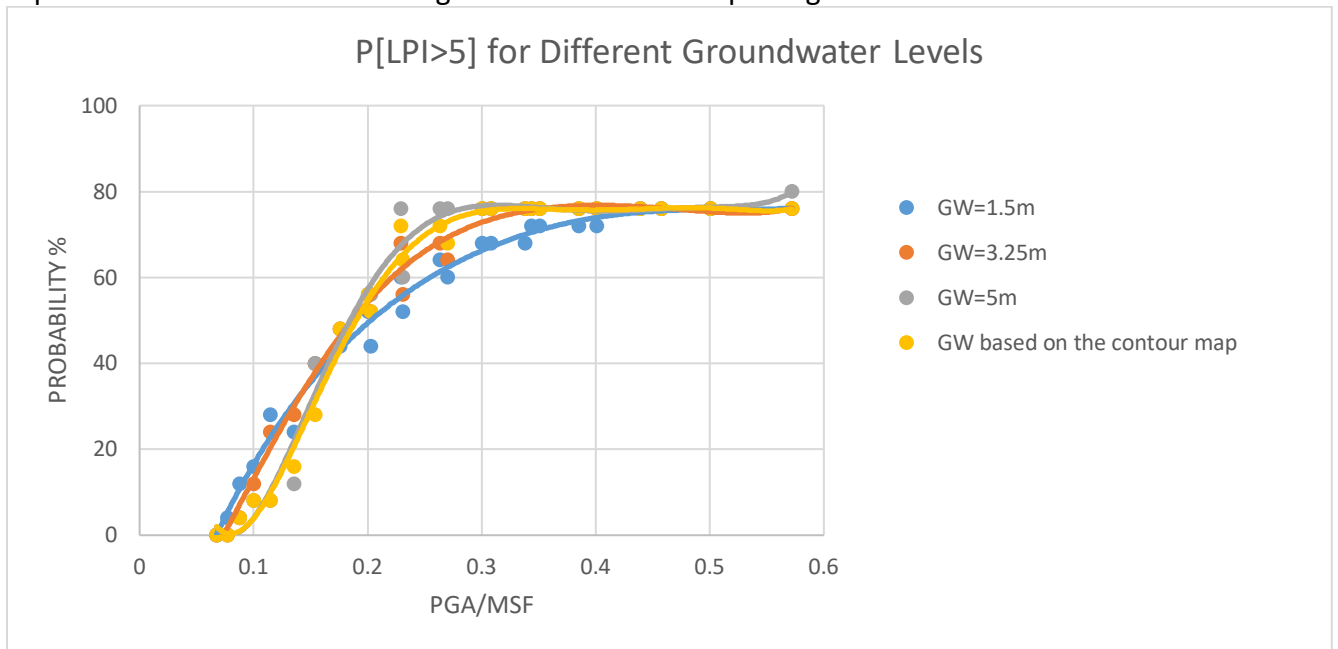
Figure 30: LPCs from shear wave velocity data for LPI>5.
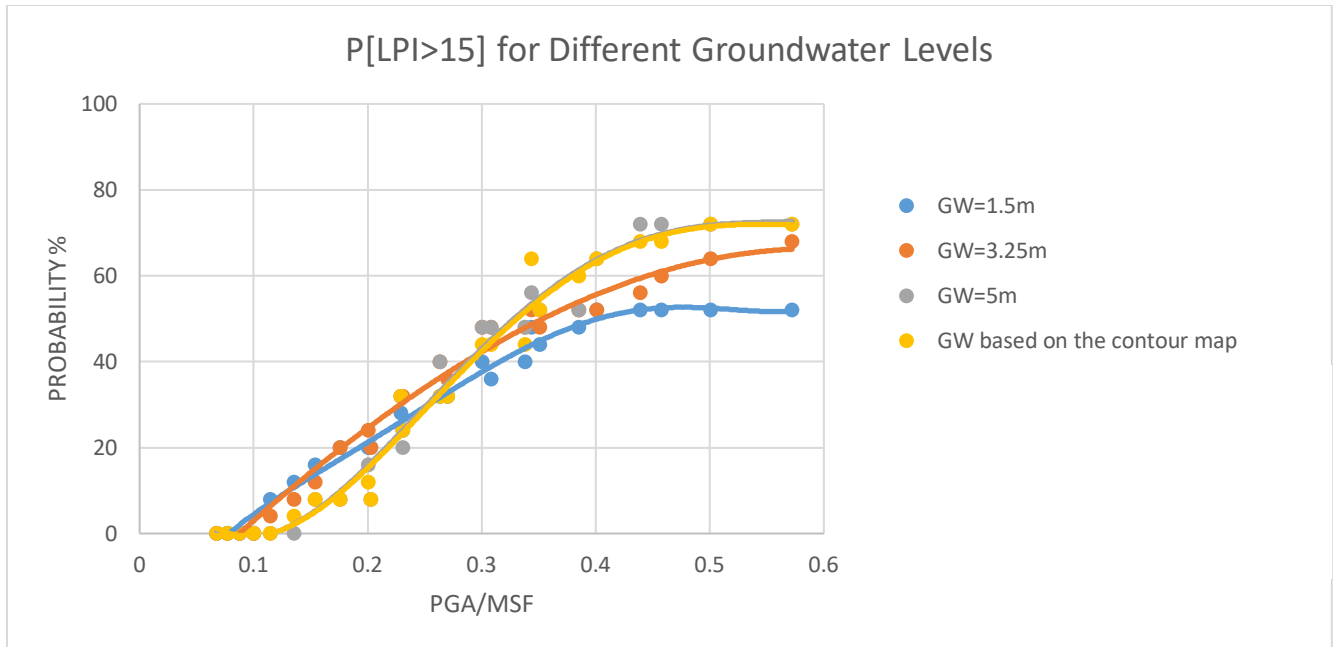
Figure 31: LPCs from shear wave velocity data for LPI>15.

The LPCs for groundwater levels of 1.5, 3.25, and 5 m in Figures 30 and 31 indicate a higher probability of exceeding an LPI of 5 or 15 with an increase in groundwater level depth, which is not in agreement with the Shelby County maps (Cramer et al. 2015, 2018). The probability of liquefaction should decrease with an increase in groundwater level depth. The limitation of developing LPCs using the Vs profile data we obtained is that soil boring data with USCS classifications were not available.

At P[LPI>5] the LPC obtained with the groundwater levels at each Vs profile using the contour map of Figure 24 yielded lower probabilities than groundwater levels of 1.5, 3.25, and 5 m at lower PGA/MSF ratios of less than about 0.15 and higher probabilities nearly the same as the 5 m water level at higher PGA/MSF ratios of about 0.15. At P[LPI>15] the LPC obtained with the groundwater levels at each Vs profile using the contour map of Figure 23 yielded lower probabilities than groundwater levels of 1.5, 3.25, and 5 m at lower PGA/MSF ratios of less than about 0.25 and higher probabilities nearly the same as the 5 m water level at higher PGA/MSF ratios of about 0.3. The groundwater levels obtained from the contour map of Figure 24 may be a better representation of groundwater levels within Lake County than the assumptions of 1.5, 3.25, and 5 m.

Liquefaction Probability Curves Based on the Cone Penetration Test (CPT)

As noted in the CPT data section, the total number of CPT borings within Lake County was only five, which is not sufficient to develop LPCs. Thus, LPCs were not developed based on CPT data. However, as part of the Lake County portion of the project, we performed a literature search to obtain the relationships needed to develop LPCs if additional CPT data is obtained within Lake County in the future and to utilize for the other portions of this project involving the other TN

counties. Equations 11 through 20 is a summary of relationships that can be used to compute CRR with CPT data. To calculate the CSR and FS Equations 10 and 8 can be used respectively.

$$q_{CN} = \frac{q_c}{P_a} \tag{11}$$

$$q_{C1N} = C_N \cdot q_{CN} \tag{12}$$

$$C_N = (P_a/\sigma'_v)^m, \tag{13}$$

$$Q = (\frac{q_c - \sigma_v}{P_a})(\frac{P_a}{\sigma'_v})^n \tag{14}$$

$$F = \left(\frac{f_s}{q_c - \sigma_v}\right) \cdot 100\%, \tag{15}$$

$$I_C = \sqrt{\{(3.47 - \log Q)^2 + (1.22 + \log F)^2\}} \tag{16}$$

$$FC = 80(I_C + C_{FC}) - 137 \tag{17}$$

$$\Delta q_{c1N} = \left(11.9 + \frac{q_{C1N}}{14.6}\right) \exp\left(1.63 - \frac{9.7}{FC + 2} - (\frac{15.7}{FC + 2})^2\right) \tag{18}$$

$$q_{C1NCS} = q_{C1N} + \Delta q_{c1N} \tag{19}$$

$$CRR = \exp\left(\frac{q_{C1NCS}}{113} + \left(\frac{q_{C1NCS}}{1000}\right)^2 - \left(\frac{q_{C1NCS}}{140}\right)^3 + \left(\frac{q_{C1NCS}}{137}\right)^4 - 2.8\right) \cdot MSF \cdot K_\sigma \qquad (20)$$

Once $CRR_{7.5}$, CSR, and FS are estimated for each 0.5m depth interval up to a depth of 20m at each CPT profile location, then the same procedure described in the Liquefaction Probability Curves Based on Standard Penetration Test (SPT) section of this report can be used to obtain LPCs.

Comparison of Liquefaction Probability Curves Based on Different Methods

As noted in the Preliminary Liquefaction Probability Curves Based on Holzer's Study section, the liquefaction hazard maps for Lake County were based on an average groundwater level of 3.25 m, which is the average of the 1.5 m and 5 m levels Holzer (2011) considered. The LPCs based on the SPT N-values and Vs profiles could not be considered because of project timeline limitations. A comparison of the Holzer based LPCs and the LPCs based on N-values and Vs profiles is presented next.

Figure 32 provides a comparison between the Holzer based LPC and the LPCs based on N-values and Vs profiles at a groundwater level of 3.25 m for P[LPI>5]. A comparison was not made between LPCs for P[LPI>15] because Holzer's study did not provide an LPC for P[LPI>15]. The Vs LPC provides higher probabilities of LPI>5 and the N-value LPC provides lower probability values at PGA/MSF ratios of less than about 0.45.

Figure 33 provides a comparison between the Holzer based LPC based on a groundwater level of 3.25 m and the LPCs based on N-values and Vs profiles at a groundwater level determined from the contour map of Figure 24. The Vs LPC provides higher probabilities of LPI>5 and the N-value LPC provides lower probability values at PGA/MSF ratios of less than about 0.5.
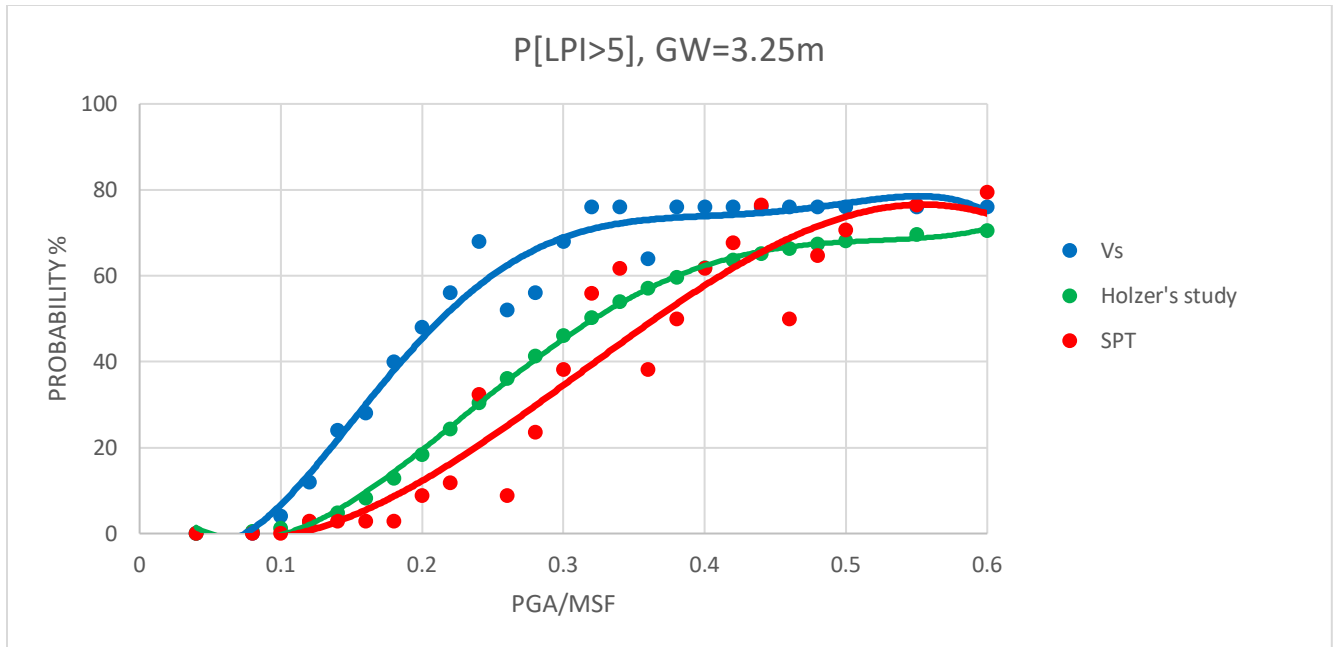
Figure 32: Comparison of obtained LPCs based on SPT data, shear wave velocity profiles and Holzer's study for GW=3.25m.
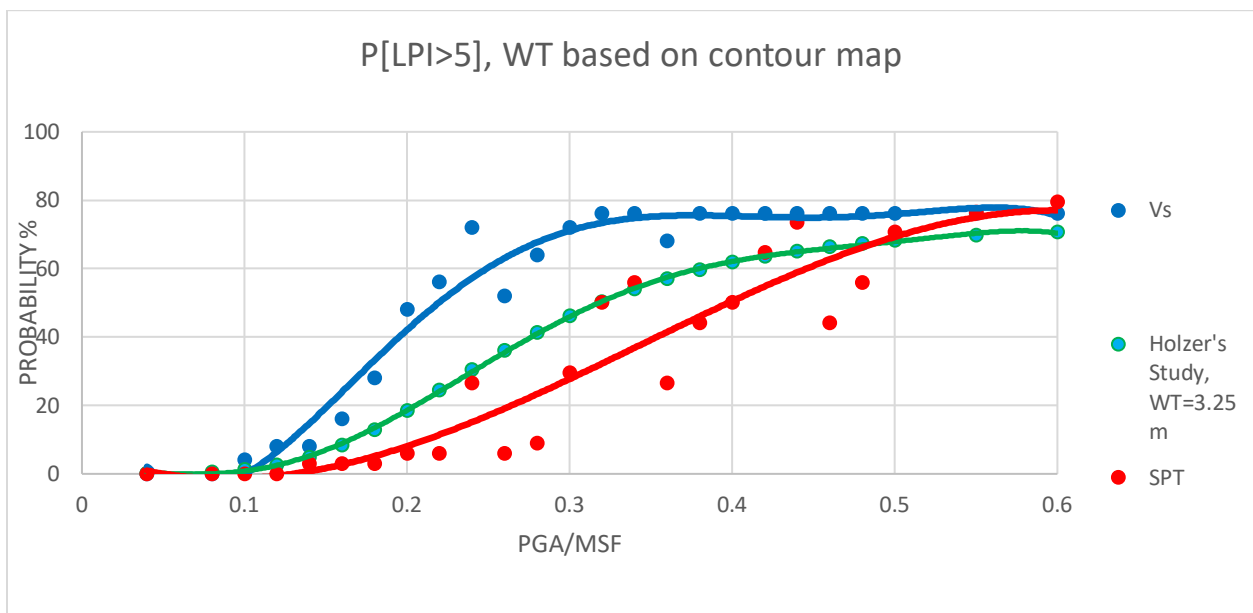
Figure 33: Comparison of obtained LPCs based on SPT data, shear wave velocity profiles (groundwater level based on the contour map) and Holzer's study (GW=3.25m).

Figures 34 and 35, which provide a comparison between the N-value LPC and the Vs LPC at both P[LPI>5] and P[LPI>15], respectively, indicate that Vs profile data yields higher probabilities of exceeding LPI of 5 and 15.
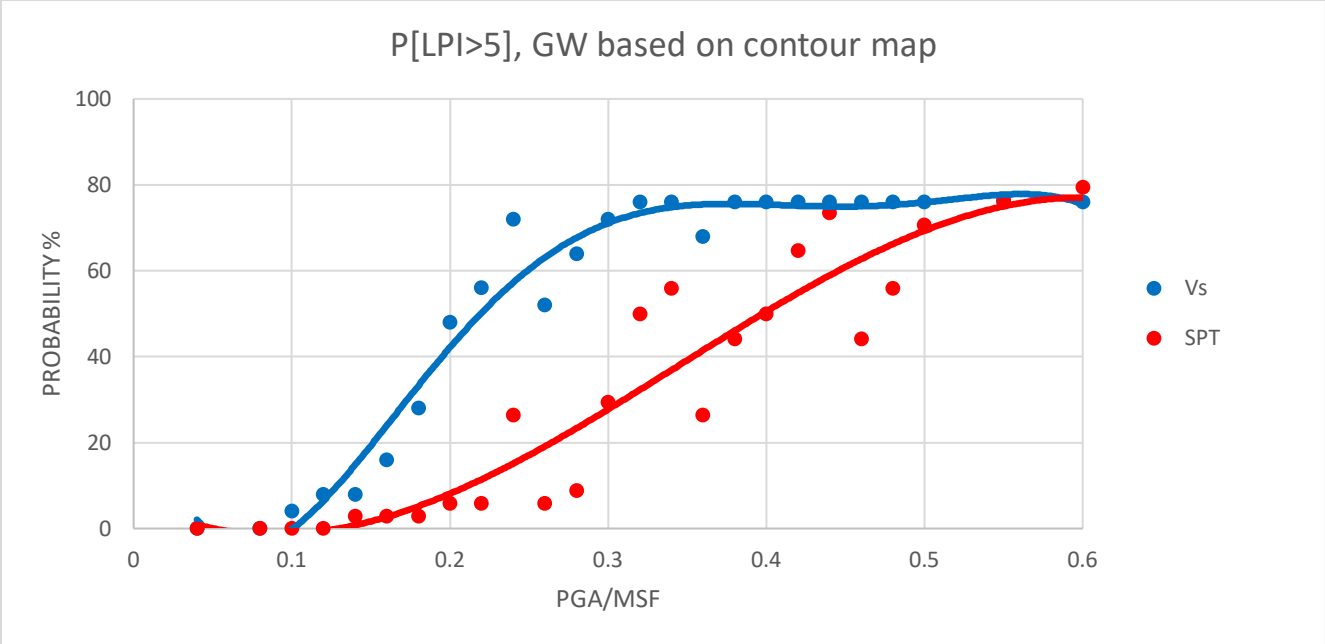
Figure 34: Comparison of obtained LPCs based on SPT data and shear wave velocity profiles for LPI>5.
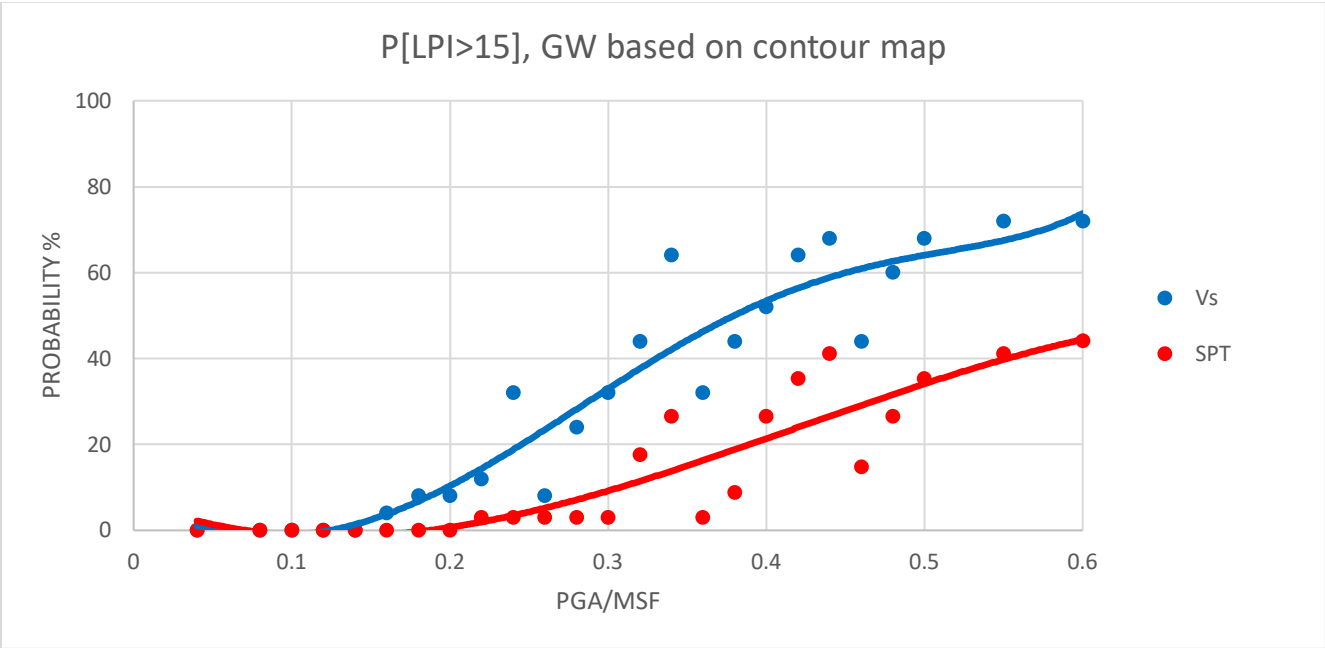
Figure 35: Comparison of obtained LPCs based on SPT data and shear wave velocity profiles for LPI>15.

It should be noted that the soil boring locations representing the N-values used for the LPCs in Figures 32 and 33 are different from the Vs profile locations used in the LPCs in Figures 34 and 35. Therefore, to better compare LPCs between data obtained with N-values and Vs profiles, we analyzed data included in the Pezeshk et al. (1998) study, which includes both N-value data and

Vs profile data obtained at the same locations at ten sites in west Tennessee. The results of this analysis will be presented in the Dyer County report.

As noted in the Liquefaction Probability Curves Based on the Shear Wave Velocity (Vs) section, the LPCs for groundwater levels of 1.5, 3.25, and 5 m in Figures 30 and 31 indicate a higher probability of exceeding an LPI of 5 or 15 with increase in groundwater level depth, which is not in agreement with the Shelby County maps (Cramer et al. 2015, 2018). The probability of liquefaction should decrease with an increase in groundwater level depth. The limitation of developing LPCs using the Vs profile data we obtained is that soil boring data with USCS classifications were not available. Therefore, based on existing data, it is suggested that future hazard maps of Lake County be based on LPCs obtained from SPT N-values instead of Vs profiles. LPCs based on SPT N-value data collected during this study is presented in Figure 36.
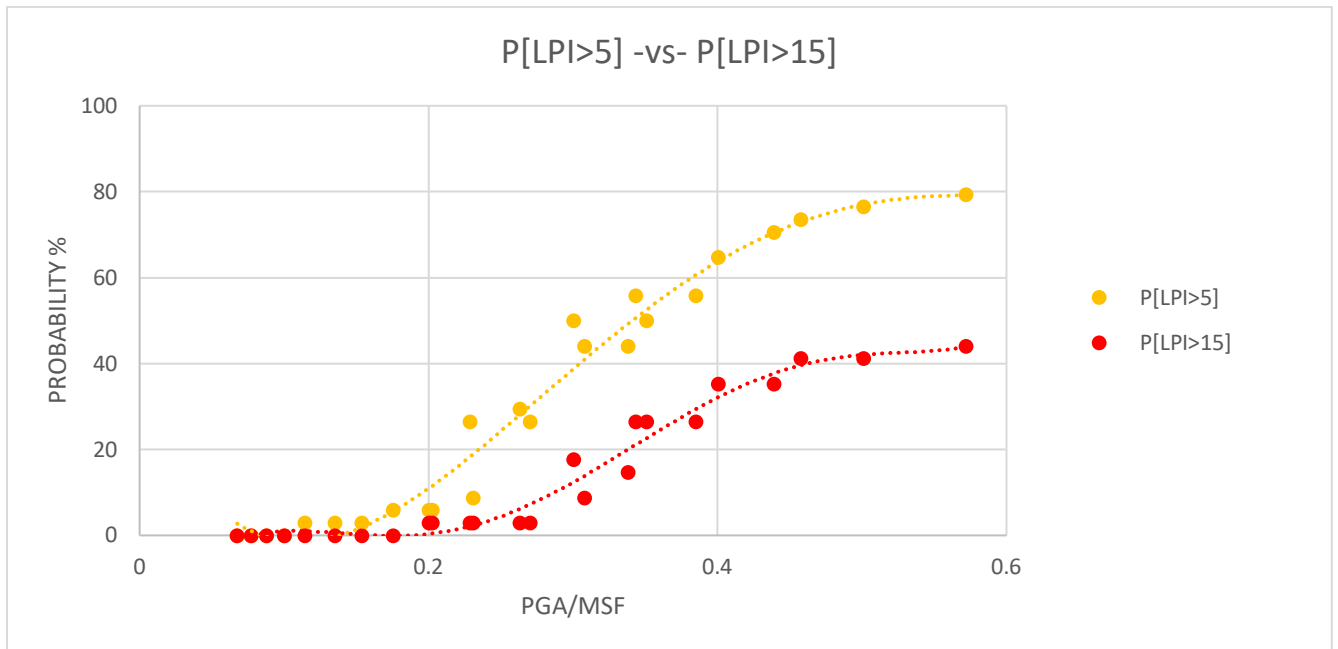
Figure 36: Liquefaction probability curves using SPT boring data.

Geotechnical Summary

The main objective of geotechnical analyses portion of the research was to develop LPCs to prepare the liquefaction hazard maps. LPCs were developed from SPT, Vs, and groundwater subsurface data obtained within Lake County. However, the project team required LPC curve data by March 2018 to develop the liquefaction hazard maps by the May 2018 due date. Because the actual project started about three months after the planned start date, the geotechnical data collection including groundwater level data was not yet completed to develop LPCs by the March deadline. Therefore, we used the six curves shown in Figure 25, which were determined by Holzer (2011) for Mississippi embayment soils, to obtain an average

LPC. The average LPC shown in Figure 26 is the curve used to develop the Lake County liquefaction hazard maps. It is suggested that future hazard maps of Lake County be based on the LPCs obtained from SPT N-values, shown in Figure 36, instead of the Vs profiles.

Seismic Measurements

Introduction

Multichannel Analysis of Surface Waves (MASW) is a geophysical exploration technique that measures shear-wave velocity of underground layers using the dispersion of surface waves along an array of geophones. The MASW seismic survey obtains velocity structure of the layers using surface waves.

The seismic refraction method is sensitive to low velocity layers. If low velocity layers are not detected, the results of seismic refraction may be compromised, while seismic reflection can detect geological features not seen in refraction tests. Geophysical exploration at shallow depths (less than 50 meters) can be a challenge. Invasive procedures such as downhole and crosshole seismic surveys can be expensive. Non-invasive procedures such as MASW can be advantageous and economical and can be a viable alternative.

In the MASW method, an array of geophones captures the surface waves that are generated by an energy source such as a sledgehammer or a heavier source (Figure 37). The changes in amplitude and arrival times are measured using a post-processing software at different frequencies (e.g., SurfSeis, developed by Kansas Geological Survey, KGS). These "changes" are associated with the dispersion of surface waves. Complicated propagation of surface waves has unique characteristics that can relate the amplitude of surface waves with shear-wave velocity, depth, and frequency. In a few words, amplitude (and consequently, velocity) of certain frequency of surface waves (phase velocity) is affected by the shear-velocity structure of the ground down to certain depths. This combination provides us with valuable information called dispersion curves, which is a plot of phase velocity versus frequency. Figure 38 shows the amplitude variation of surface waves with respect to wavelength, which is the normalized depth on the vertical axis and normalized motion (amplitude at depth z over amplitude at surface) on the abscissa. As shown in Figure 39, longer wavelength (or lower frequencies) can sample larger depths.
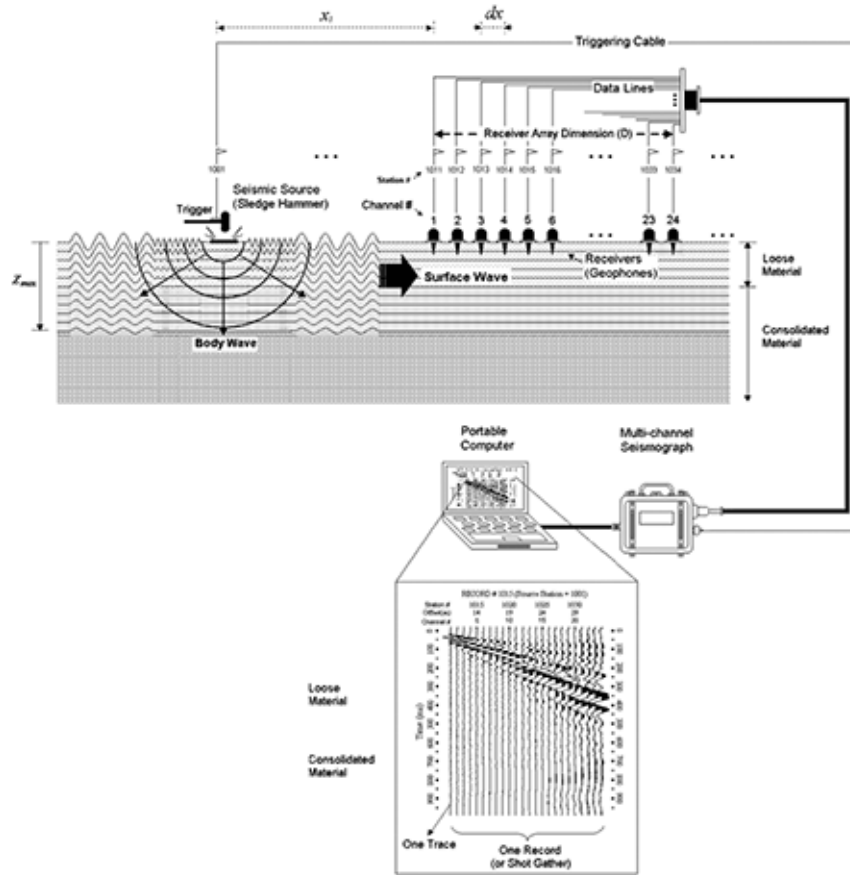
Figure 37: Active MASW test setup. (from KGS.ku.edu).
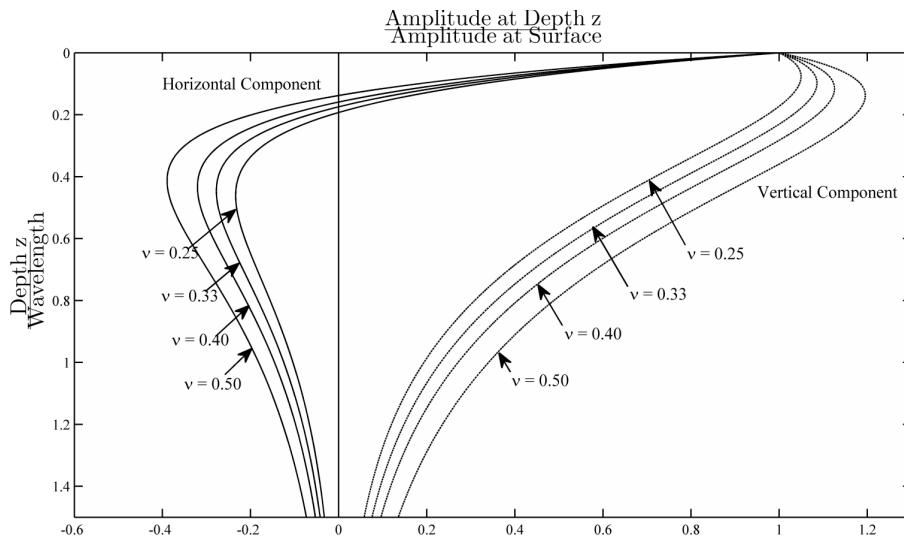
Figure 38: Variation of horizontal and vertical normalized components of displacements induced by Rayleigh waves with normalized depth in a homogeneous isotropic, elastic half-space.
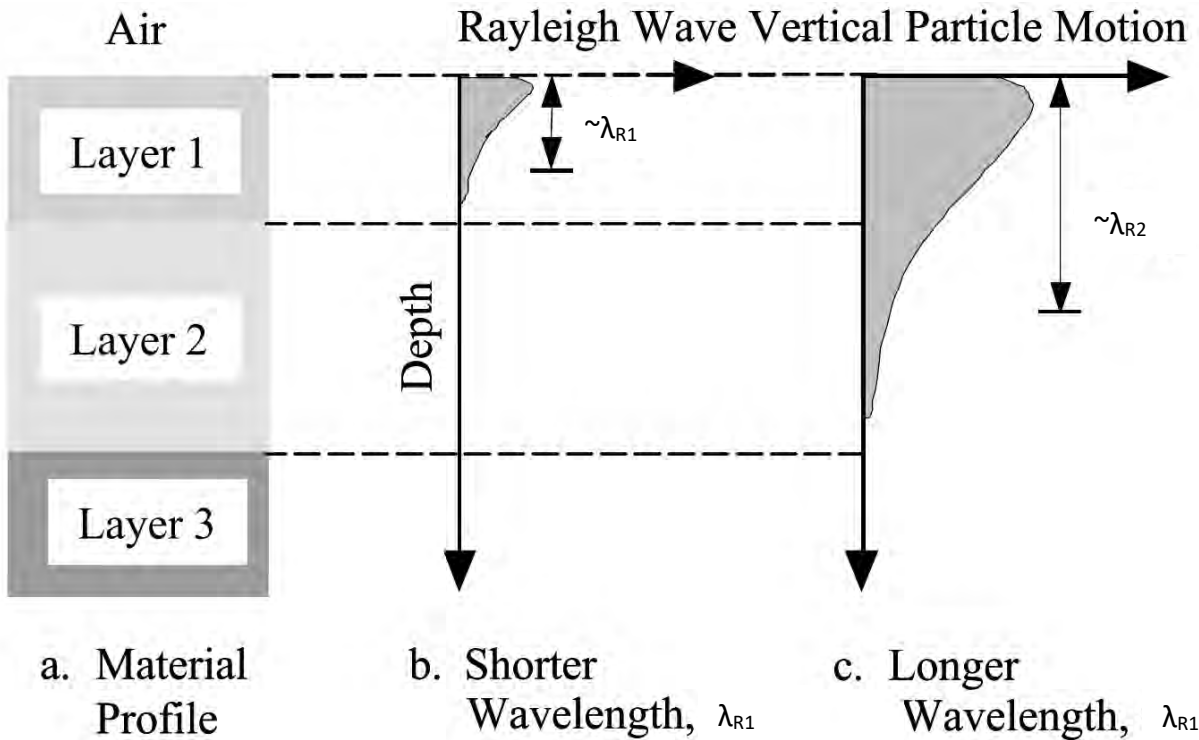
Figure 19: Depth sampled by Rayleigh waves with different wavelengths (Stokoe II and Santamarina, 2000).

Finally, through and iterative inversion process using the SurfSeis software, the best matching velocity profile is obtained. It is important to mention that the inversion process may produce several shear-wave velocity profiles with similar dispersion curves matching the experimental dispersion curve which is referred to as the non-uniqueness of the inversion process. There are some provisions embedded in the software that can remove irrelevant velocity profiles. Also, geological studies and prior expert knowledge can help mitigating the non-uniqueness issue.

MASW Equipment and Testing procedure

In all the 14 sites that we performed MASW survey in the Lake County, we used a 144 m linear array of 72 4.5 Hz geophones with 2 meters of spacing between geophones. Our active energy source was a Propelled Energy Generator (PEG – Figure 40). This device has a 40 kg mass that is driven down using an elastic band, which is stretched using the motor mounted on the device. The energy produced by quick drop of the weight was experimentally considered enough for the entire length of the array plus a 16m offset from the first geophone.

We started shooting at a 16 m offset from the first geophone and advanced every 4 meters through the middle of the spread. Each location was shot three times. Several shots per location can help reduce the effects of noise by stacking the records. Stacking will average out the noise and enhance the main signal, to reach a higher signal to noise ratio.

To obtain deeper velocity structures (e.g., lower frequency range) we recorded ambient noise using the Refraction Microtremor (ReMi) seismic survey. An array of 24 geophones with 10 ft spacing was placed at the same location and several 32s second records of data was acquired multiple times. The dispersion curve obtained using the MASW seismic survey was augmented with the dispersion curve points obtained by the ReMi procedure to better estimate the shear-wave velocity of deeper layers of the soil structure. We used the SeisOpt ReMi software to process data collected using the ReMi seismic survey.

Figure 40: Propelled Energy Generator used as an Active Source.

Data Processing

Data processing is performed using the SurfSeis software. The recordings were analyzed to obtain the "Overtone Images" (Figure 41). In Figure 41 and 42, the vertical axis is the phase velocity in m/sec and the horizontal axis is the frequency. The dispersion curves were automatically picked, and visually checked. Furthermore, the dispersion curve obtained using the ReMi procedure were combined with the MASW dispersion curve as shown in Figure 42. In some cases, dispersion curves from MASW is augmented with ReMi at low frequencies to obtain information at higher depths. Then, the dispersion curves were inverted to obtain the shear-wave velocity profile associated with the site. In Figure 42, the orange curve is the high energy (the middle of the overtone image from ReMi analysis) and the gray curve is the lower energy curve (the lower margin of the overtone image). Lower limit of the apparent phase velocities can be recognized as the true phase velocities (Louie, 2001).
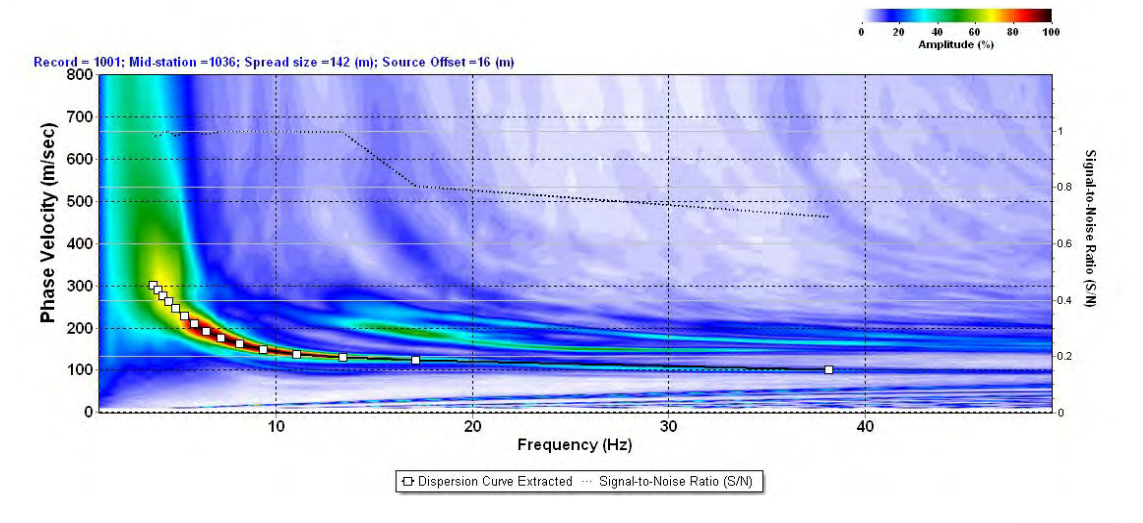
Figure 41: A sample of the dispersion curve obtained by the Surfseis Software.
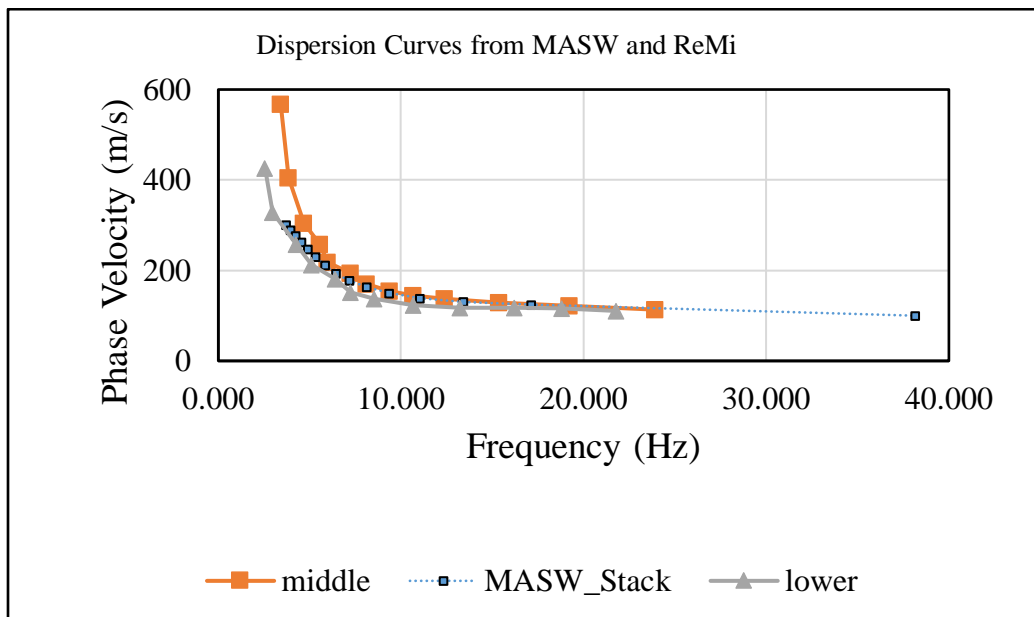
Figure 42: Comparison of dispersion curves obtained with MASW and ReMi.

Depth of investigation is proportional to the largest wavelength captured by the instruments (Schuler, 2008).

$$Depth\ of\ Investigation\ =\ 0.4\ \times\ Wavelength\ =\ 0.4\ \times\ Velocity\ /\ frequency$$

Depth of investigation depends on a few parameters.
- Corner frequency of the geophones, which was 4.5Hz in our case that is a widely and practically used device for surface exploration methods.

- Energy source. The energy source should be strong and capable of generating enough low frequencies.

- Velocity of subsurface soil. The faster the velocities, the greater depth we can measure.

- Noise in the area. A noisy location can obscure wave motion at long distances, where the wave has attenuated.

Results

The final results of 14 MASW and ReMi seismic surveys (Figure 43) in the Lake County are summarized in this section (Figure 44). We were able to obtain shear-wave velocity profiles to depths of about 30m to 70m. We performed a Bayesian averaging in depth and calculated the 90% credible interval of the velocity with depth. Our study confirms that the MASW procedure can estimate down to 50m depth with acceptable accuracy. Data quantity does not support the reliability and accuracy at depths higher than 50m. In general, uncertainty increases with depth. In some cases we included higher modes into our inversion process to enhance the resolution of the velocity profiles. Although, the estimated depth of the velocity profile is only dependent on the wavelength (frequency) of the modes, meaning that including higher modes does not increase the depth of conversion. Yet, the benefit of recognizing higher modes is to increase the resolution of the profile and decreasing the uncertainty of the inversion process.

Comparing our inversion results with previous findings of other researchers (i.e., Romero and Rix, 2005 for Shelby County) we obtained a slightly faster layer from 35m down to 50m. At shallower depths, the averaged shear-wave velocity and the velocity slope with depth matches Romero and Rix's (2005) findings. In Lake County the top of the faster velocity Eocene sediments can be as shallow as 30 m, which can start biasing the MASW profiles to faster velocities below 30 m as we observe. A check of the estimated depth to the top of the Eocene at MASW sites from the geology model with the depth at which the Vs exceeds 500 m/s (estimated Eocene Vs) in the MASW profiles shows a fairly good correlation, which is consistent with an Eocene Vs bias below 35 m in the Lake County MASW profiles. Although the posterior standard deviation barely contains Romero and Rix's profile, yet, it is doubtful if the velocity trend takes a faster trend compared to the aforementioned study, because statistically it does not fall out of our credible interval (Figure 45).

Lake Co MASW Sites
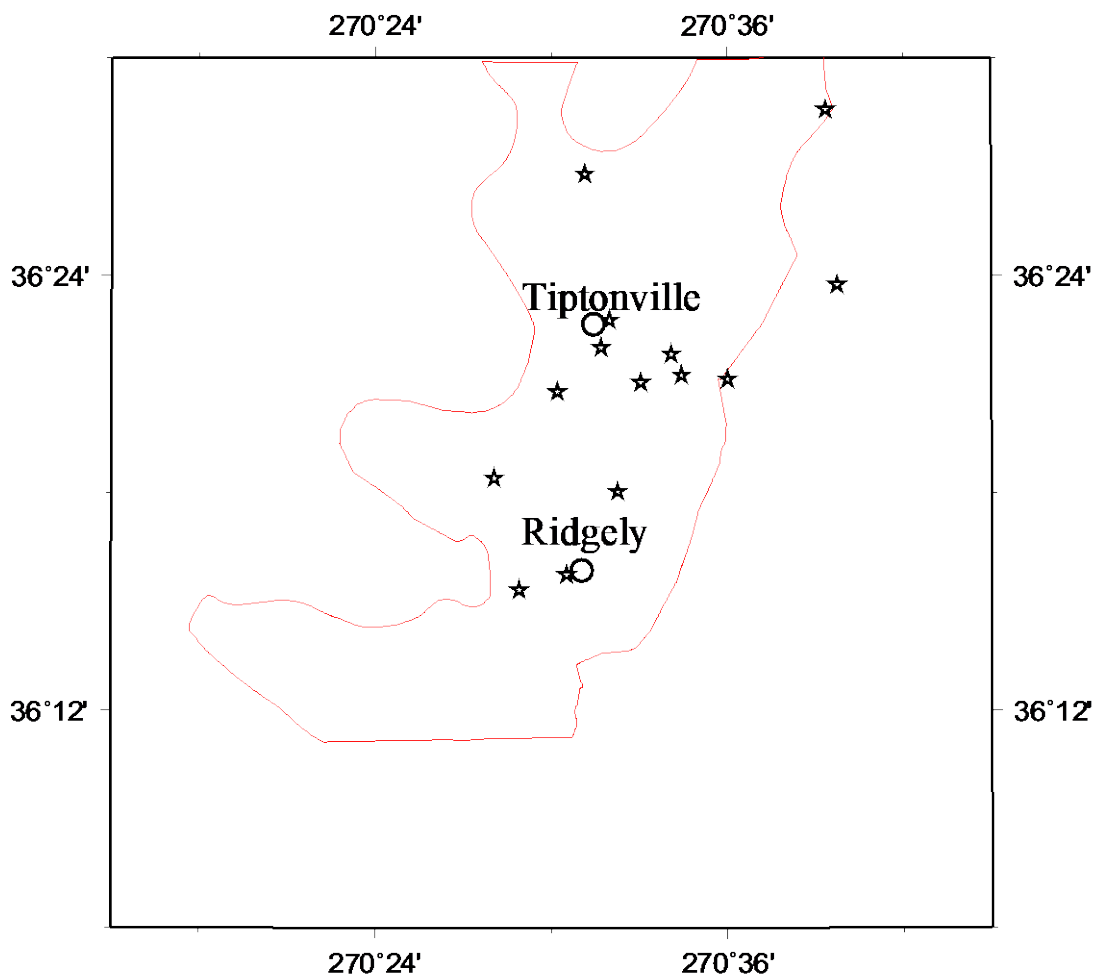
Figure 43: Location of MASW measurements (stars) in and near Lake County (red outline).
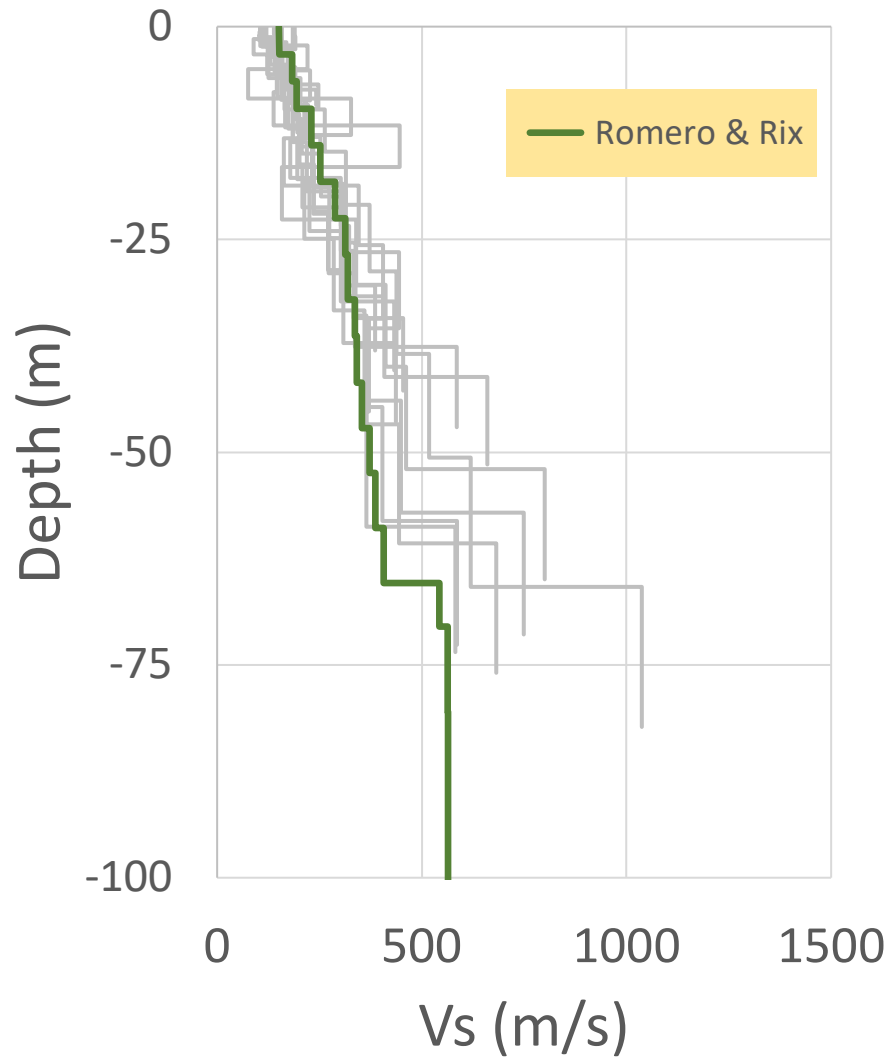
Figure 44: Comparing the velocity profiles obtained via testing and findings of Romero and Rix (2005).
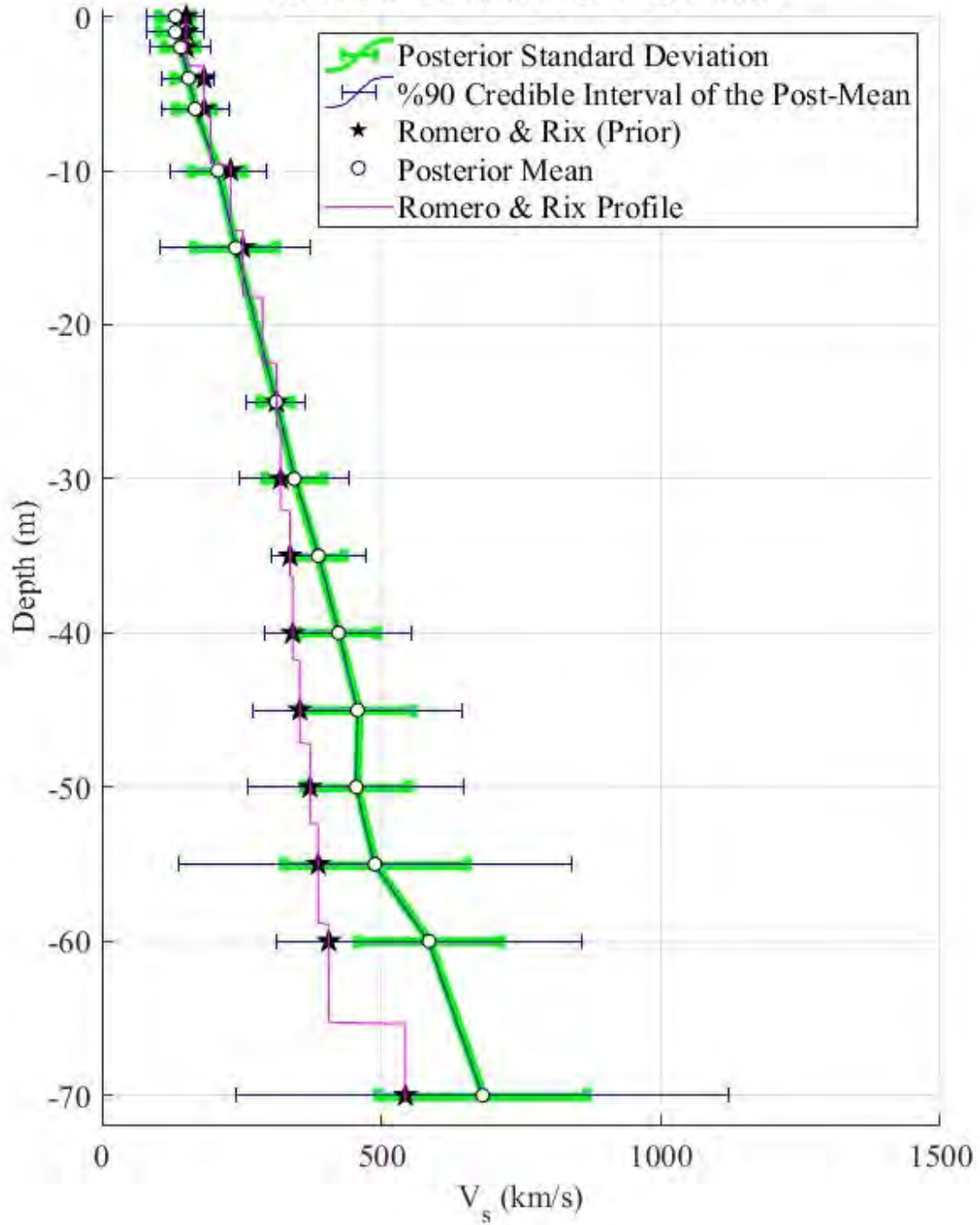
Figure 45: Bayesian Average of the 14 velocity profiles.

Hazard Maps Development

Methodology

A standard methodology for including the effects of local geology in seismic and liquefaction hazard estimates was used in this study. We followed the approach of Cramer et al. (2006, 2008, 2014, 2017, and 2018) of developing site amplification distributions on a grid, applying those distributions to modify hard rock hazard curves to geology-specific hazard curves and develop seismic hazard maps, and then applying geology-specific liquefaction probability curves to develop liquefaction hazard maps. The site amplification distributions are based on the 3D geological, geotechnical, and seismological models developed above for Lake County. The 2014 U.S. Geological Survey (USGS) National Seismic Hazard Project's seismic hazard model (seismic sources and ground motion attenuation model of Petersen et al., 2014) for hard rock was modified using our Lake County site amplification distributions. Probabilistic seismic hazard maps were generated from the USGS probabilistic model and scenario (deterministic) seismic hazard maps were generated using selected scenario fault ruptures (earthquakes) and the USGS ground motion attenuation model. The resulting peak ground acceleration (PGA) seismic hazard maps were then modified using appropriate Lake County liquefaction probability curves (discussed above) to generate liquefaction hazard maps (both probabilistic and scenario).

Lake County Shear-wave Velocity Model

Seismic hazard maps with the effects of local geology depend on developing site amplification distributions on a grid for the 3D geology of the study area. The 3D geology is converted to geologic (sediment) profiles on a uniform grid. The geology layers are converted to shear-wave velocity (Vs) profiles at each grid point and input to a geotechnical soil response program (SHAKE91), along with appropriate geotechnical properties, to develop site response distributions at each grid point using the University of Memphis High Performance Computing (HPC) facility. The site amplification distributions model frequency and amplitude dependent amplification/deamplification at the surface of hard rock ground motions input at the bottom of the sediment profile.

The Lake County velocity model used was developed from published and measured Vs profiles in and near the county. Two separate models were developed for Lake County, one for the Quaternary sediments above the top of the Eocene deposits and one for the geologic layers from the Eocene to the Paleozoic.

The Quaternary Vs model is a step-wise gradient model developed from the shallow Vs observations (both published and our own MASW measurements at 14 sites in Lake County). Figure 46 shows the model developed from averaging the observations from these profiles. The depth to the top of the Eocene layer varies for each profile between 30 and 70 meters depth so the gradient trend was projected downward from the all Quaternary sediment trend above 30 m to 70 m in 5 m depth steps. The Eocene Vs jumps to 515 m/s at the top of that

layer. Appropriate uncertainties based on the statistics (standard deviation) of the profile averaging at each depth interval were developed and applied in the sediment profile randomization process employed in the development of the site amplification distributions at each grid point.
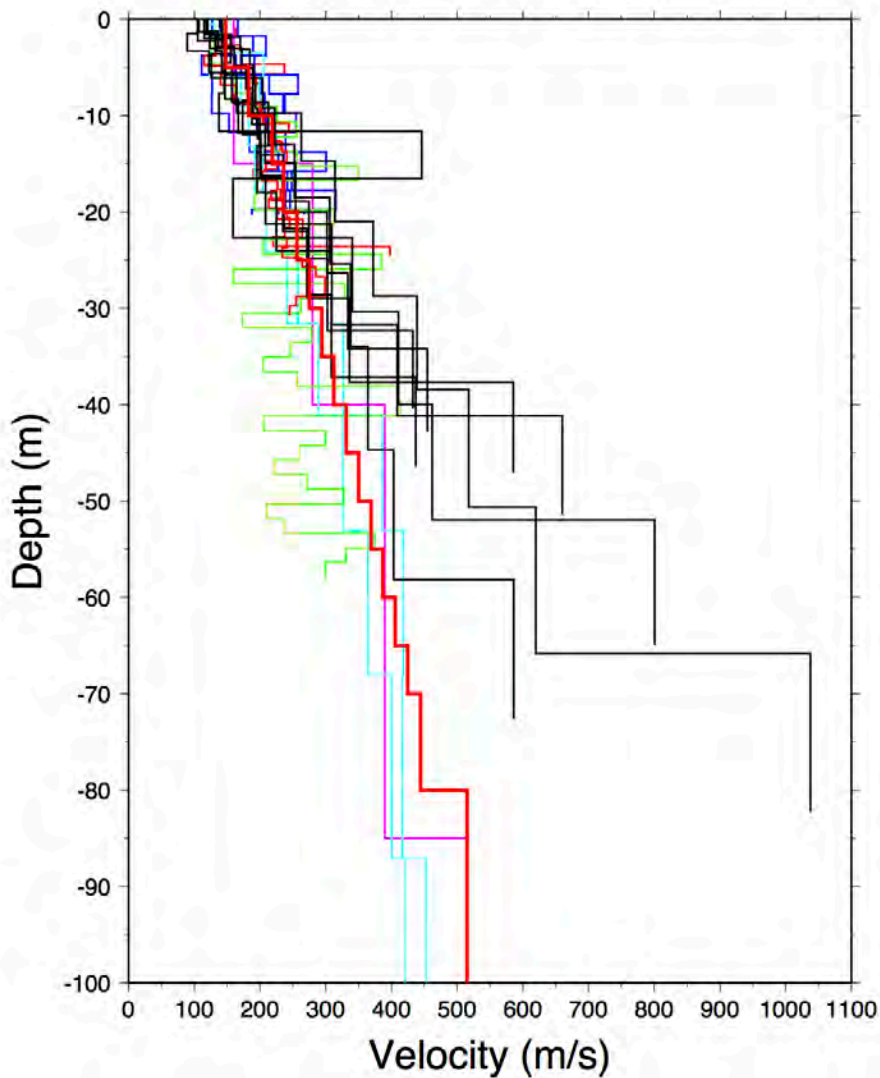

Figure 46: Vs profiles down to 100 m depth with Lake County Quaternary Vs model shown in heavy red line. Thin colored lines are published Vs profiles. Thin black lines are MASW profiles measured as a part of this study.

The Eocene to Paleozoic Vs model was developed from the CUSSO deep hole site in Kentucky (Woolery et al., 2016) and published deeper embayment measurements in and near Lake County (refs) plus Vs models from Shelby County (Cramer et al., 2006). The borehole geological information mainly constrained the depths to the top of the Eocene, Cretaceous, and Paleozoic (bedrock) layers. In Lake County, very limited observations were available for other intermediate geological layers such as the top of the Memphis Sand, Flour Island clay, Fort Pillow sand, and Old Breastworks clay. The depth to the top of these four geological layers are needed to define the geology and Vs profiles beneath Lake County. Using the limited observations for these four layers and the better constrained isopachs for the top of the Eocene and Cretaceous, we developed a scheme to estimate the depth to the tops of the four intermediate layers between the Eocene and Cretaceous layers. Taking the depth difference between the tops of the Eocene and Cretaceous layers as unity, statistical estimates (average and standard deviation) were determined from the few available measurements for the depth difference between the top of the Eocene and the tops of each intermediate layer. The results in Table 9 are in fraction of the distance between the tops of the Eocene and Cretaceous. We then used these averages and standard deviations to estimate the depth with uncertainty to the top of the intermediate layers at each grid point. Vs values and uncertainties assigned to each intermediate layer was determined from the CUSSO Vs profile and checked and adjusted with available deeper Vs profile observations in Lake County and from the Shelby Co model. Figure 47 and Table 10 show the resulting deeper Vs model and uncertainties used in the site amplification distribution calculations at each grid point.

As a further check on the intermediate Vs profile model developed for Lake County, we compared our model and available observations with the Vs profile from ambient noise (surface-waves) based Vs profile by Chunyu Liu (Figure 47). Liu's results are from the Non-Volcanic Tremor (NVT) L-shaped array of 19 broadband stations with a 60m spacing (600 m on a side). The NVT array was located near Mooring in Lake County. Clearly in Figure 48 below 150 m depths the Liu profile agrees with our model and other observations within the uncertainty. Above 150 m the Liu profile estimates of Vs are lower, but still within uncertainty, although with a loss of resolution in Liu's profile above 50 m. Liu did find an Vs anisotropy between 100 and 140 m depths.

Grids

There are two grid sizes used in our study. The 3D geology for the depth to the top of the Cretaceous and Paleocene layers where provided on a 0.001 degree grid (~100 m). The depth to the top of the Eocene was provided on a 0.0015 degree grid and resampled to a 0.001 degree grid in Generic Mapping Tools (GMT) (Wessel and Smith, 1991). These geology inputs were desampled to a 0.005 degree profile grid (~500 m) using the Quaternary and deeper Vs models discussed above for site amplification distribution and seismic hazard calculations. The final seismic and liquefaction hazard maps use the 0.005 degree grid spacing.
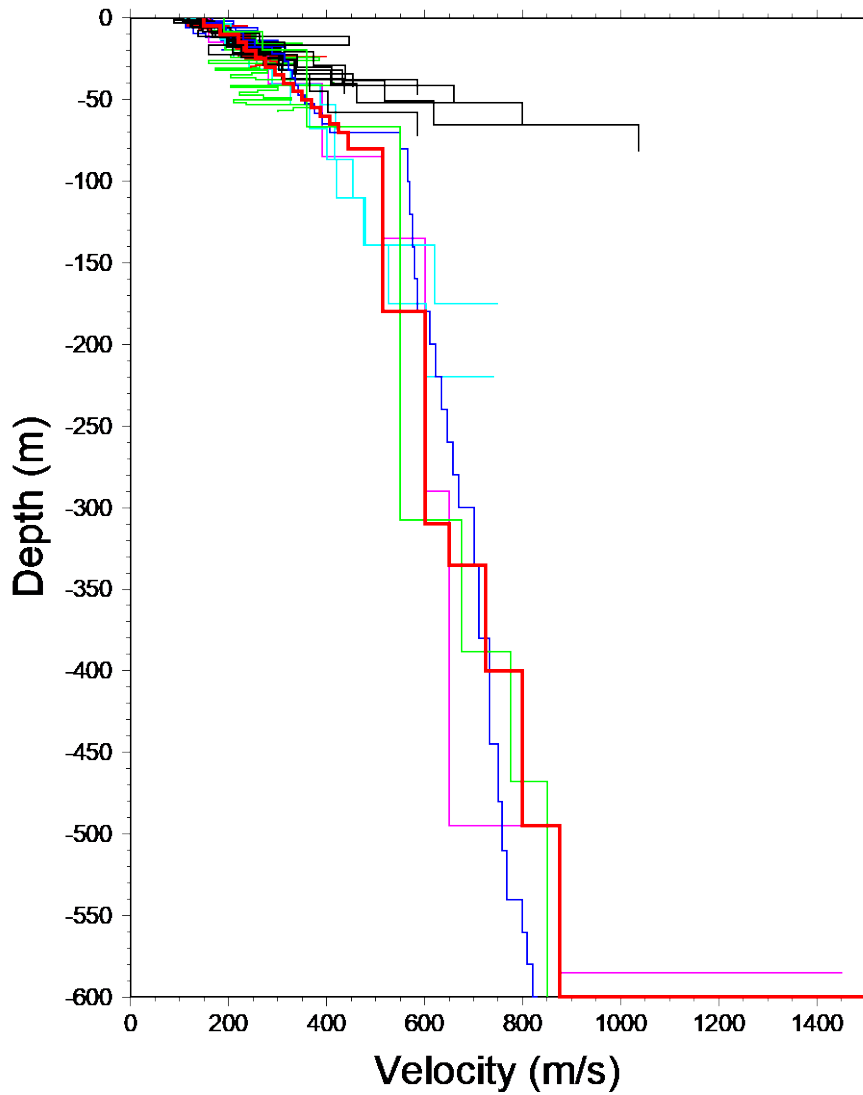
Figure 47: Vs profiles down to 600 m depth with Lake County Quaternary Vs model shown in heavy red line. Thin colored lines are published Vs profiles. Thin black lines are MASW profiles measured as a part of this study. The magneta profile is the CUSSO (Kentucky) deephole profile. The deeper green profile is the Shelby County reference profile. The blue profile is the Romero and Rix (2001) profile.

Table 9: Intermediate layer statistics in fraction of Cretaceous-Eocene depth difference.

Top of Formation	Fractional Distance	Fractional Std. Deviation	# of Observations
Memphis Sand	0.234	±0.029	6
Flour Island (clay)	0.546	±0.034	6
Fort Pillow (sand)	0.611	±0.048	5
Old Breastworks (clay)	0.771	±0.035	5

Table 10: Geotechnical profile used in 3D geology hazard model. Uncertainties are one std. deviation.

Formation	DepthToTop(m)	Damping	Density(g/cc)	Velocity(m/s)
Alluvium	0.	0.05	2.00	148±13
	5.±0.75	0.05	2.00	183±15
	10.±0.75	0.03	2.00	219±30
	15.±0.75	0.03	2.00	236±26
	20.±0.75	0.03	2.00	259±31
	25.±0.75	0.03	2.00	275±34
	30.±0.75	0.02	2.00	294±35
	35.±0.75	0.02	2.00	312±35
	40.±0.75	0.02	2.00	331±35
	45.±0.75	0.02	2.00	350±35
	50.±0.75	0.02	2.00	369±35
	55.±0.75	0.02	2.00	387±35
	60.±0.75	0.02	2.00	406±35
	65.±0.75	0.02	2.00	425±35
	70.±0.75	0.02	2.00	444±35
Eocene	80.±1.00	0.02	2.00	515±127
Memphis Sand	180±12	0.02	2.00	600±50
Flour Island	310±7.5	0.02	2.00	650±25
Fort Pillow	335±15	0.01	2.00	725±15
Old Breastworks	400±13	0.01	2.00	800±25
Cretaceous	495±13	0.01	2.50	875±63
Paleozoic	600±13	0.001	2.80	2800
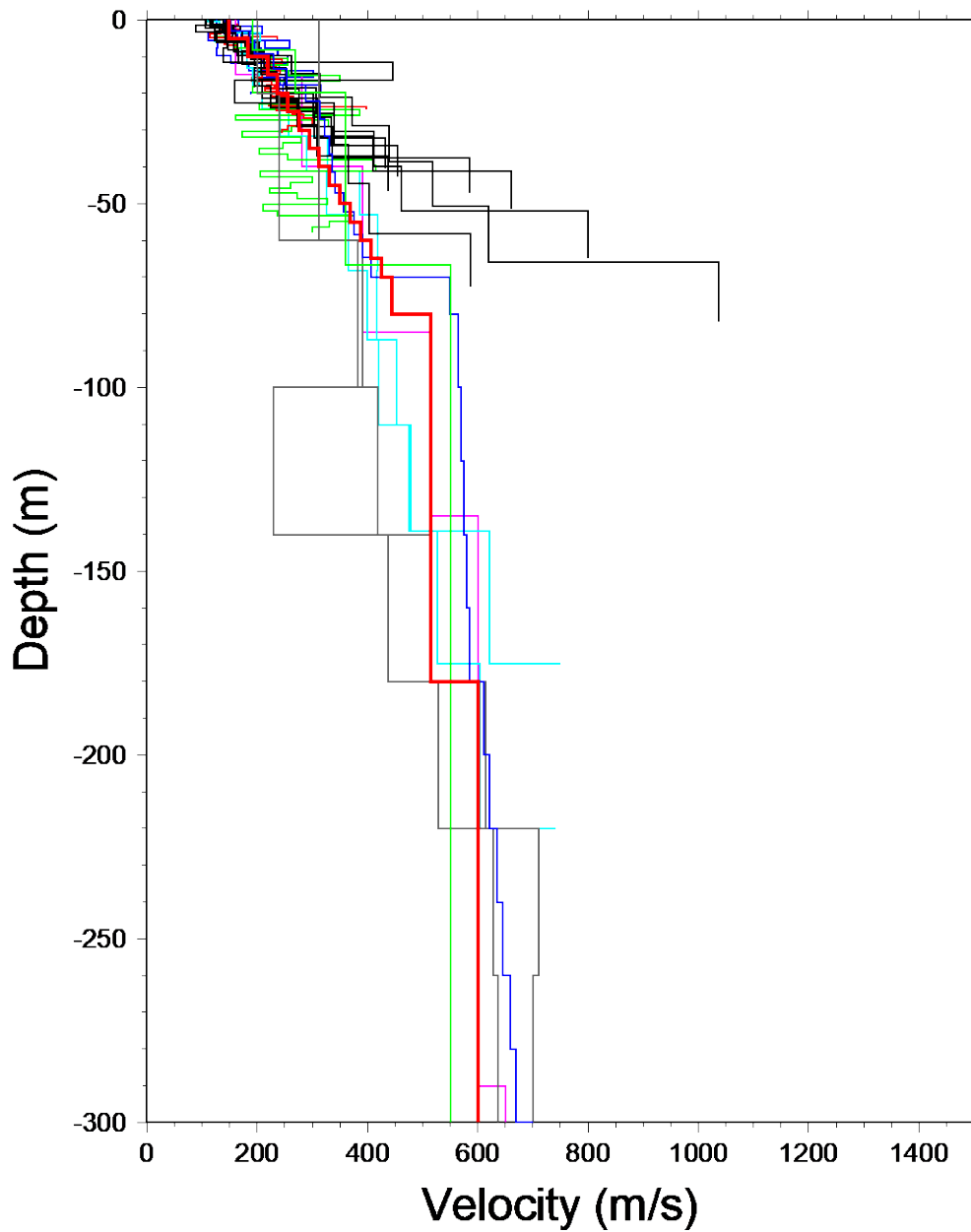
Figure 48: Vs profiles down to #00 m depth with Lake County Quaternary Vs model shown in heavy red line. The grey lines are Chunyu Liu's NVT profiles. The other profiles are colored as indicated in Figure 47.

Time History Database

The site amplification distribution calculations use a suite of input time histories (seismograms) at the bedrock/sediment interface to estimate sediment response. Time histories are required by soil response computer programs to estimate site response. The time histories used are listed in Table 11 and have been used by Cramer et al. (2006, 2017, and 2018) in similar seismic hazard analyses. At each grid point, the time history used is randomly selected for each iteration in the soil profile randomization to properly include uncertainty in the site amplification distribution calculations.

Table 11: Strong motion time series on rock used in the analysis (Cramer, 2006).

Earthquake	Station	Components
1989 **M** 6.9 Loma Prieta, California	G01	E, N
1992 **M** 7.1 Cape Mendocino, California	CPM	E, N
1992 **M** 7.3 Landers, California	JOS	E, N
1995 **M** 6.9 Kobe, Japan	KJM	E, N
1999 **M** 7,4 Kocaeli, Turkey	GBZ	W
	IZT	S
1999 **M** 7.6 Chi-Chi, Taiwan	TCU	N, W
1999 **M** 7.1 Duzce, Turkey	1060	E, N
Atkinson and Beresnev (2002)	**M** 7.5 and **M** 8.0 at Memphis, Tennessee	

Hazard Maps

Seismic and liquefaction hazard maps have been developed for both probabilistic and scenario cases. Probabilistic hazard maps have been generated for 10%, 5%, and 2% probability of exceedance in 50 years. The 2% in 50 year maps correspond to current building code standards and represent up to the 80 percentile New Madrid seismic ground motions. 5% in 50 year maps are similar to median scenario ground motion maps for the **M**7 earthquakes in the New Madrid seismic zone and represent up to 60 percentile ground motions. The 10% in 50 year maps correspond to an older design standard and only represent up to 35 percentile ground motions from the New Madrid seismic zone (NMSZ) sources. The 10% in 50 year maps do not adequately represent expected median ground motions from New Madrid 1811-1812 earthquakes, are no longer recommended for design purposes by regulatory agencies, and are not presented here.

Median ground motion scenario (deterministic) hazard maps have been generated for eight scenario earthquakes (Table 12 and Figure 49A,B) and represent median expected ground motions from those earthquakes. The scenarios are for the largest earthquakes from the 1811-1812 New Madrid sequence, two **M**6 earthquakes in 1843 and 1895, and for a hypothetical **M**5.8 earthquake in Lake County. The latter scenario represents the effects of recent **M**5.5-6.0

Central and Eastern North American earthquakes if a similar size earthquake were to occur in Lake County.

The ground motion periods represented in the Lake County seismic hazard maps are peak ground acceleration (PGA), 0.2 s, and 1.0 s. 0.3 s maps have also been generated for compatibility with HAZUS, a risk and loss assessment package commonly used in loss analysis. The 0.2 and 0.3 s hazard maps are similar so the 0.3 s hazard maps are not shown in this report.

Table 12: Scenario earthquakes used in Lake County study.
M 7.7 on the Reelfoot Thrust (central segment)
M 7.5 on the Cottonwood Grove Fault (SW segment)
M 7.3 on the New Madrid North Fault (NE segment)
M 6.9 "Dawn" Aftershock (2 alternatives)
M 6.2 near Marked Tree, Arkansas (1843 earthquake)
M 6.2 near Charleston, Missouri (1895 earthquake)
Hypothetical M 5.8 earthquake between Tiptonville and Ridgely (recent CEUS earthquakes)
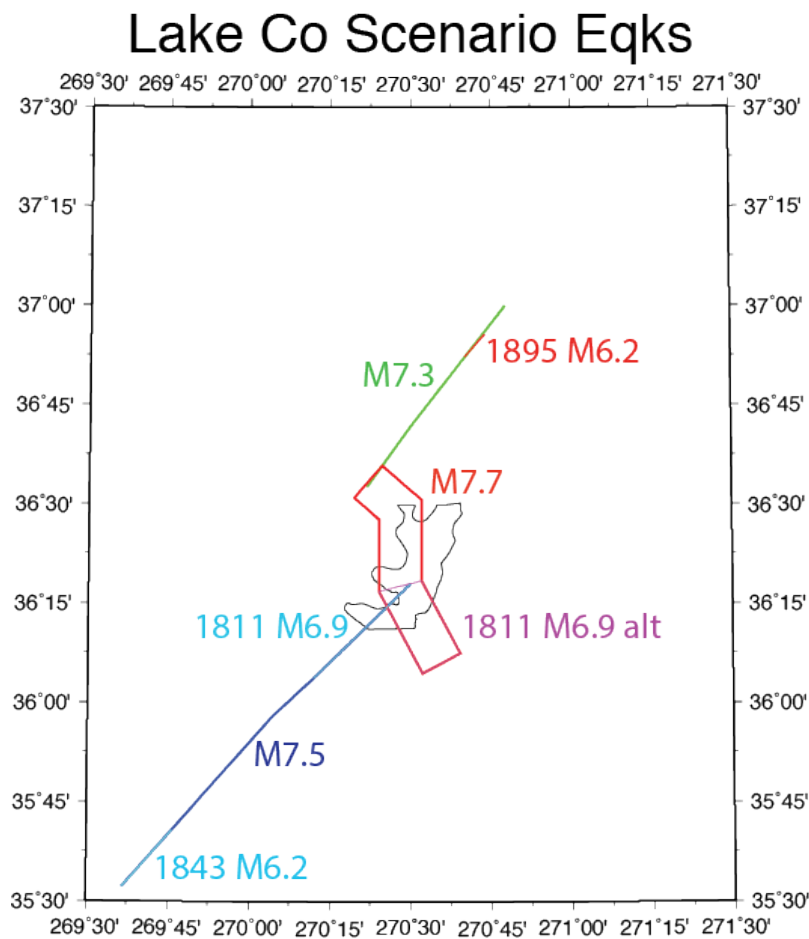
Figure 49A: Scenario ruptures for Lake County. 1811–1812 **M**7 ruptures indicted by **M**7.5, **M**7.3, and **M**7.7. 1811 **M**6.9s indicate two alternative "Dawn" aftershock ruptures. 1843 and 1895 **M**6.2s indicate historic end of seismic zone ruptures.
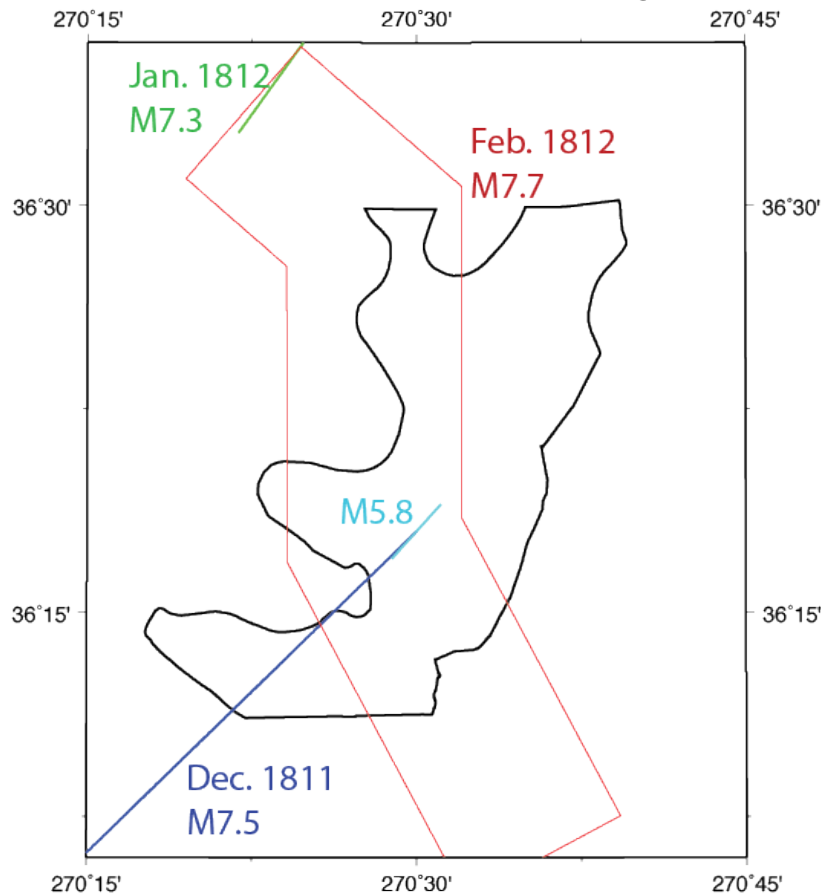
Figure 49B: Scenario ruptures close to Lake County. Dec. 1811 and Jan. 1812 are strike-slip mainshock ruptures extending out of the map view. Feb. 1812 is trust mainshock rupture mostly in map view. **M**5.8 is hypothetical earthquake in Lake County.

Seismic Hazard Maps

Figures 50 - 52 show the 5% in 50 year probabilistic seismic hazard maps for Lake County for PGA, 0.2 s, and 1.0 s. The background maps are the equivalent USGS national seismic hazard maps for B/C boundary conditions (Vs30 = 760 m/s). At short periods (PGA and 0.2 s) the Lake County range of values is 0.5 – 0.8 g (g is the acceleration of gravity at the earth's surface – 9.80665 m/s). At long periods (1.0 s) the range is 0.4 – 0.7 g. Short period seismic hazard is for 1-2 story buildings, while long period hazard is for ~10 story buildings.

Figure 50: 5% in 50 year PGA hazard map for Lake County with the effects of local geology inset on the U.S. Geological Survey's national seismic hazard map for BC boundary conditions.

Figure 51: 5% in 50 year 0.2 s hazard map for Lake County with the effects of local geology inset on the U.S. Geological Survey's national seismic hazard map for BC boundary conditions.

Figure 52: 5% in 50 year 1.0 s hazard map for Lake County with the effects of local geology inset on the U.S. Geological Survey's national seismic hazard map for BC boundary conditions.

Figures 53 - 55 show the 2% in 50 year probabilistic seismic hazard maps for Lake County. The hazard range is high than the 5% in 50 year maps: 0.9 – 1.3 g for PGA, 0.9 – 1.5 g for 0.2 s, and 0.9 – 1.4 g for 1.0 s.

The probabilistic seismic hazard maps with the effect of local geology show a short period reduction of about 50% and a long period amplification of about 10% relative to the USGS national seismic hazard maps at the same periods. The short period reduction is due to estimated ground motion nonlinear soil effects strongly reducing the high ground motions expected near the earthquake sources. The long period amplification is due to the reduced nonlinear effects and increase dominance of soil column resonant effects amplifying ground motions. As we progress further from the earthquake sources the ground motion level decreases, the nonlinear effects decrease, and the dominance of resonance effects increases. In Shelby County, about 50 km from the New Madrid earthquake sources, Cramer et al. (2018) show Shelby County seismic hazard maps with 40 – 60% decreases at short period and 50 – 100 % increases at long period over the USGS national seismic hazard maps.

Figure 53: 2% in 50 year PGA hazard map for Lake County with the effects of local geology inset on the U.S. Geological Survey's national seismic hazard map for BC boundary conditions.

Lake Co 0.2s Hazard
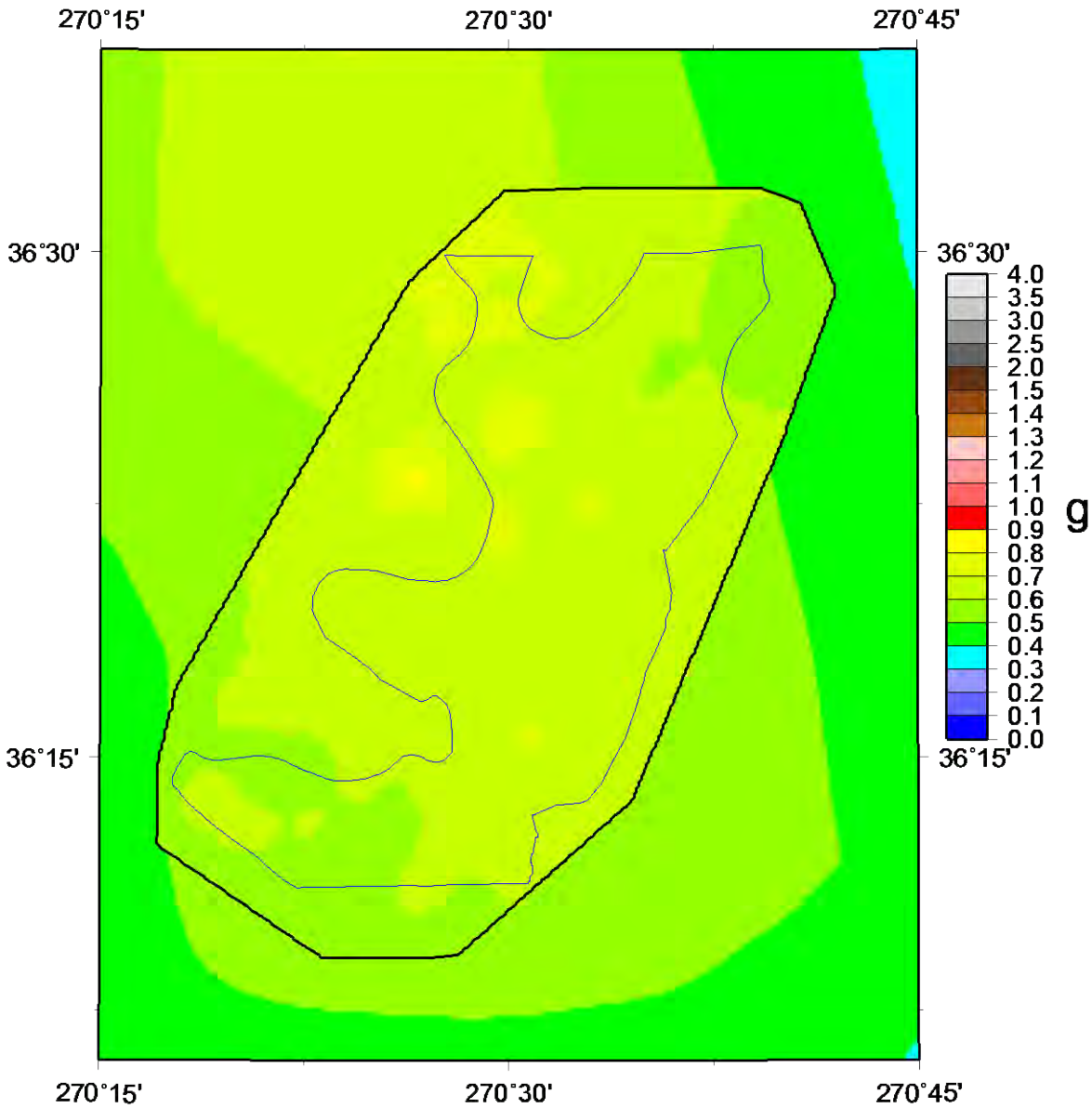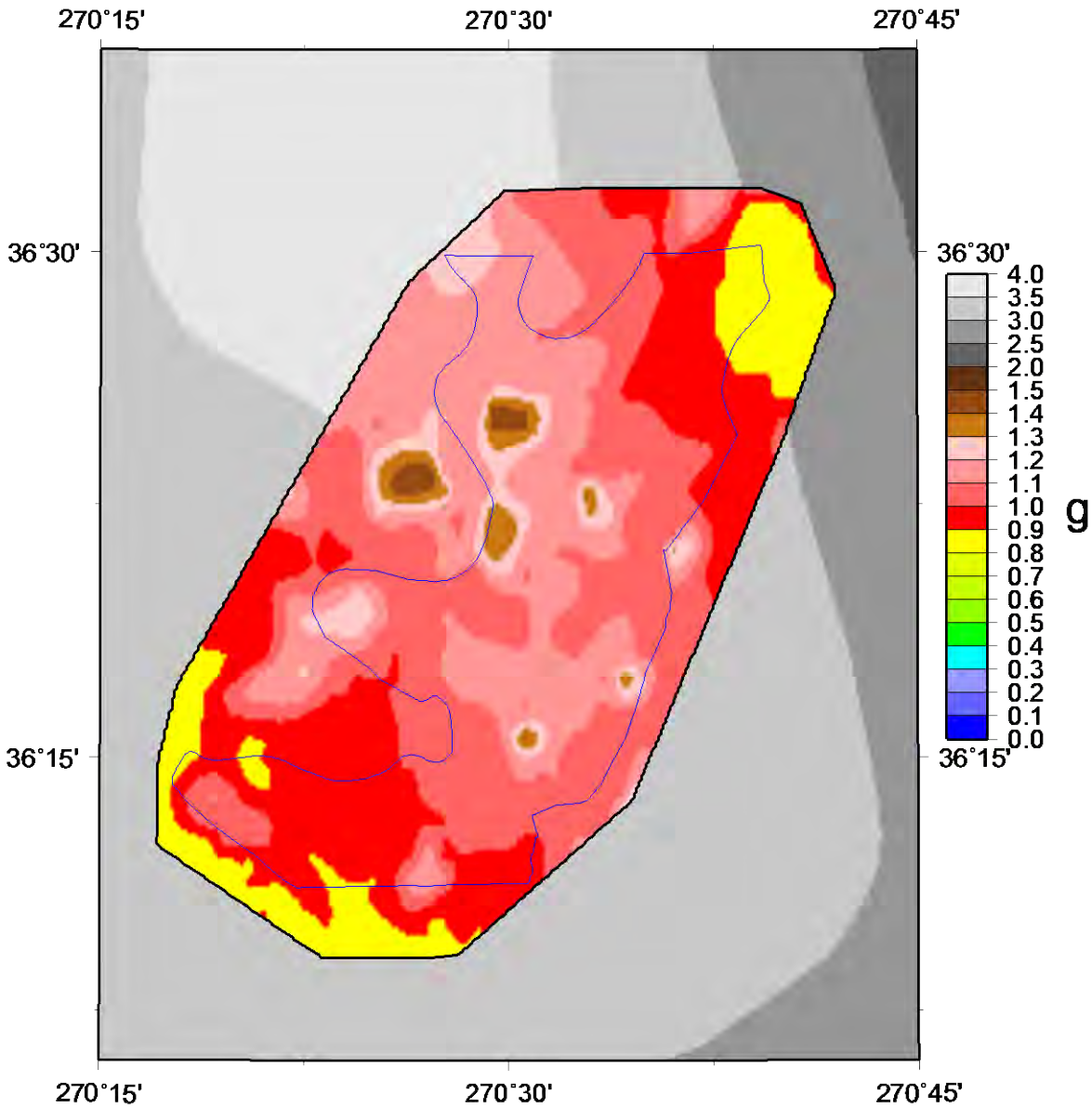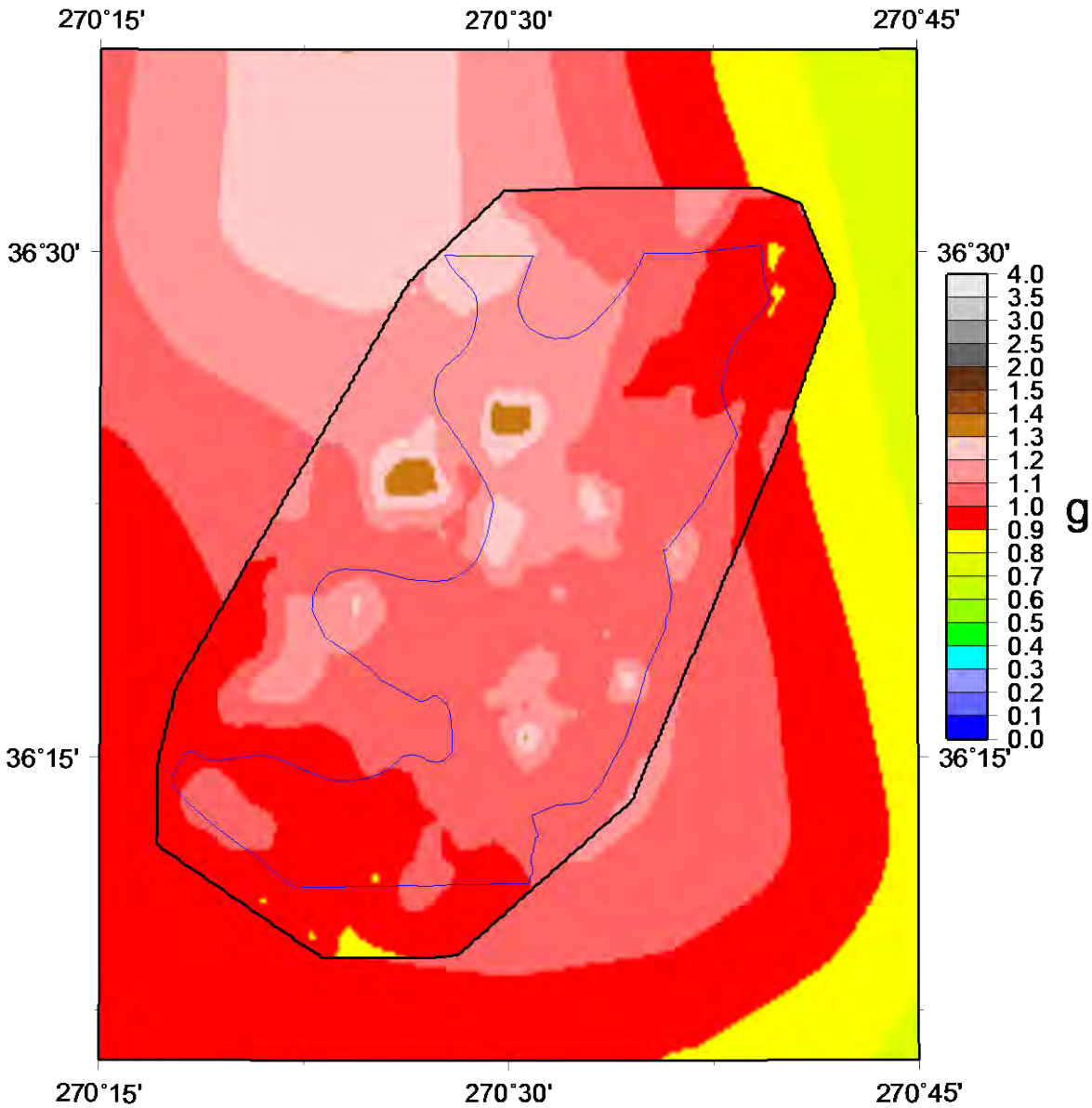
2% in 50 year, October 2018

Figure 54: 2% in 50 year 0.2 s hazard map for Lake County with the effects of local geology inset on the U.S. Geological Survey's national seismic hazard map for BC boundary conditions.

Figure 55: 2% in 50 year 0.1 s hazard map for Lake County with the effects of local geology inset on the U.S. Geological Survey's national seismic hazard map for BC boundary conditions.

Figures 56 - 63 present the PGA, 0.2 s, and 1.0 s seismic hazard maps for the eight scenarios of Table 12. There are no equivalent comparisons to the USGS probabilistic maps for these scenarios. At all periods shown, the M7 New Madrid scenario hazard maps range from 0.2 – 0.8 g, the M6.9 largest aftershock alternatives range from 0.3 – 0.6 g, the M6.2 1843 and 1895 scenarios are about 0.1 g, and the M5.8 hypothetical Lake County earthquake ranges from 0.2 – 0.4 g. Thus both the scenario and probabilistic seismic hazard maps show similar ground motion levels at short and long periods due to the close proximity of ruptures and the effect of soils of the Mississippi embayment.
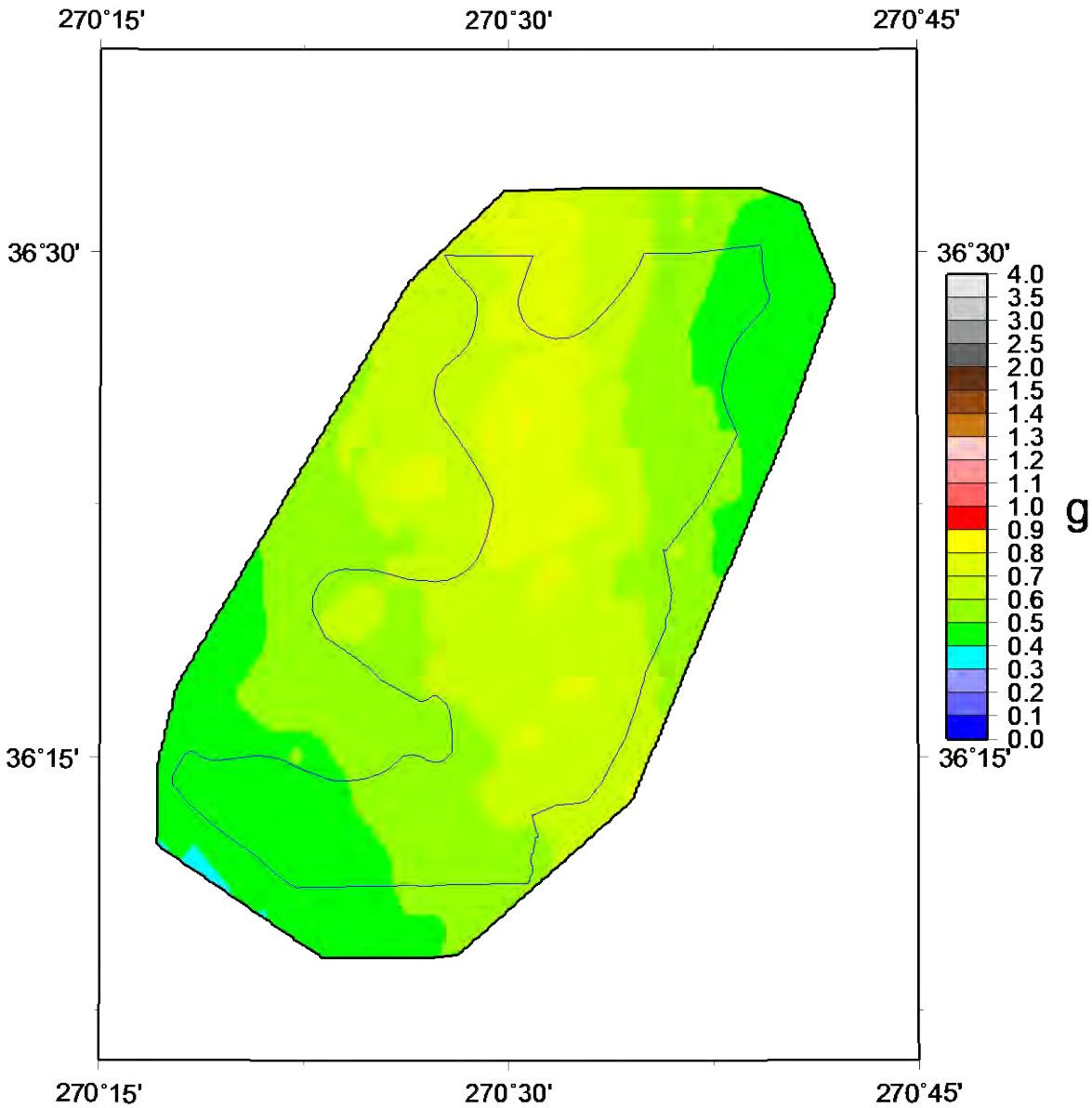
Figure 56A: Scenario PGA hazard map for a M7.7 earthquake on the Reelfoot Thrust (central segment of NMSZ) for Lake County with the effects of local geology.
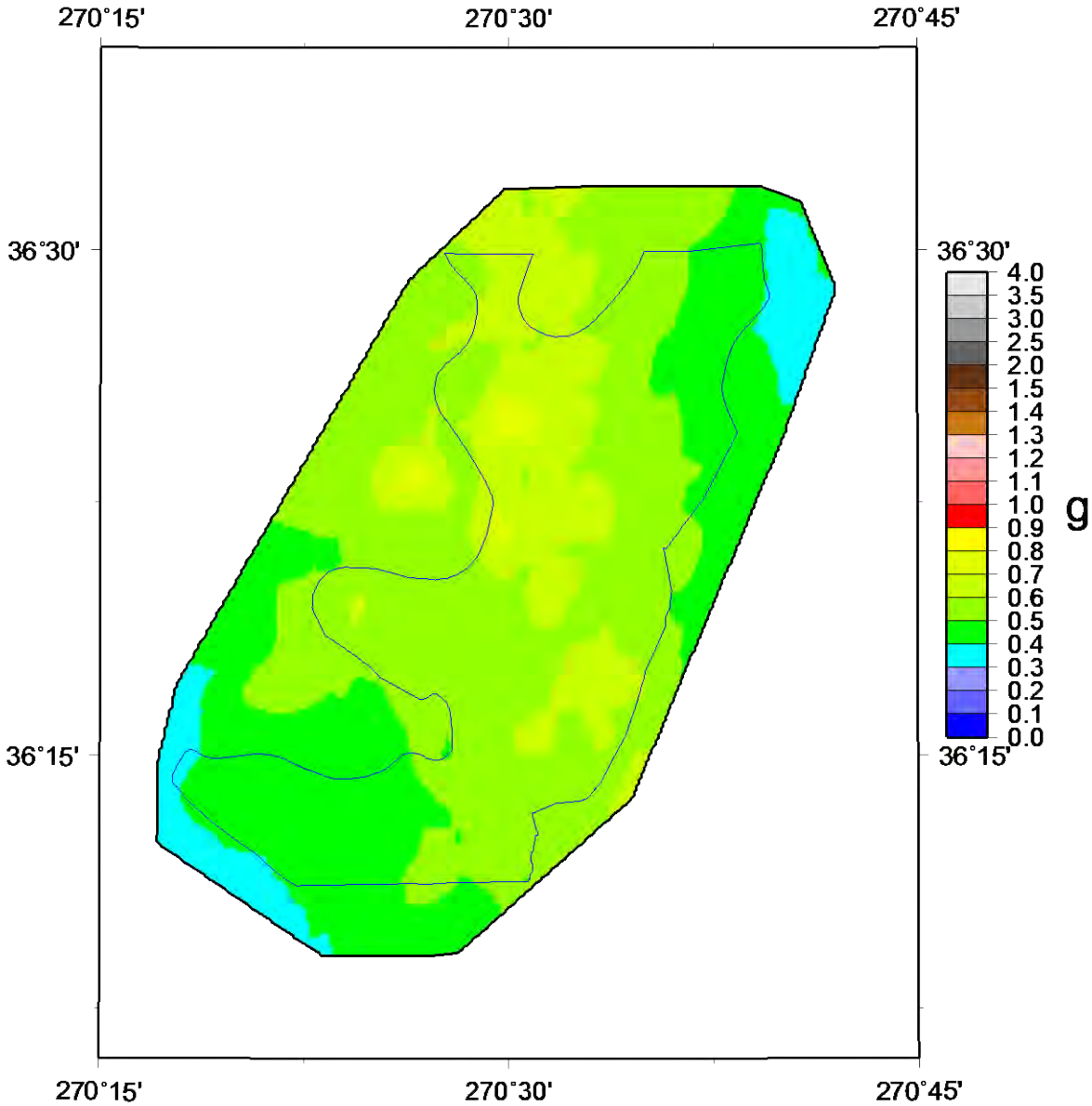
Figure 56B: Scenario 0.2 s hazard map for a M7.7 earthquake on the Reelfoot Thrust (central segment of NMSZ) for Lake County with the effects of local geology.
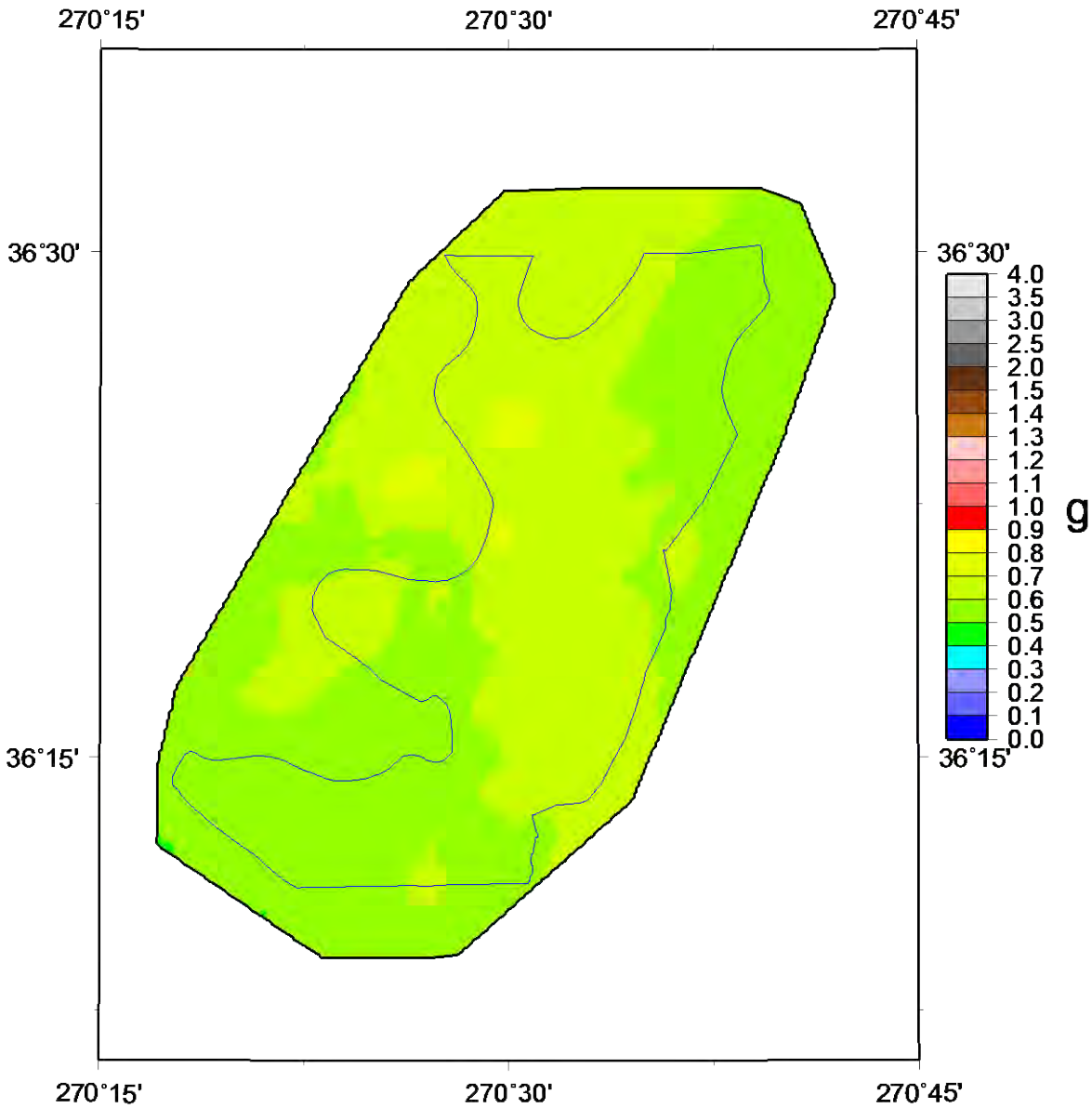
Figure 56C: Scenario 1.0 s hazard map for a M7.7 earthquake on the Reelfoot Thrust (central segment of NMSZ) for Lake County with the effects of local geology
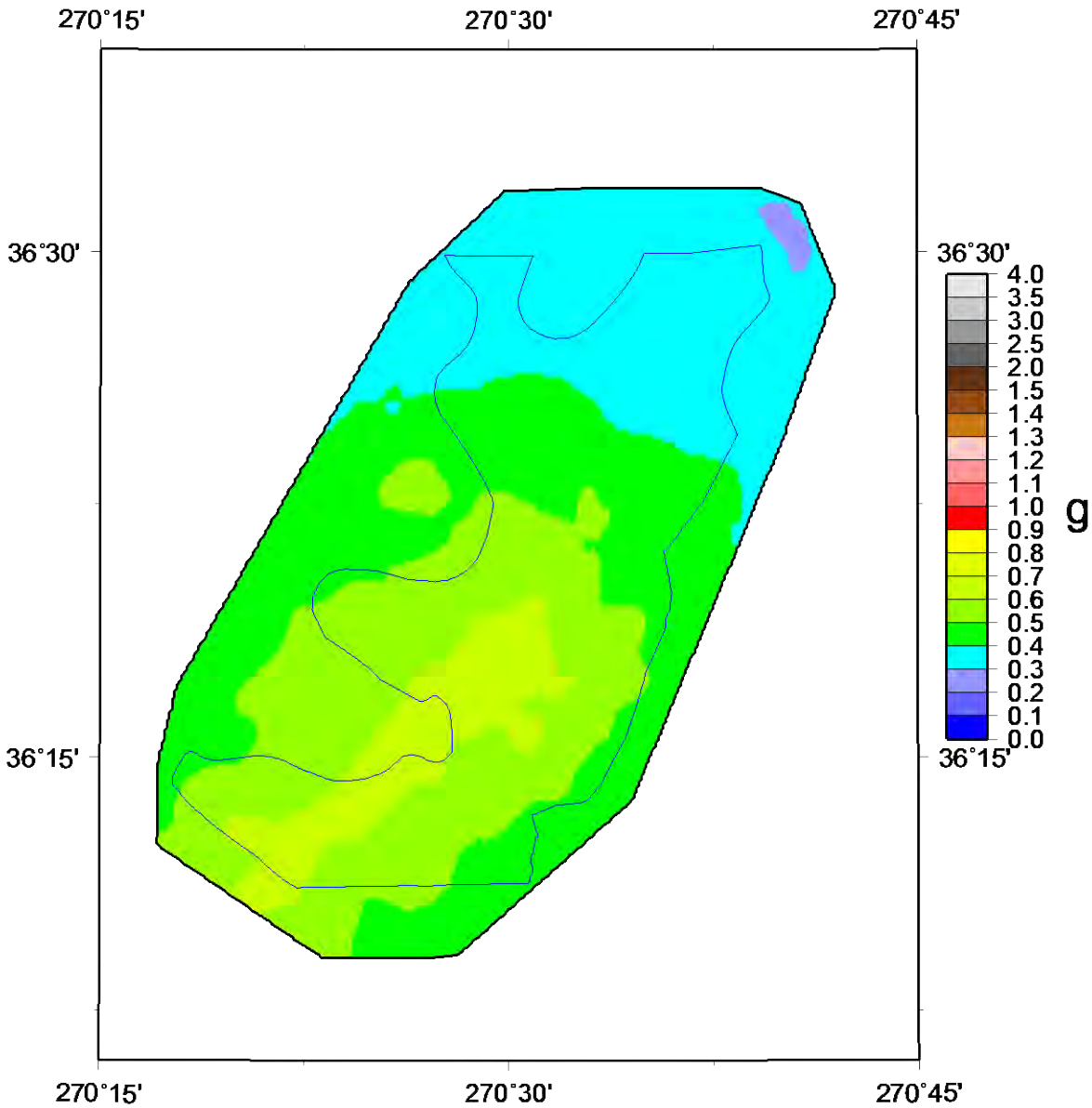
Lake Co PGA Hazard

NMSW M7.5, March 2018

Figure 57A: Scenario PGA hazard map for a M7.5 earthquake on the Cottonwood Grove Fault (SW segment of NMSZ) for Lake County with the effects of local geology.
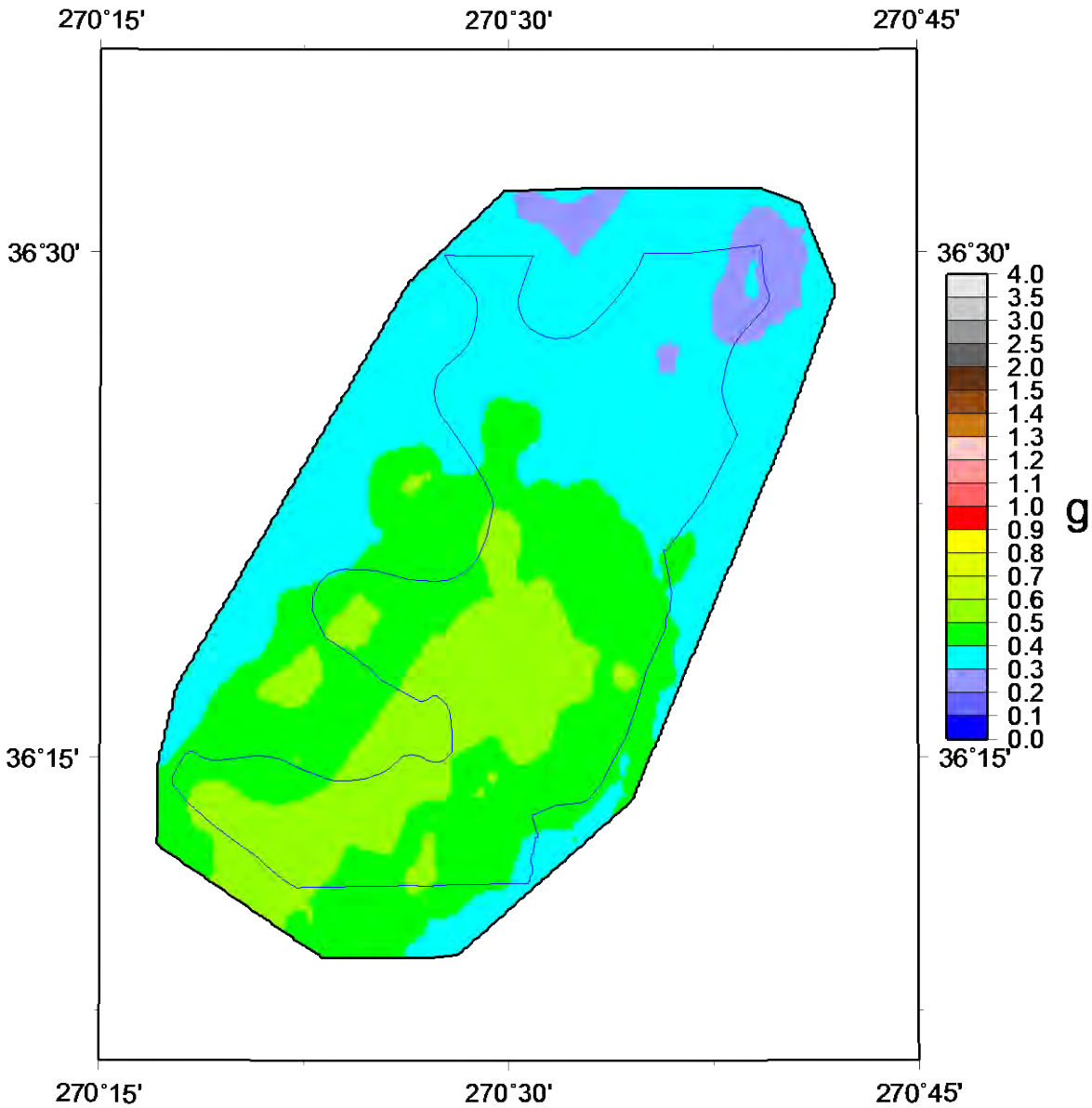
Lake Co 0.2s Hazard

Figure 57B: Scenario 0.2 s hazard map for a M7.5 earthquake on the Cottonwood Grove Fault (SW segment of NMSZ) for Lake County with the effects of local geology.
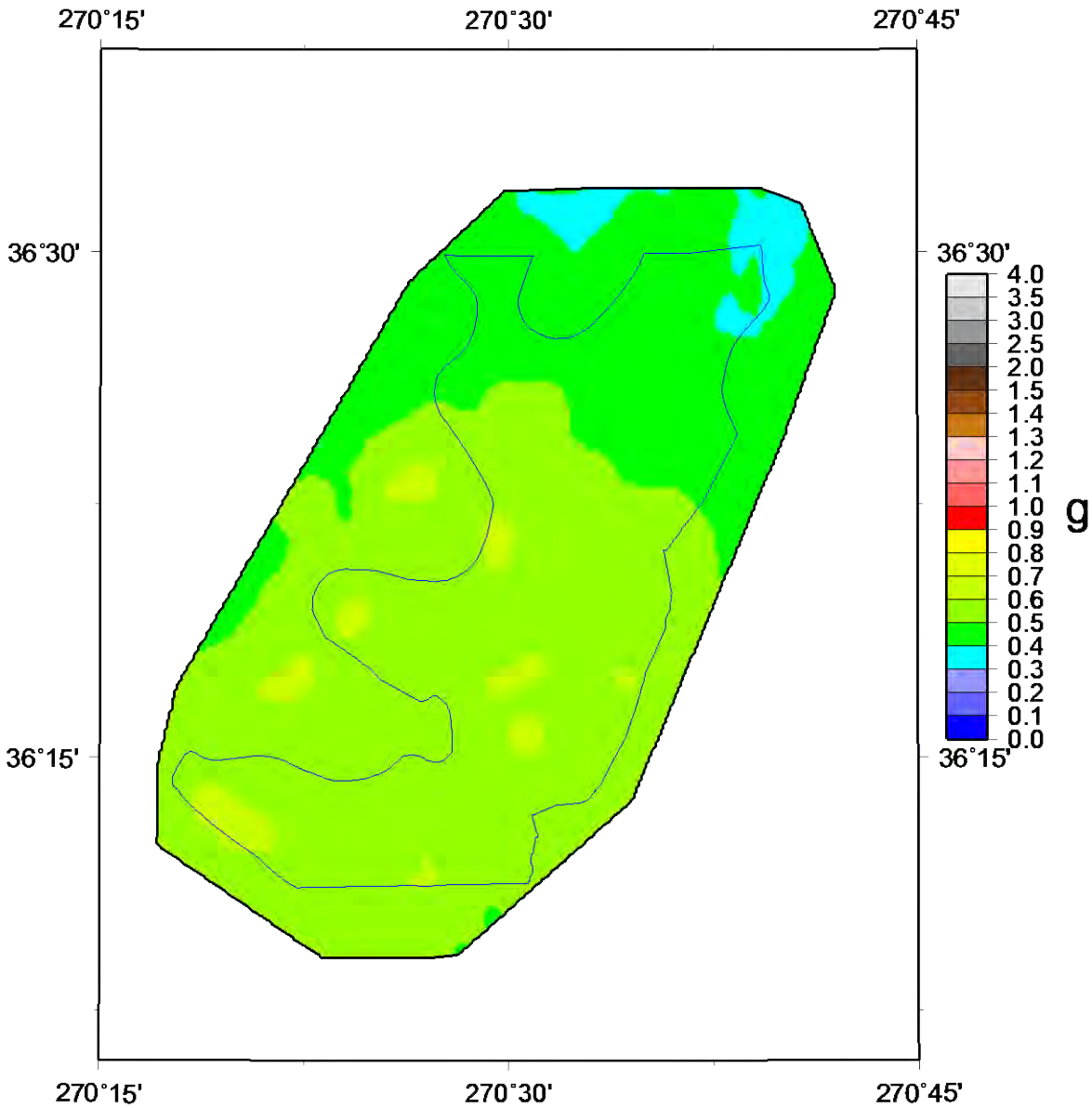
Lake Co 1.0s Hazard

NMSW M7.5, March 2018

Figure 57C: Scenario 1.0 s hazard map for a M7.5 earthquake on the Cottonwood Grove Fault (SW segment of NMSZ) for Lake County with the effects of local geology.
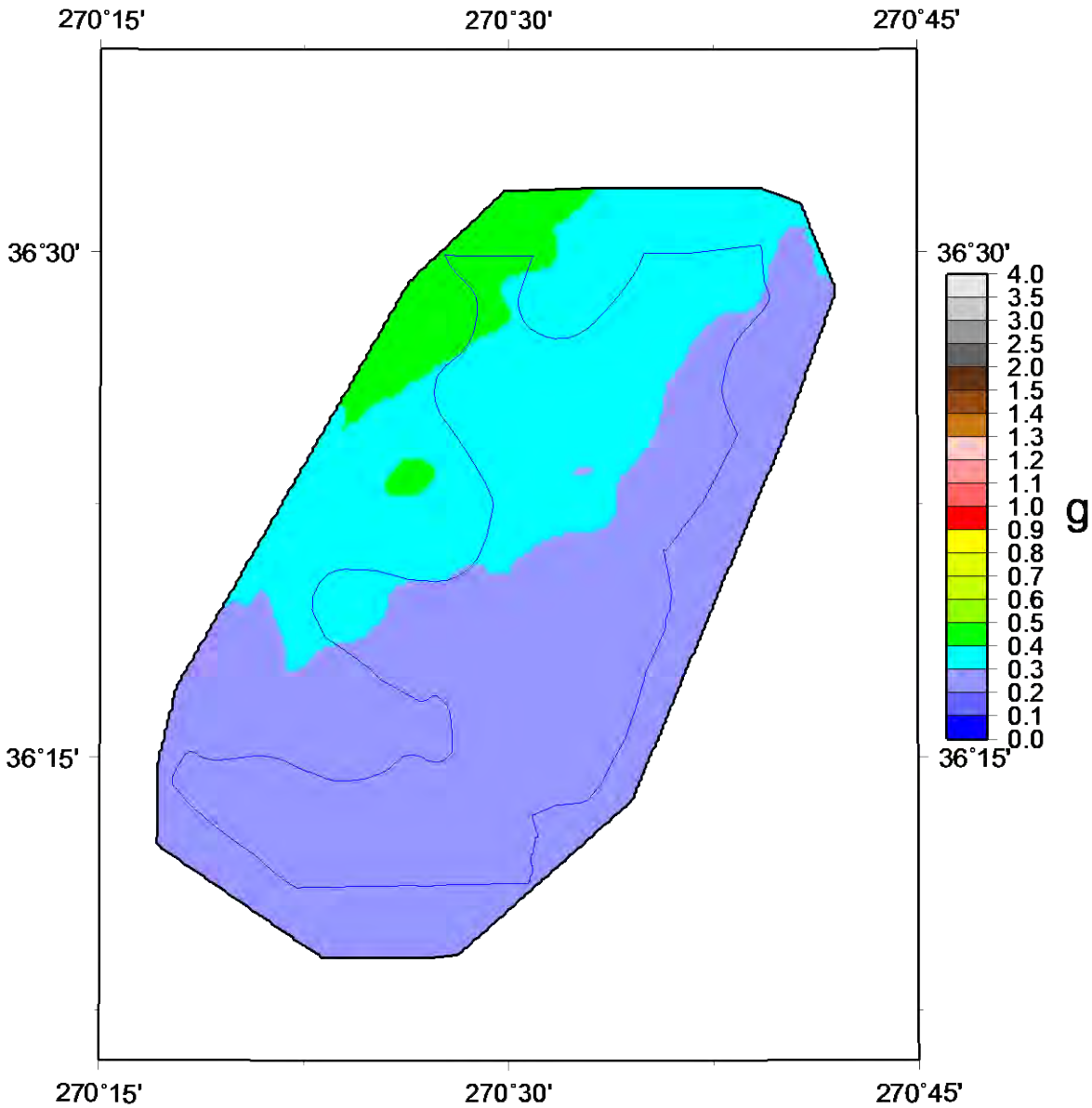
Figure 58A: Scenario PGA hazard map for a M7.3 earthquake on the New Madrid North Fault (NE segment of NMSZ) for Lake County with the effects of local geology.
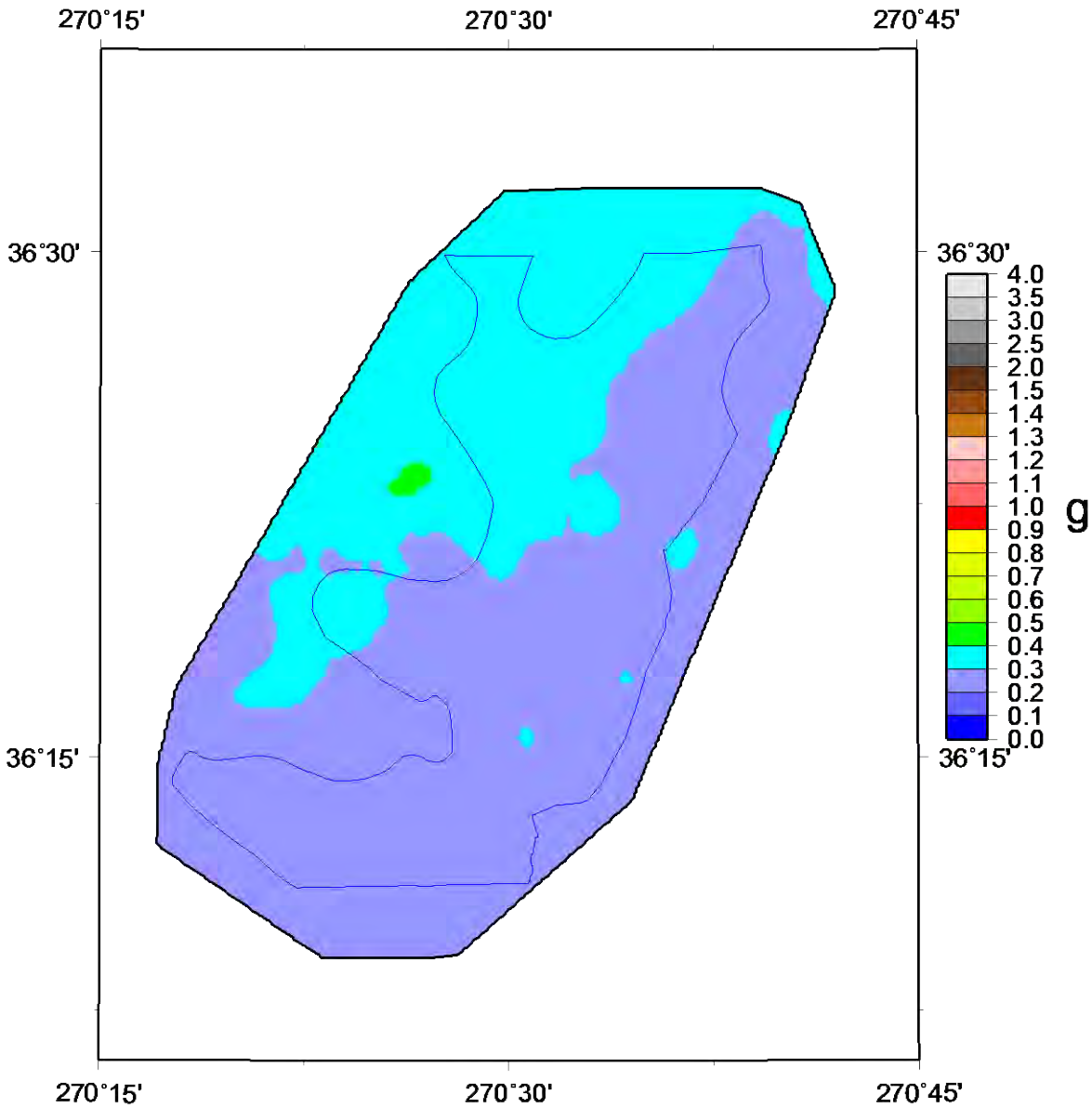
Lake Co 0.2s Hazard

NMNE M7.3, March 2018

Figure 58B: Scenario 0.2 s hazard map for a M7.3 earthquake on the New Madrid North Fault (NE segment of NMSZ) for Lake County with the effects of local geology.
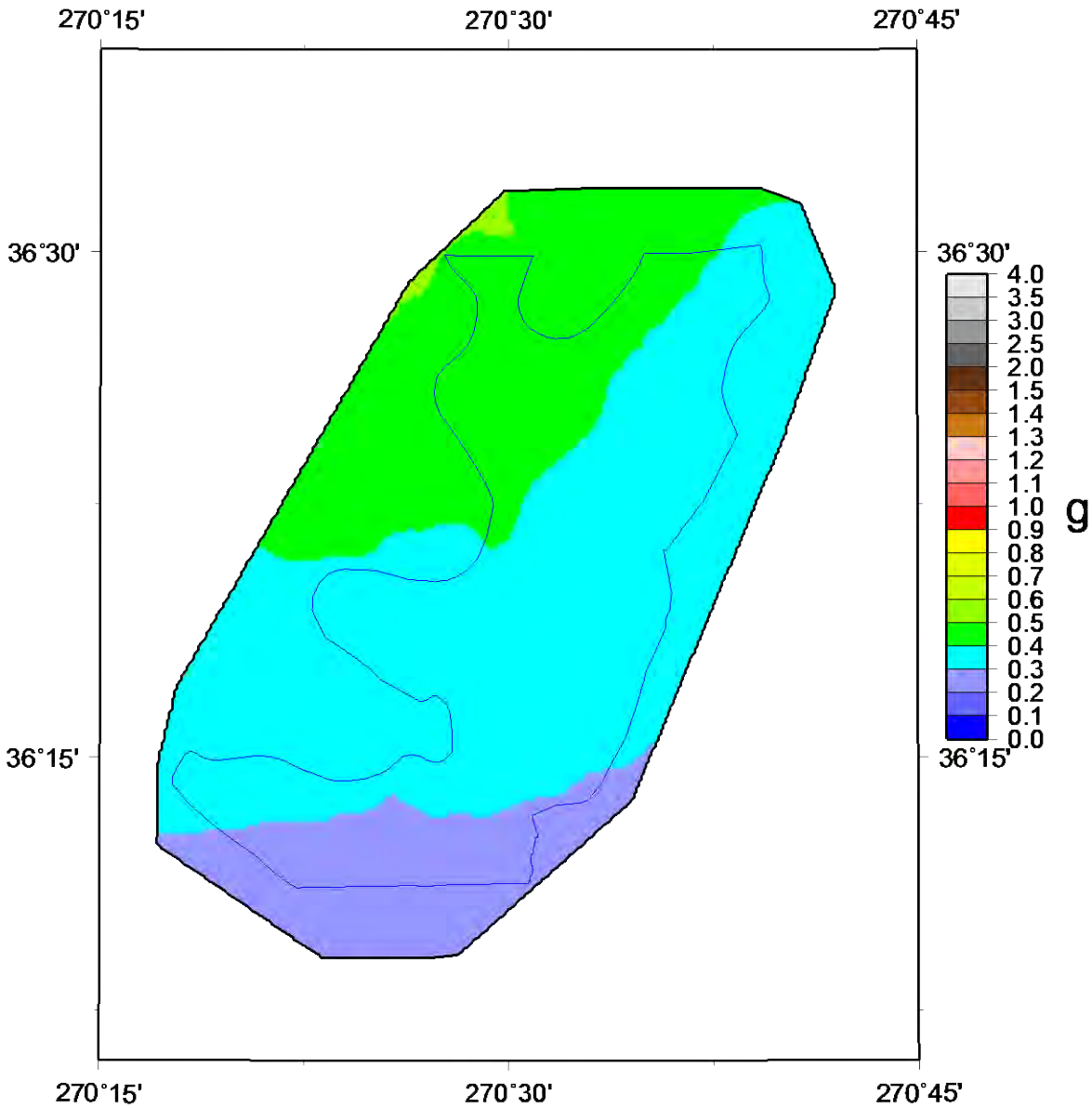
Lake Co 1.0s Hazard

NMNE M7.3, March 2018

Figure 58C: Scenario 1.0 s hazard map for a M7.3 earthquake on the New Madrid North Fault (NE segment of NMSZ) for Lake County with the effects of local geology.
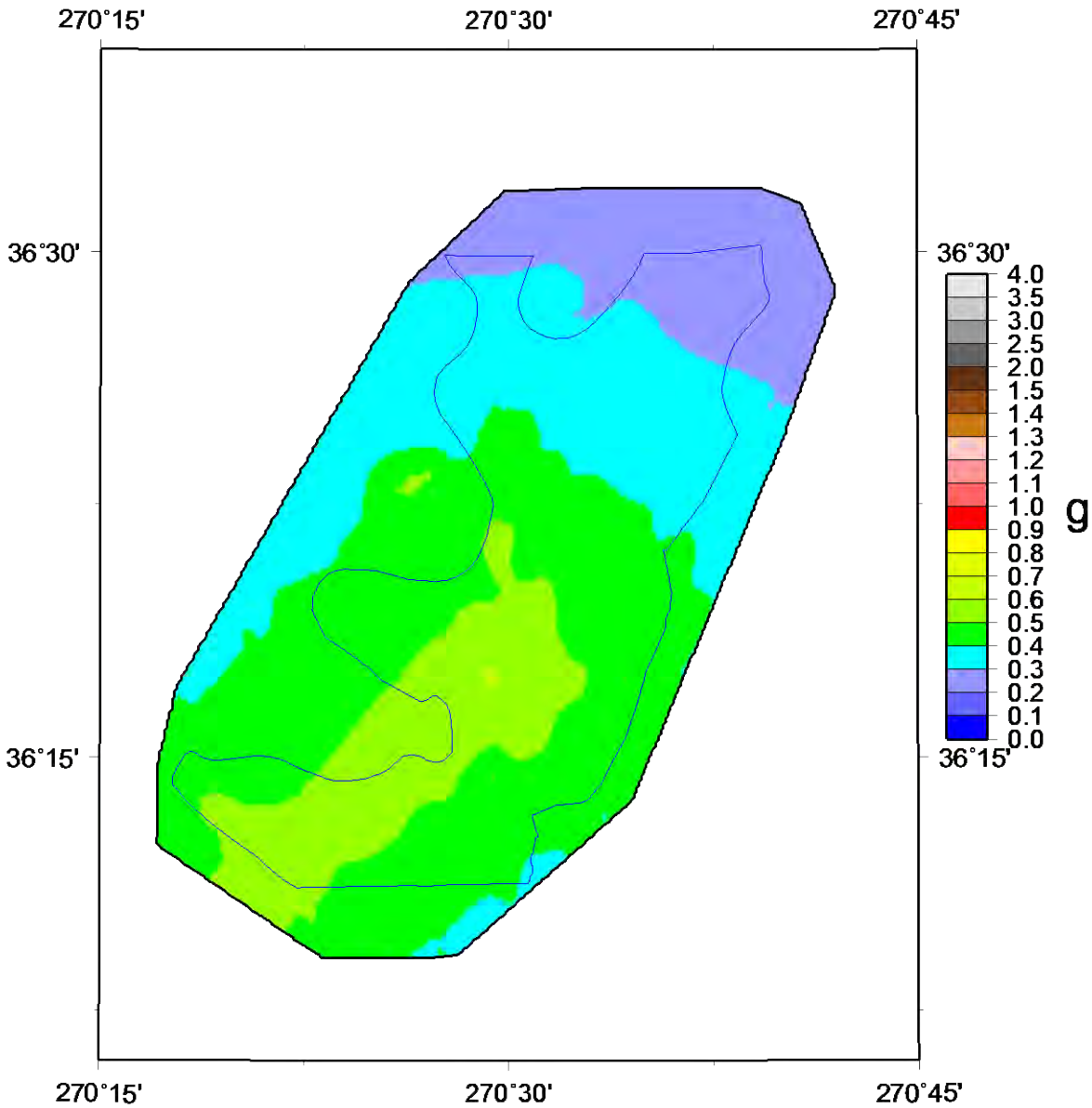
Figure 59A: Scenario PGA hazard map for a M6.9 "Dawn" aftershock (alt. 1) on the Cottonwood Grove Fault (SW segment of NMSZ) for Lake County with the effects of local geology.
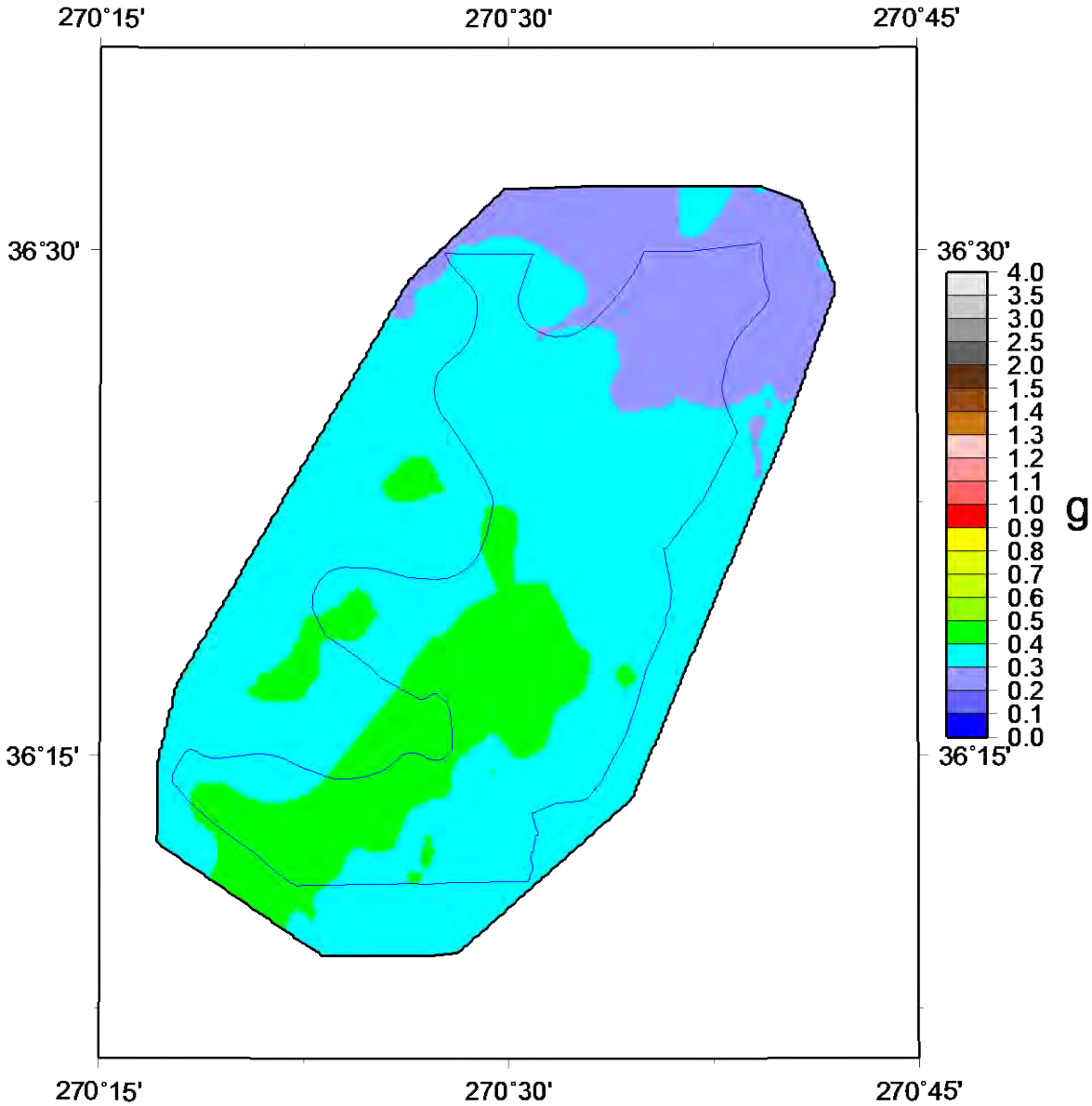
Figure 59B: Scenario 0.2 s hazard map for a M6.9 "Dawn" aftershock (alt. 1) on the Cottonwood Grove Fault (SW segment of NMSZ) for Lake County with the effects of local geology.
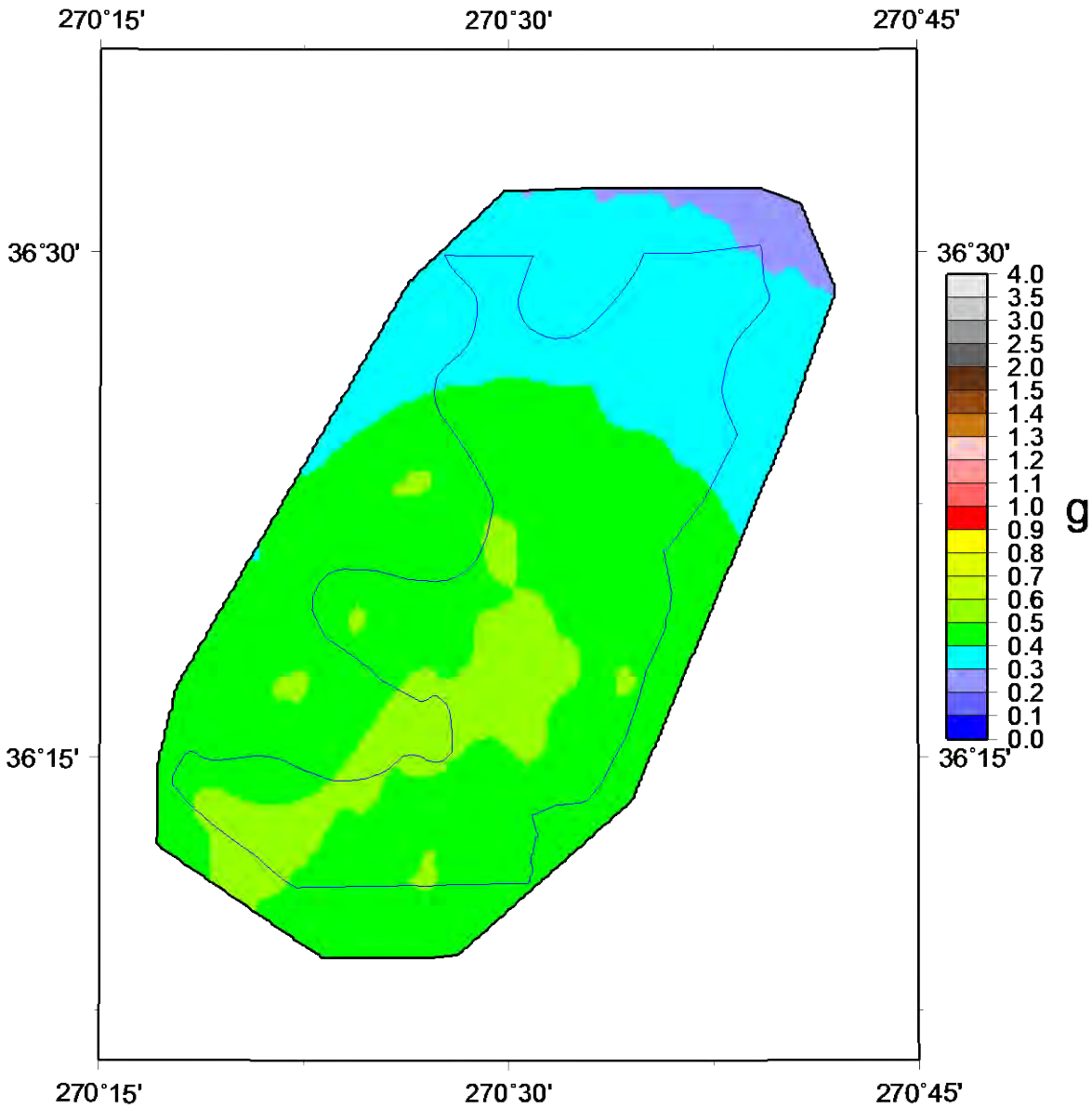
Figure 59C: Scenario 1.0 s hazard map for a M6.9 "Dawn" aftershock (alt. 1) on the Cottonwood Grove Fault (SW segment of NMSZ) for Lake County with the effects of local geology.
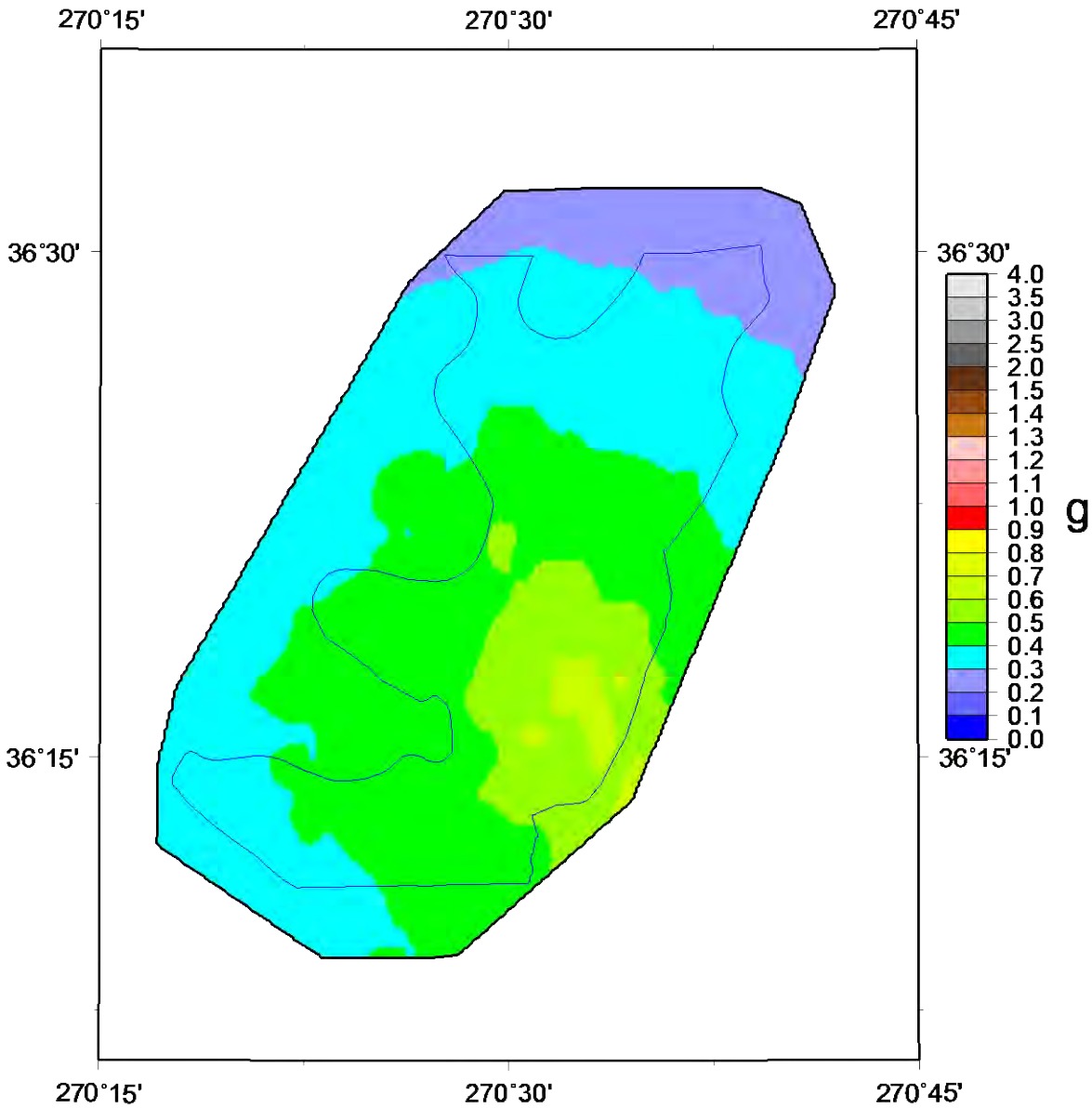
Lake Co PGA Hazard

NMRTA M6.9, March 2018

Figure 60A: Scenario PGA hazard map for a M6.9 "Dawn" aftershock (alt. 2) on the Reelfoot Thrust (central segment of NMSZ) for Lake County with the effects of local geology.

Figure 60B: Scenario 0.2 s hazard map for a M6.9 "Dawn" aftershock (alt. 2) on the Reelfoot Thrust (central segment of NMSZ) for Lake County with the effects of local geology.

Figure 60C: Scenario 1.0 s hazard map for a M6.9 "Dawn" aftershock (alt. 2) on the Reelfoot Thrust (central segment of NMSZ) for Lake County with the effects of local geology.
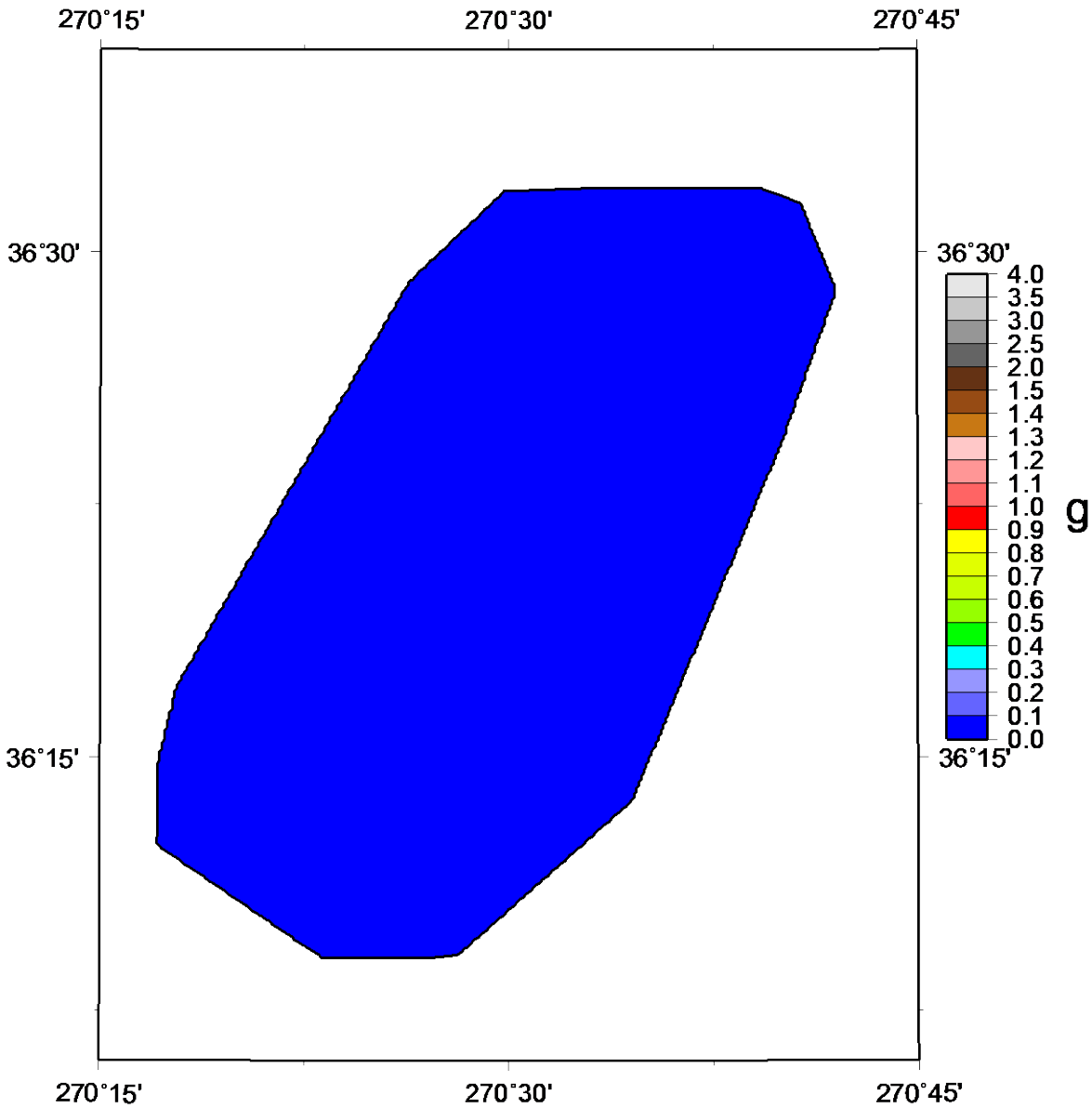
Lake Co PGA Hazard

NMMT M6.2, March 2018

Figure 61A: Scenario PGA hazard map for a M6.2 on the Cottonwood Grove Fault (1843 Marked Tree – SW segment of NMSZ) for Lake County with the effects of local geology.
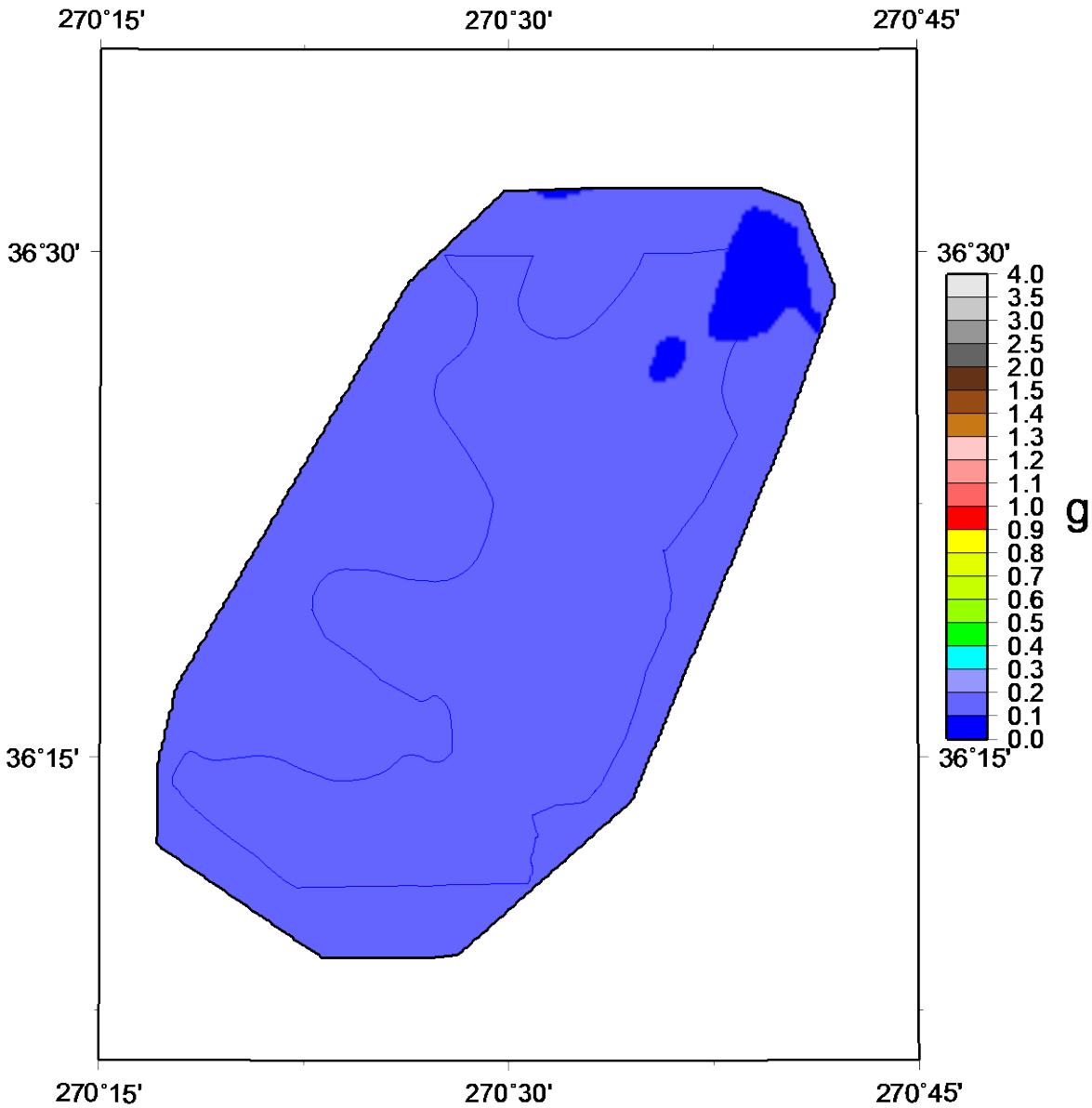
Figure 61B: Scenario 0.2 s hazard map for a M6.2 on the Cottonwood Grove Fault (1843 Marked Tree – SW segment of NMSZ) for Lake County with the effects of local geology.
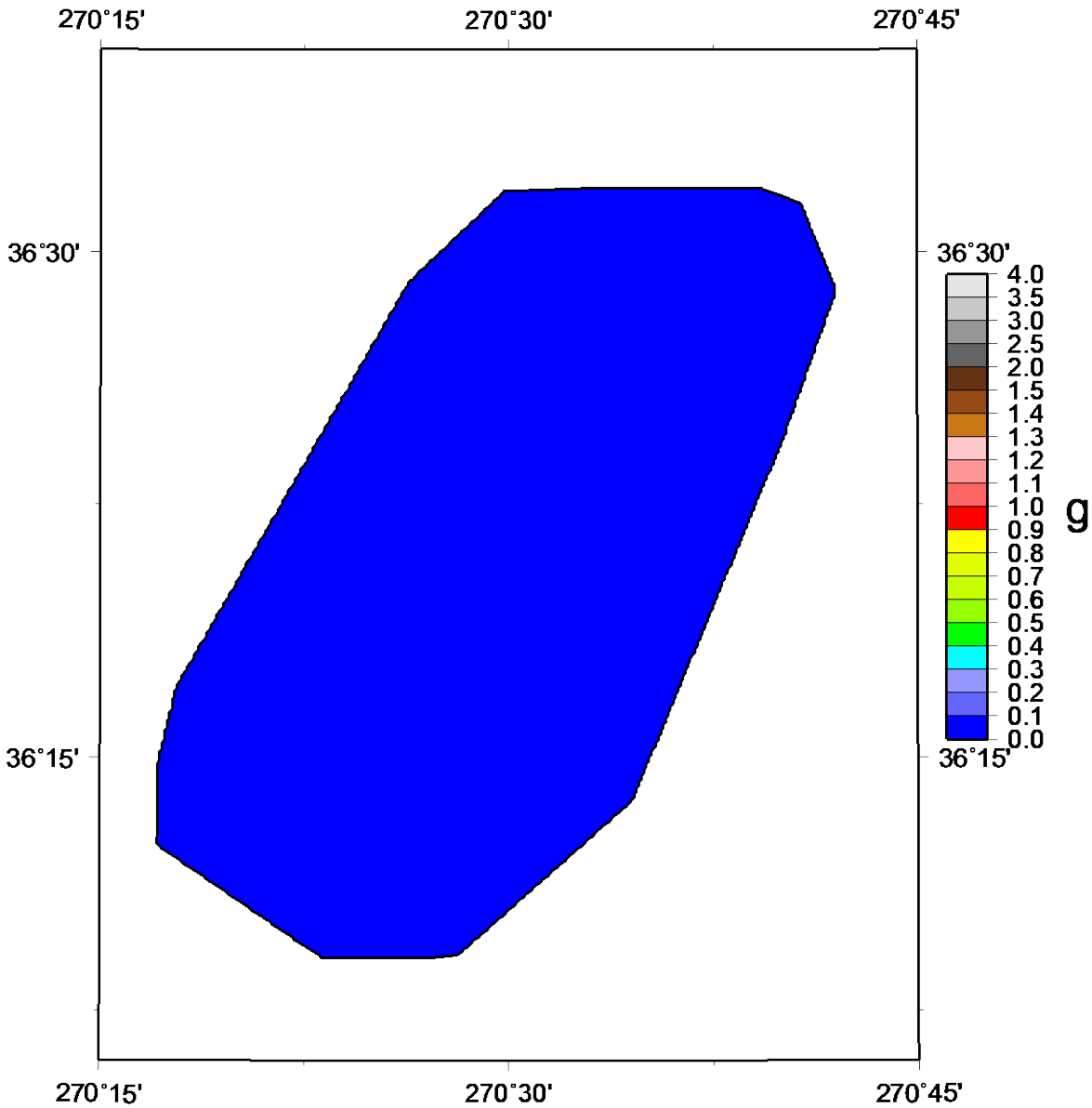
Figure 61C: Scenario 1.0 s hazard map for a M6.2 on the Cottonwood Grove Fault (1843 Marked Tree – SW segment of NMSZ) for Lake County with the effects of local geology.
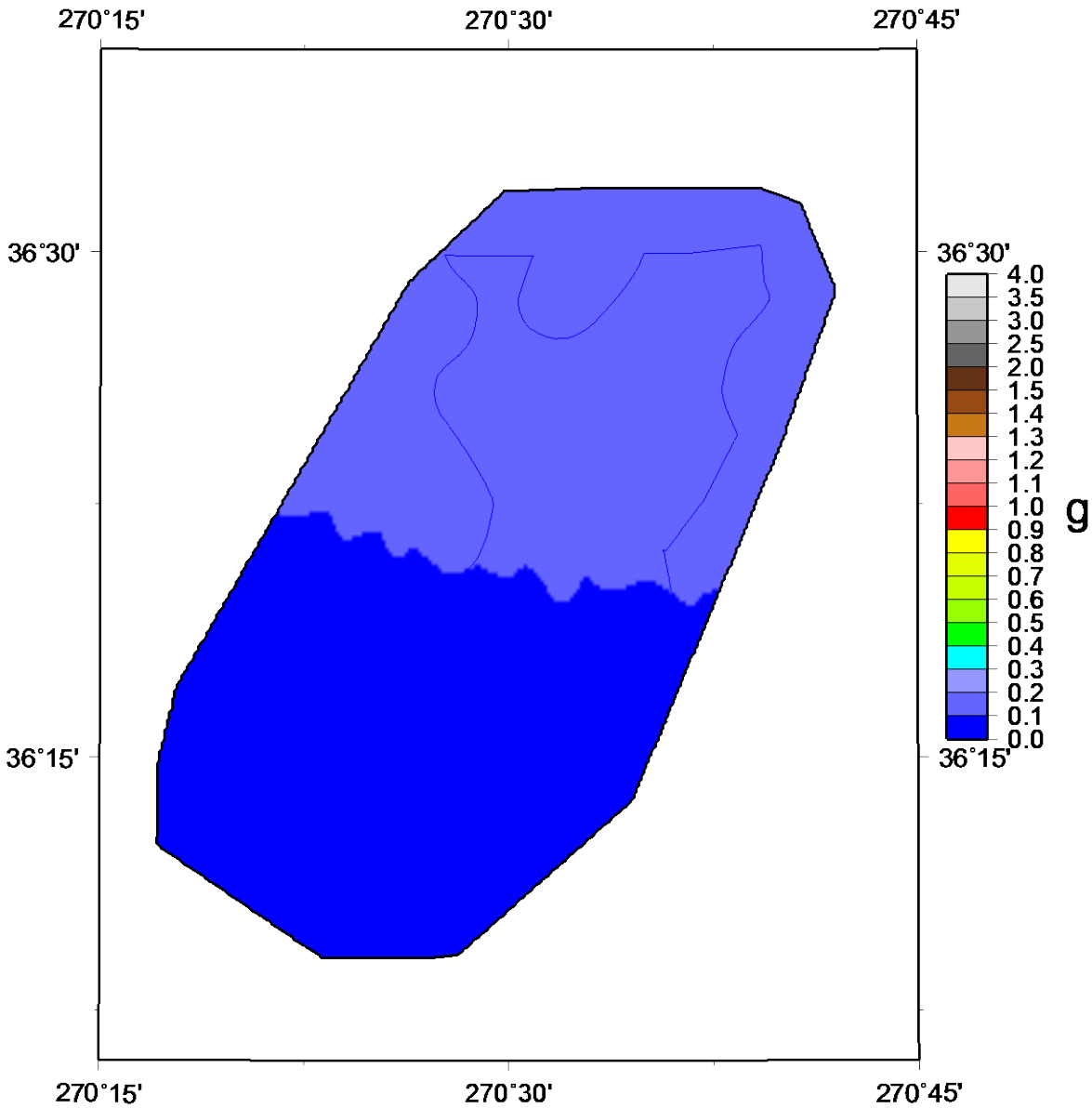
Figure 62A: Scenario PGA hazard map for a M6.2 on the New Madrid North Fault (1895 Charleston, MO – SW segment of NMSZ) for Lake County with the effects of local geology.
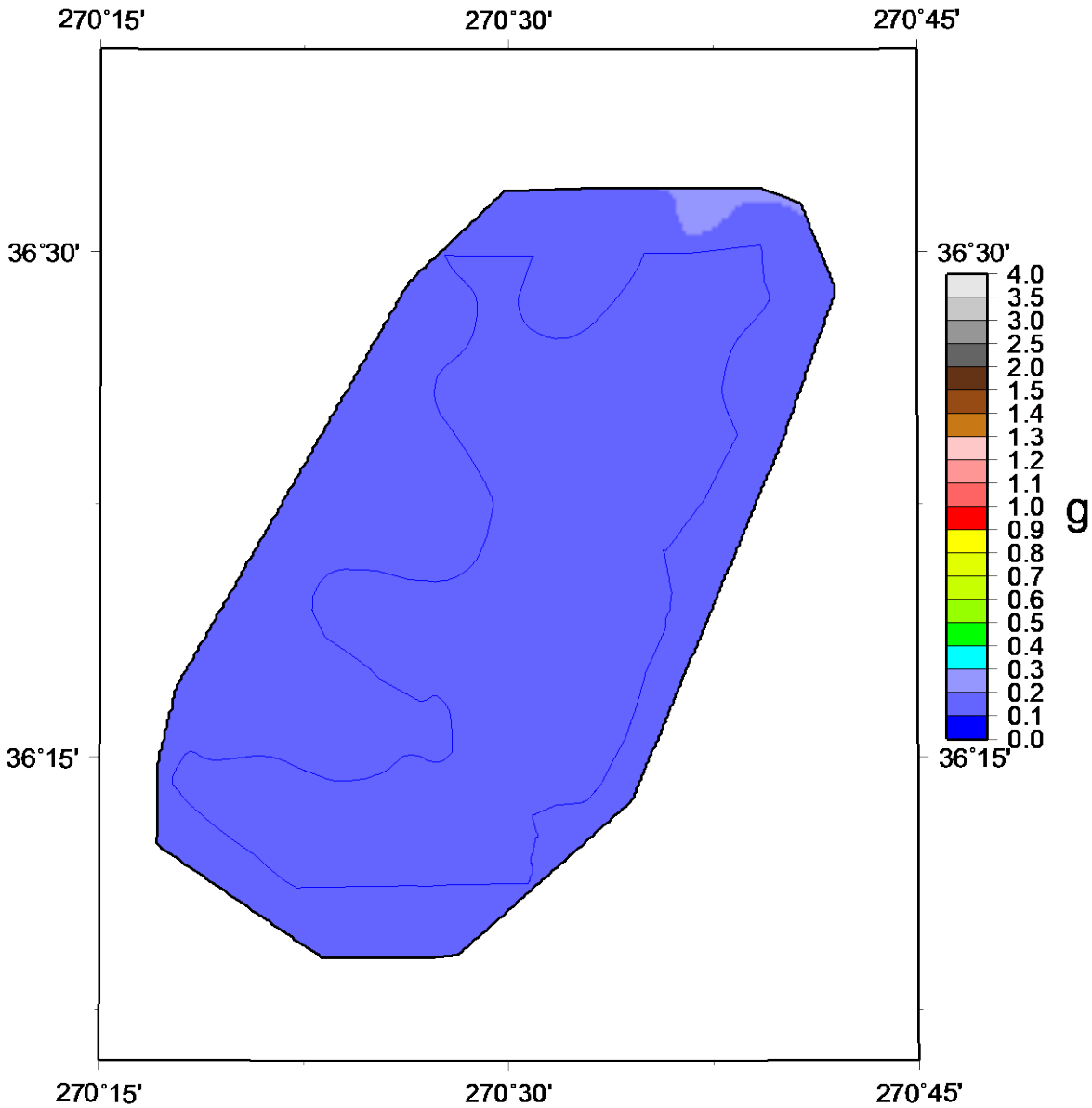
Lake Co 0.2s Hazard

NMCM M6.2, March 2018

Figure 62B: Scenario 0.2 s hazard map for a M6.2 on the New Madrid North Fault (1895 Charleston, MO – SW segment of NMSZ) for Lake County with the effects of local geology.
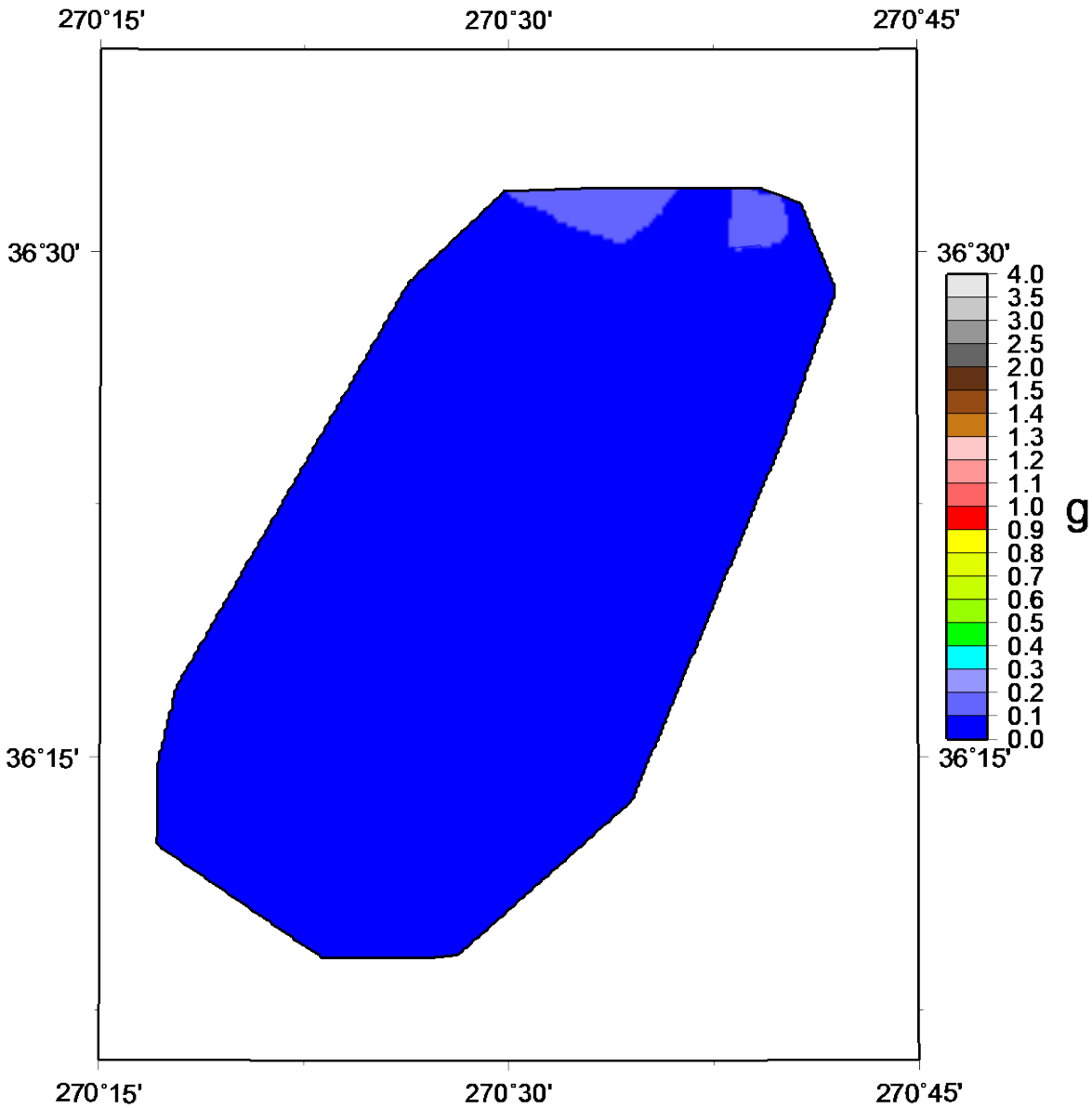
Figure 62C: Scenario 1.0 s hazard map for a M6.2 on the New Madrid North Fault (1895 Charleston, MO – SW segment of NMSZ) for Lake County with the effects of local geology.
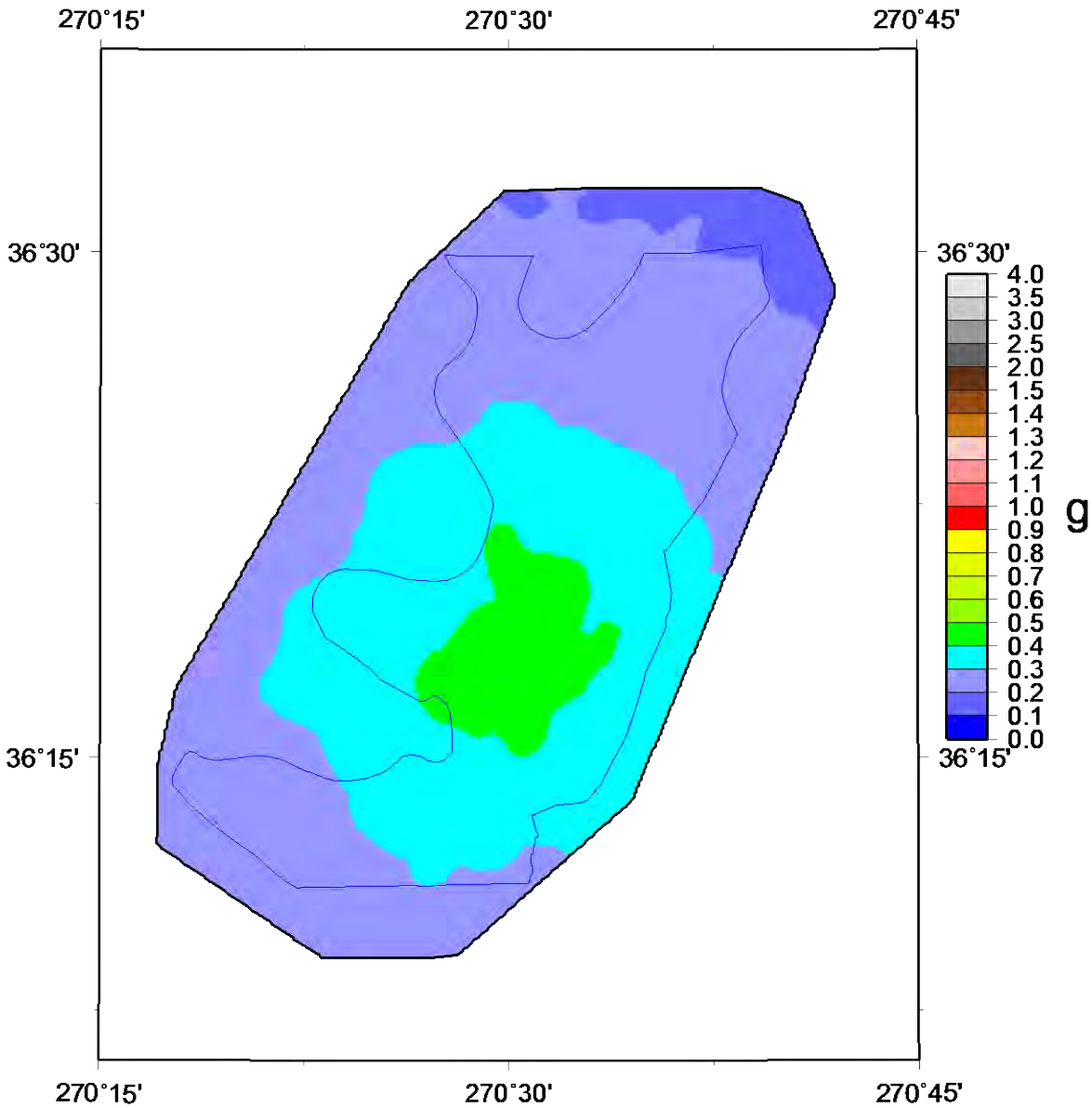
Lake Co PGA Hazard

LACO M5.8, March 2018

Figure 63A: Scenario PGA hazard map for a M5.8 hypothetical Lake County earthquake (between Tiptonville and Ridgely) for Lake County with the effects of local geology.
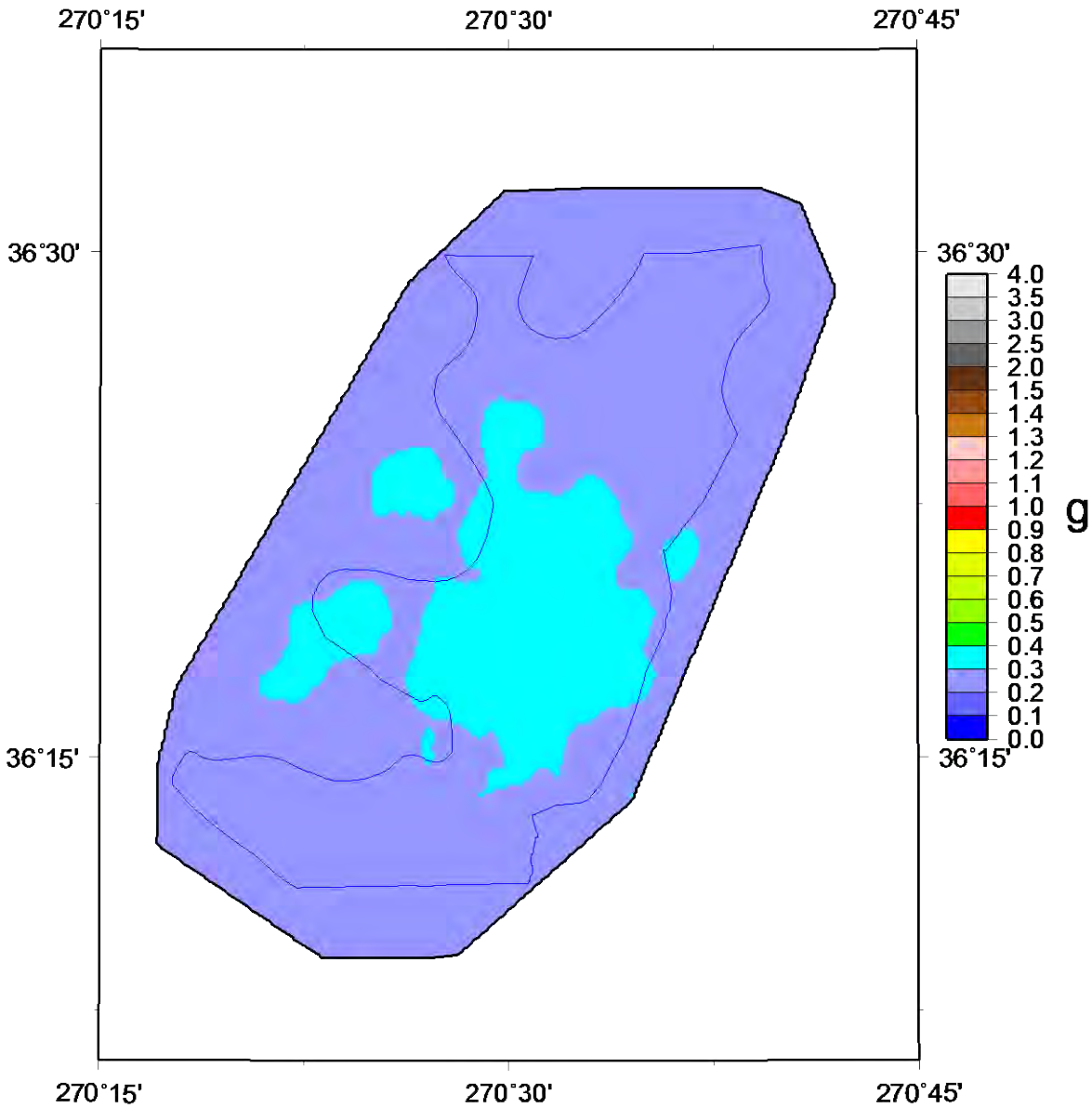
Lake Co 0.2s Hazard

LACO M5.8, March 2018

Figure 63B: Scenario 0.2 s hazard map for a M5.8 hypothetical Lake County earthquake (between Tiptonville and Ridgely) for Lake County with the effects of local geology.
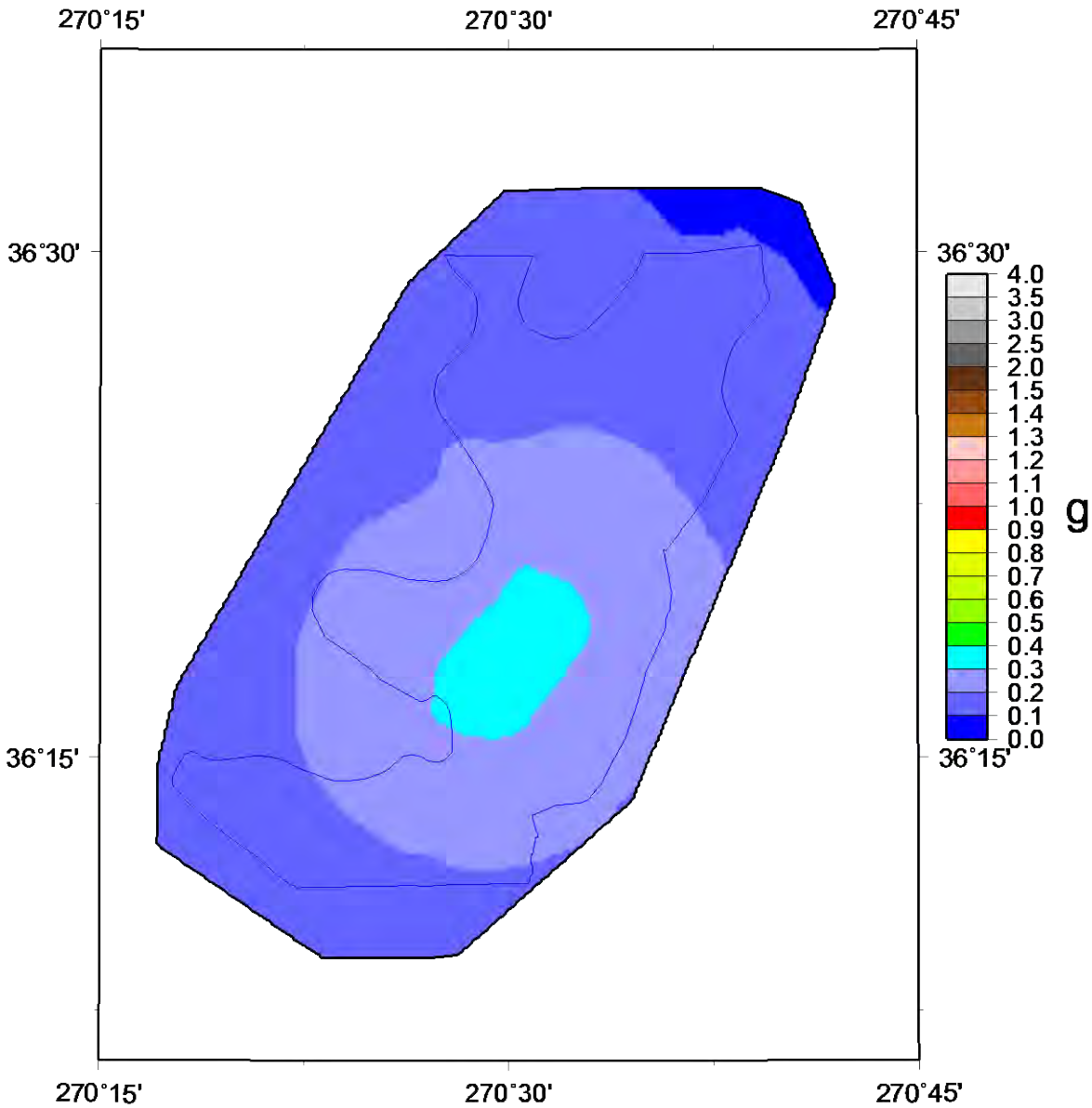
Figure 63C: Scenario 1.0 s hazard map for a M5.8 hypothetical Lake County earthquake (between Tiptonville and Ridgely) for Lake County with the effects of local geology.

Liquefaction Hazard Maps

To generate the initial liquefaction hazard maps for Lake County, we used the liquefaction probability curves (LPCs) of Holzer et al. (2011) (Figure 24), which are the available published curves for the study area. We found the water table to be mostly between 1.5 and 5.0 m in Lake County, both from refraction measurements and the boring database for the county. Holzer et al. (2011) had three Mississippi alluvial flood plain LPCs (surface geology based) for two different water table levels (1.5 and 5.0 m). The LPCs are for Liquefaction Probability Index (LPI) exceeding 5, which is for the manifestation of liquefaction at the surface (moderate to severe liquefaction). Thus our liquefaction hazard maps are for the probability of moderate to severe liquefaction. To produce our initial liquefaction hazard maps we averaged the 6 Holzer et al. (2011) LPCs appropriate for Lake County (Figure 26).

Figures 64 - 71 show the two probabilistic and six scenario liquefaction hazard maps derived from the equivalent PGA seismic hazard maps show above. The probabilistic liquefaction hazard maps show 80 – 100% (2% in 50 years) and about 75% (5% in 50 years) probability of liquefaction in Lake County, which corresponds with the observed prevalence of sand blow and liquefaction features in the county. The scenario M7 SW arm and Reelfoot Thrust liquefaction hazard maps show 60 – 80% probability of liquefaction. The M7 NE arm New Madrid scenario shows 20 -70% probability of liquefaction. The largest aftershock alternatives show 30 – 70% probability of liquefaction. And the M5.8 hypothetical Lake County earthquake shows 0 – 40% probability of liquefaction (low). The 1843 and 1895 M6.2 scenarios do not produce any significant liquefaction hazard and are not shown. The liquefaction hazard is high for the near M7 and greater earthquake scenarios.
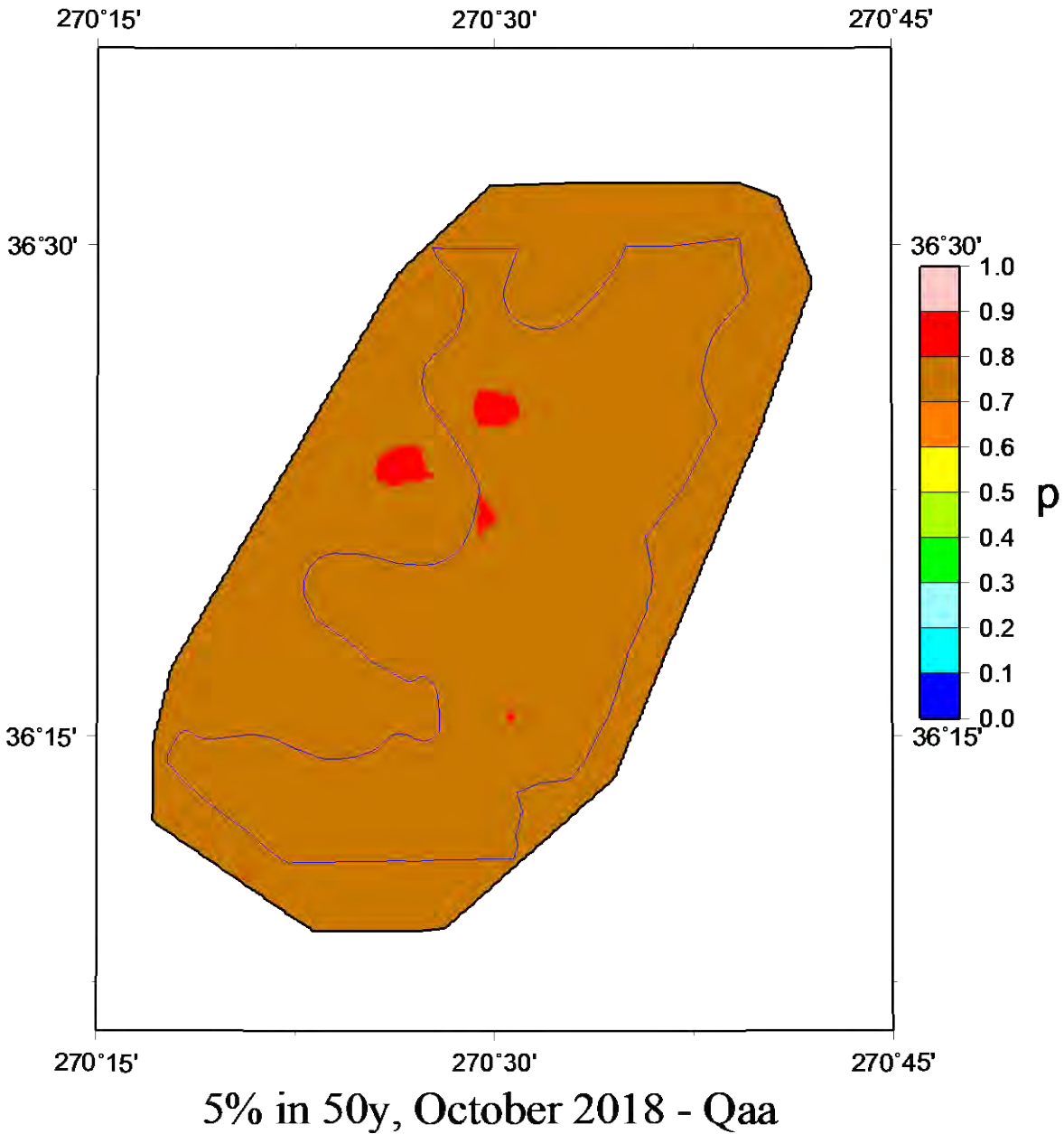
Figure 64: 5% in 50 year liquefaction hazard map for moderate to severe liquefaction at the surface (LPI > 5) for Lake County including the effects of local geology.
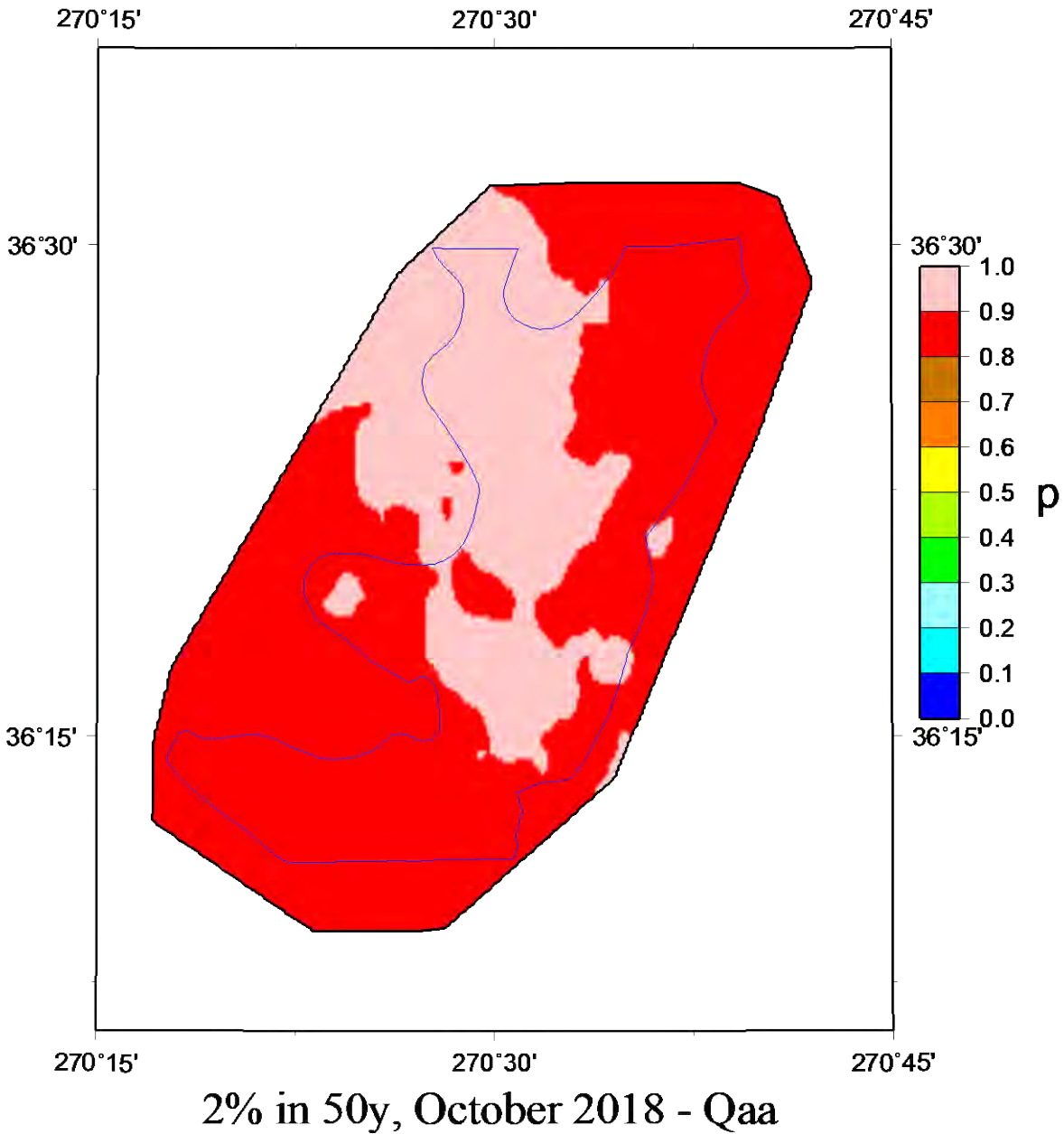
Figure 65: 2% in 50 year liquefaction hazard map for moderate to severe liquefaction at the surface (LPI > 5) for Lake County including the effects of local geology.
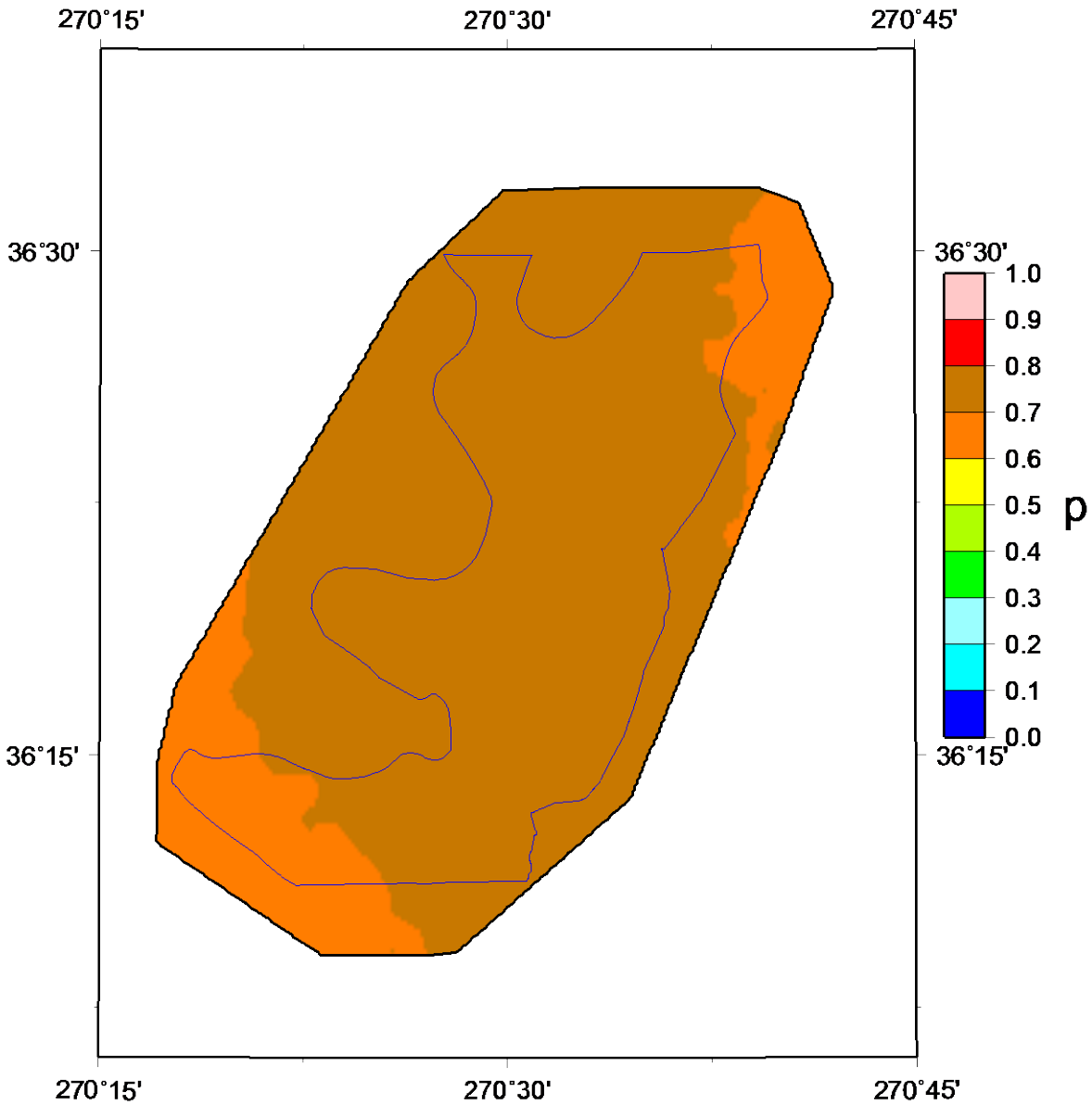
Figure 66: Scenario liquefaction hazard map for moderate to severe liquefaction at the surface (LPI > 5) for a M7.7 earthquake on the Reelfoot Thrust (central segment of NMSZ).
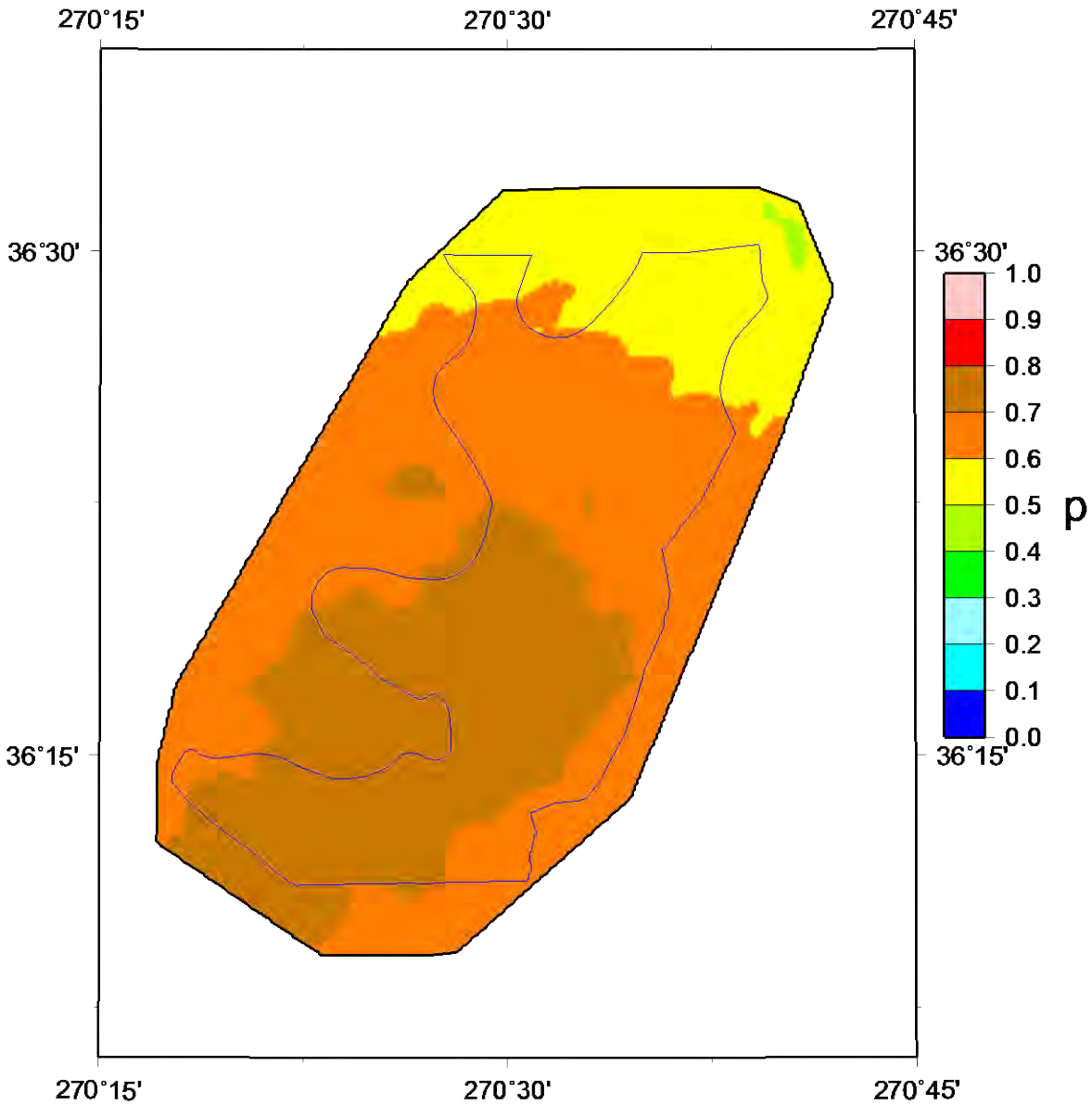
Figure 67: Scenario liquefaction hazard map for moderate to severe liquefaction at the surface (LPI > 5) for a M7.5 earthquake on the Cottonwood Grove Fault (SW segment of NMSZ).
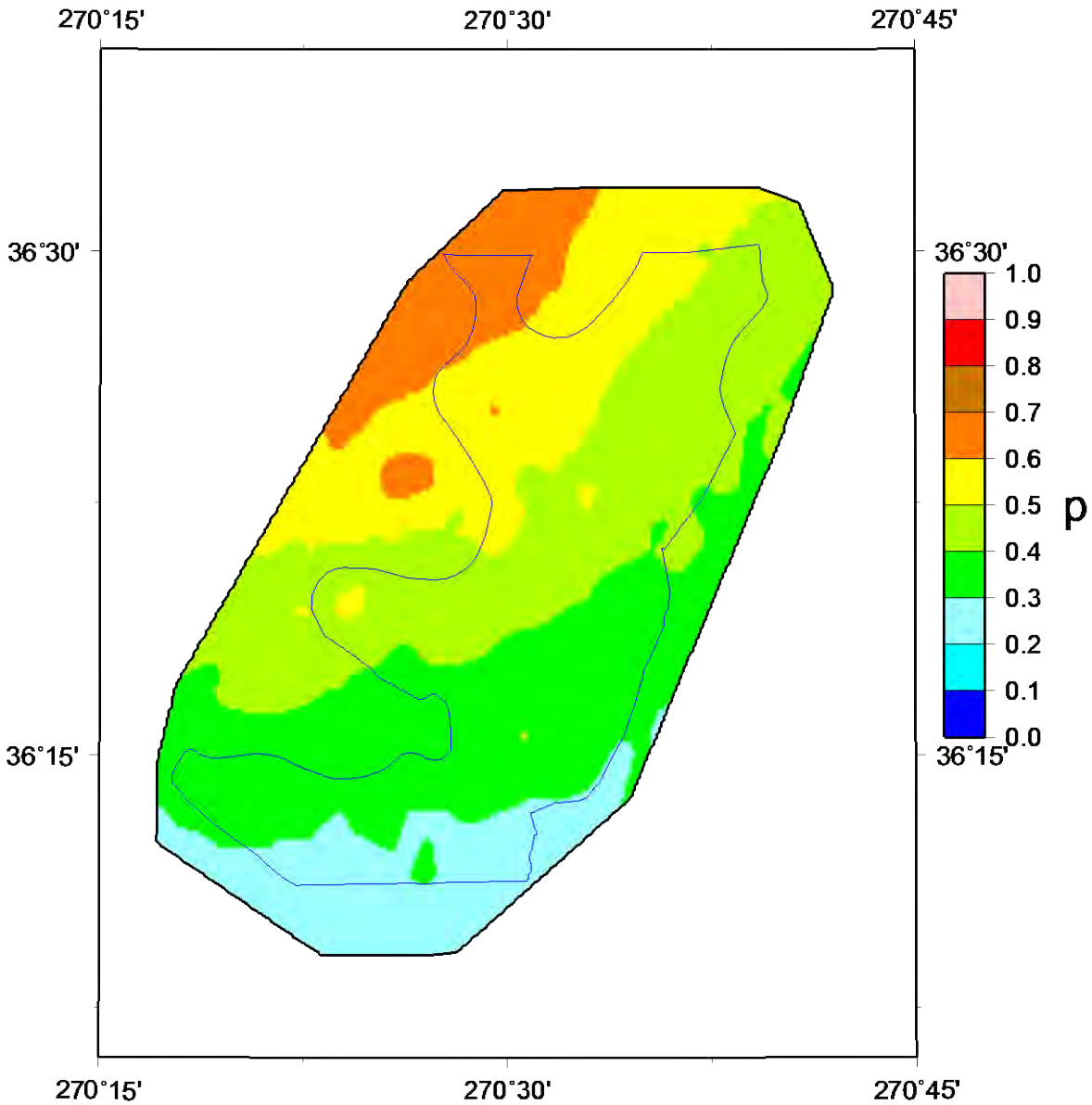
Figure 68: Scenario liquefaction hazard map for moderate to severe liquefaction at the surface (LPI > 5) for a M7.3 earthquake on the New Madrid North Fault (NE segment of NMSZ).
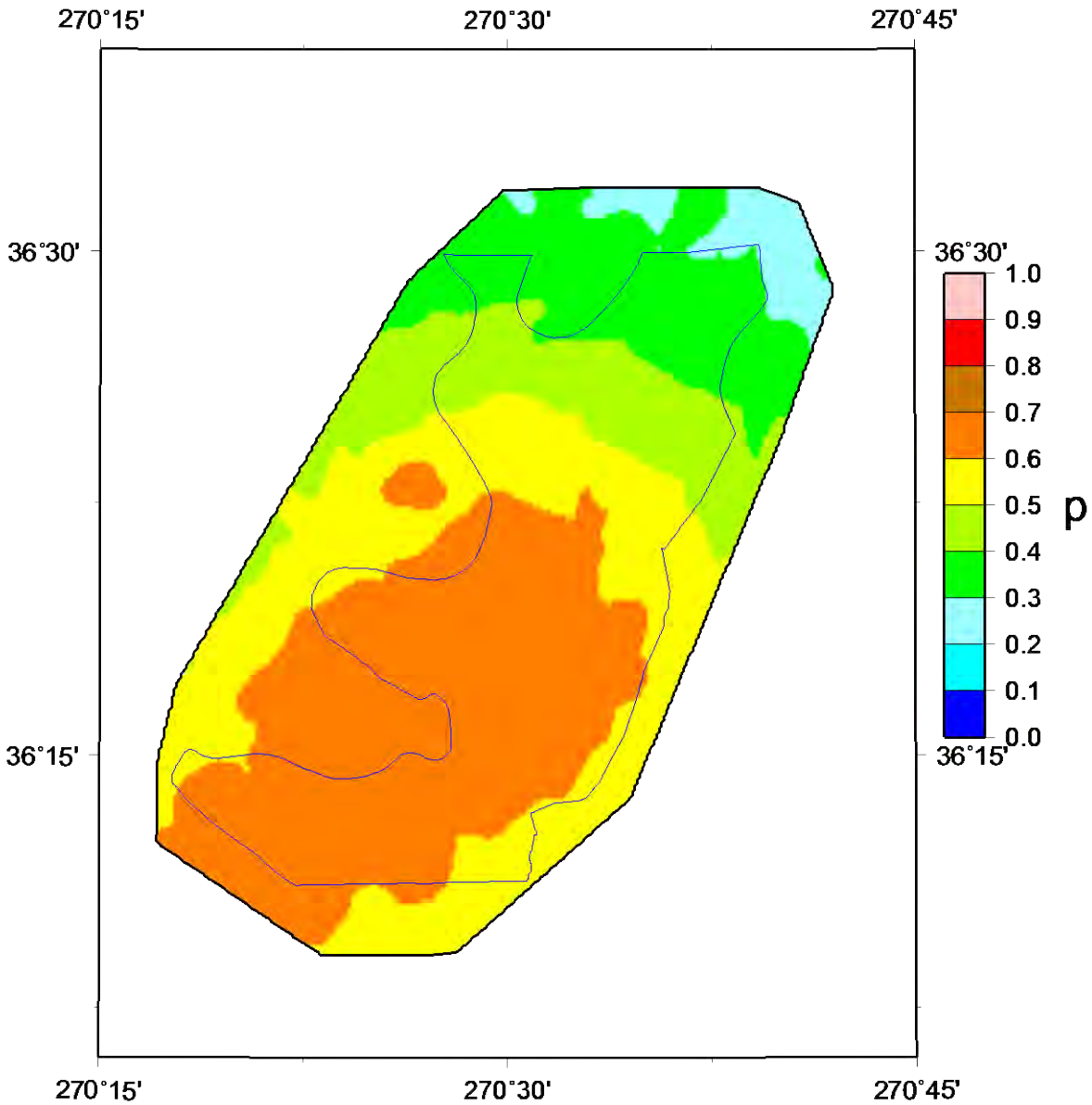
Figure 69: Scenario liquefaction hazard map for moderate to severe liquefaction (LPI > 5) for a M6.9 "Dawn" aftershock (alt. 1) on the Cottonwood Grove Fault (SW segment of NMSZ).
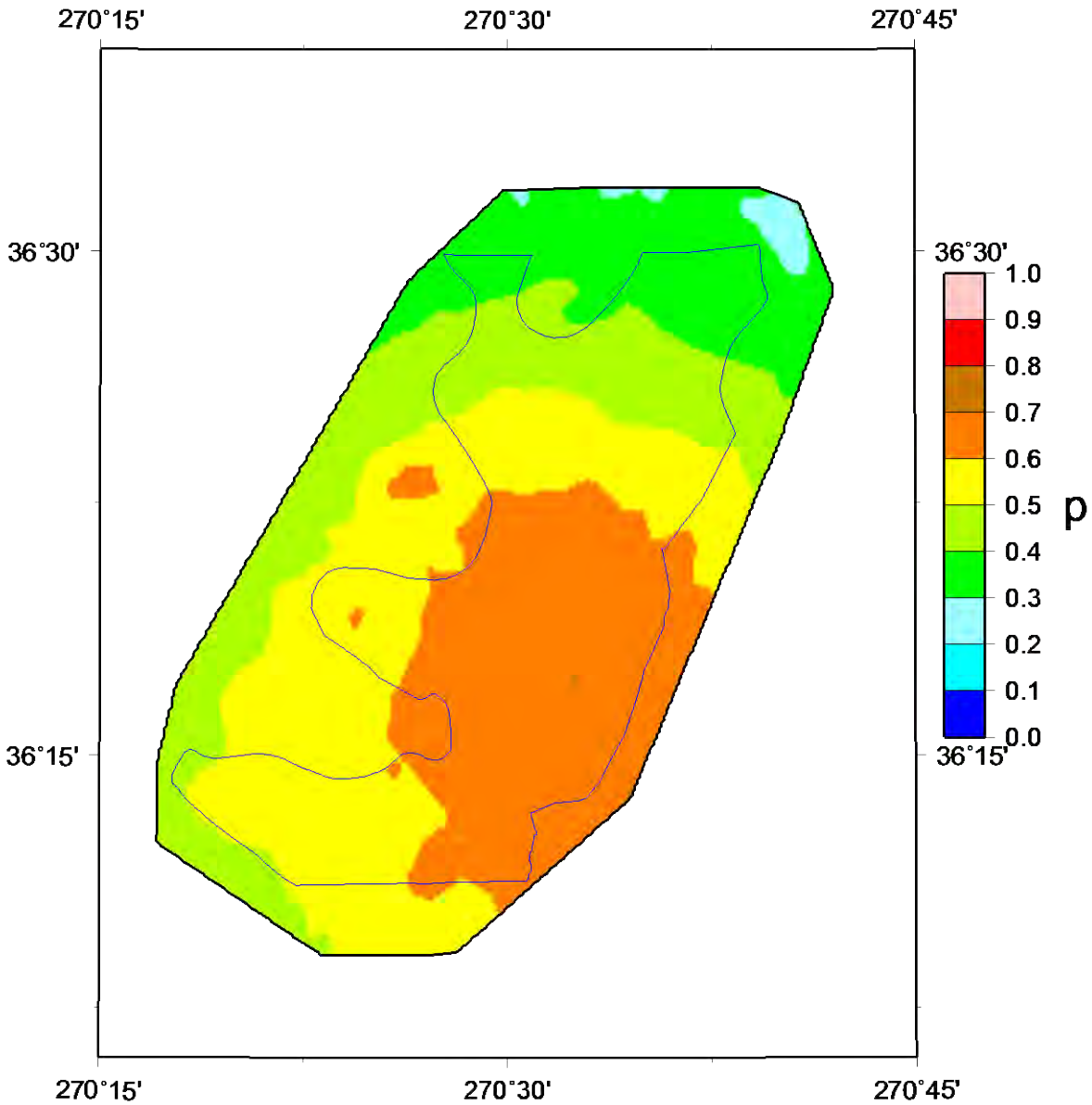
Figure 70: Scenario liquefaction hazard map for moderate to severe liquefaction (LPI > 5) for a M6.9 "Dawn" aftershock (alt. 2) on the Reelfoot Thrust (central segment of NMSZ).
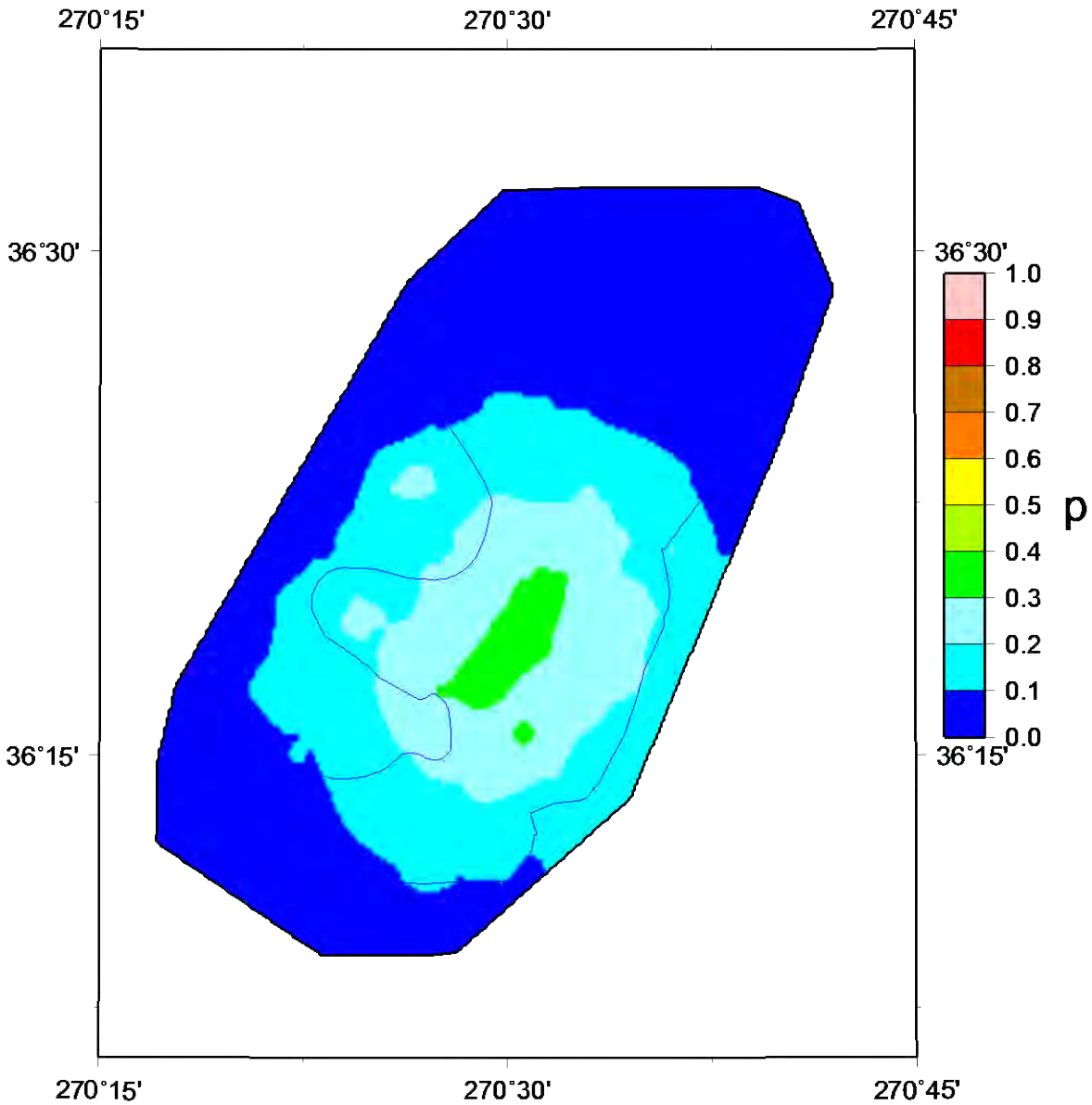
Figure 71: Scenario liquefaction hazard map for moderate to severe liquefaction (LPI > 5) for a M5.8 hypothetical Lake County earthquake (between Tiptonville and Ridgely).

Conclusions

We have produced seismic and liquefaction hazard maps that include the effects of local geology for Lake County. The products from this effort include a 3D geology database and model, a geotechnical database and liquefaction probability curves (LPCs), shear-wave velocity (Vs) measurements and models, and probabilistic and scenario hazard maps for Lake County. The geology model is detailed for the Quaternary sediments down to depths of 300 ft (100 m) and more generalized for the Eocene to Paleozoic formations. Paleozoic limestones form the bedrock of the model. The geotechnical database includes information on water table depths, standard penetration tests (SPT), seismic cone penetration tests (CPT), and shallow Vs information. It was used to generate LPCs based on SPT and Vs measurements to add to the published LPCs based on Mississippi embayment CPT measurements. The liquefaction hazard maps for Lake County were based on the average of published LPCs due to time constraints in hazard map production, but comparisons and recommendations are made to guide future liquefaction hazard map generation. Shallow Vs measurements were made at 14 Lake County sites and added to 9 published Vs profiles from the region. The Vs measurements were used to generate a typical Quaternary Vs profile. Deeper published information from the region were used to constrain the Eocene to Paleozoic Vs reference profile used in this study. Seismic and liquefaction hazard maps were generated that include the new geological, geotechnical, and seismological information gathered. The hazard maps are both probabilistic (5% and 2% probability of being exceeded in 50 years) and for eight earthquake scenarios. Seismic hazard maps at PGA and 1.0 s show a 50% decrease in hazard at short periods and a 10% increase at long periods compared with USGS NSHMP maps, which are for a uniform standard geology not found in western Tennessee. Liquefaction hazard maps show high hazard in Lake County for the five M7 New Madrid scenarios, and low hazard for the M5.8 hypothetical Lake County earthquake. The 1843 and 1895 M6.2 scenarios do not produce any significant liquefaction hazard due to more distant epicenters and a shorter duration of strong shaking.

References

Andrus, R. D., and Stokoe, K. H., II, 1997. ''Liquefaction resistance based on shear wave velocity.'' Proc., NCEER Workshop on Evaluation of Liquefaction Resistance of Soils, Nat. Ctr. for Earthquake Engrg. Res., State Univ. of New York at Buffalo, 89–128.

Arango, I., 1996. ''Magnitude scaling factors for soil liquefaction evaluations.'' J. Geotech. Engrg., ASCE, 122(11), 929–936.

Ashford, S.A., Jakrapiyanum, W., Lukkanaprasit, P., 1996. Amplification of earthquake ground motions in Bangkok.

Boulanger, R. W., and Idriss, I. M., 2007. "Evaluation of cyclic softening in silts and clays." J. Geotechnical and Geoenvironmental Eng., ASCE 133(6), 641–52.

Boulanger, R. W., and Idriss, I. M., 2012a. "Probabilistic SPT-based liquefaction triggering procedure."Journal of Geotechnical and Geoenvironmental Engineering, ASCE, 138(10), 1185-1195.

Boulanger, R. W., and Idriss, I. M., 2012b. "Evaluation of overburden stress effects on liquefaction resistance at Duncan Dam." Canadian Geotechnical Journal, 49, 1052-1058.

Boulanger, R. W., and Idriss, I. M., 2014. CPT AND SPT BASED LIQUEFACTION TRIGGERING PROCEDURES. CPT AND SPT BASED LIQUEFACTION TRIGGERING PROCEDURES, rep., Center for Geotechnical Modeling, Department of Civil and Environmental Engineering, University of California, Davis, California.

Bowles, J. E., 1977. Foundation Analysis and Design, McGraw-Hill, Inc., New York.

Burns, S. E., and Mayne, P. W. M., 1996. "Small- and High-Strain Measurements of in Situ Soil Properties Using the Seismic Cone Penetrometer." Transportation Research Record: Journal of the Transportation Research Board, 1548(1), 81–88.

Clark, B.R., Hart, R.M., and Gurdak, J.J., 2011. Groundwater availability of the Mississippi embayment: U.S. Geological Survey Professional Paper 1785, 62 p.

Cramer, C.H., J.S. Gomberg, E.S. Schweig, B.A. Waldron, and K. Tucker, 2006. First USGS urban seismic hazard maps predict the effects of soils, *Seism. Res. Lett.* **77**, 23-29.

Cramer, C.H., G. Rix, and K. Tucker, 2008. Probabilistic liquefaction hazard maps for Memphis, Tennessee, *Seis. Res. Lett.* **79**, 416-423.

Cramer, C.H., R.B. Van Arsdale, M.S. Dhar, D. Pryne, and J. Paul, 2014. Updating of urban seismic-hazard maps for Memphis and Shelby County, Tennessee: geology and Vs observations, *Seis. Res. Lett.* **85**, 986-996.

Cramer, C.H., R.A. Bauer, J. Chung, J.D. Rogers, L. Pierce, V. Voigt, B. Michell, D. Gaunt, R.A. Williams, D. Hoffman, G.L. Hempen, P.J. Steckel, O.S. Boyd, C.M. Watkins, K. Tucker, and N. McCallister, 2017. St. Louis area earthquake hazards mapping projects: seismic and liquefaction hazard maps, *Seis. Res. Lett.* **88**, 206-223.

Cramer, C.H., M.S. Dhar, and D. Arellano, 2018. Update of the urban seismic and liquefaction hazard maps for Memphis and Shelby County, Tennessee: liquefaction probability curves and 2015 hazard maps, *Seis. Res. Lett.* **89**, 688-701.

Csontos, R., and Van Arsdale, R., 2008, New Madrid seismic zone fault geometry. Geosphere, v. 4, p. 802-813.

Dhar, M.S., and C.H. Cramer, 2018. Probabilistic seismic and liquefaction hazard analysis of the Mississippi embayment incorporating nonlinear effects, *Seis. Res. Lett.* **89**, 253-267, published online 13 December 2017.

Final Technical Report to the USGS, USGS grant 06HQGR0131, 24 pp.

Golesorkhi, R., 1989. ''Factors influencing the computational determination of earthquake-induced shear stresses in sandy soils.'' Ph.D. dissertation, University of California at Berkeley.

Greenwood, M.L., Woolery, E.W., Van Arsdale, R.B., Stephenson, W.J., and Patterson, G.L., 2016, Continuity of the Reelfoot Fault across the Cottonwood Grove and Ridgely Faults of the New Madrid Seismic Zone. Seismological Society of America Bulletin, v. 106, p. 2674-2685. doi: 10.1785/0120150290.

Guo, L**.,** M. B. Magnani, K. McIntosh, and B. Waldron, 2014, Quaternary deformation and fault structure in the Northern Mississippi Embayment as imaged by near-surface seismic reflection data,   Tectonics, 33, doi:10.1002/2013TC003464.

Holzer T.L. Noce, T.E., and Bennett, M.J., 2011. Liquefaction Probability Curves for Surficial Geologic Deposits. Environmental & Engineering Geoscience, Vol. XVII, No. 1pp. 1–21.

Idriss, I. M., 1999. An update to the Seed-Idriss simplified procedure for evaluating liquefaction potential, in Proceedings, TRB Workshop on New Approaches to Liquefaction, Publication No. FHWARD- 99-165, Federal Highway Administration, January.

Idriss, I. M., and Boulanger, R. W., 2008. Soil liquefaction during earthquakes. Monograph MNO-12, Earthquake Engineering Research Institute, Oakland, CA, 261 pp.

Idriss, I. M., and Boulanger, R. W.. 2010. "SPT-based liquefaction triggering procedures." Report UCD/CGM-10/02, Department of Civil and Environmental Engineering, University of California, Davis, CA, 259 pp.

IRIS: "How Shallow Earth Structure Is Determined." http://www.iris.edu/hq/resource/how_shallow_earth_structure_is_determined. National Science Foundation, n.d. Web. 23 Oct. 2013.'

Iwasaki, T., Tatsuoka, F., Tokida, K. and Yasuda, S., 1978. A practical method for assessing soil liquefaction potential based on case studies at various sites in Japan, Second International Conference on Mierozonation for Safer Construction Research and Application 1978.

Iwasaki, T. and Tokida, K., 1981. Soil liquefaction potential evaluation with use of the simplified procedure, Proc. International Conference on Recent Advances in Geotechnical L2zrthquake Engineering and Soil Dynamics, 1981.

Iwasaki, T., Arakawa, T., and Tokida, K.-I.. 1984. "Simplified procedures for assessing soil liquefaction during earthquakes." International Journal of Soil Dynamics and Earthquake Engineering, 3(1), 49–58.

Kayen, R. E., Mitchell, J. K., Seed, R. B., Lodge, A., Nishio, S., and Coutinho, R., 1992. ''Evaluation of SPT-, CPT-, and shear wave-based methods for liquefaction potential assessment using Loma Prieta data.''

Kelson, K.I., Simpson, G.D., Van Arsdale, R.B., Harris, J.B., Haraden, C.C., and Lettis, W.R., 1996, Multiple Late Holocene earthquakes along the Reelfoot fault, central New Madrid seismic zone. Journal of Geophysical Research, v. 101, n. B-3, p. 6151-6170.

Levesques, C.L., Locat, J., Leroueil, S., 2007. Characterization of postglacial sediments of the Saguenay Fjord, Quebec. In: Tan, T.S., Phoon, K.K., HIght, D.W. & Leroueil, S. (eds.) Characterization and Engineering Properties of Natural Soils. Taylor & Francis Group, London, 2645-2677.

Liao, S., and Whitman, R. V., 1986a. ''Overburden correction factors for SPT in sand.'' J. Geotech. Engrg., ASCE, 112(3), 373–377.

Liao, S. S. C., and Whitman, R. V., 1986b. ''Catalogue of liquefaction and non-liquefaction occurrences during earthquakes.'' Res. Rep., Dept. of Civ. Engrg., Massachusetts Institute of Technology, Cambridge, Mass.

Long, M., Quigley, P., O'Connor, P., 2013. Undrained shear strength and stiffness of Irish glacial till from shear wave velocity. Ground Engineering, 26-27.

Louie, J.N., 2001. Faster, Better: Shear-Wave Velocity to 100 Meters Depth from Refraction Microtremor Arrays. Bulletin of the Seismological Society of America; 91 (2): 347–364.

Mayne, P.W., 2001. Stress-strain-strength-flow parameters from seismic cone tests. Intl. Conf. on In-Situ Measurement of Soil Properties & Case Histories, Bali, Indonesia, 27-48.

Mayne, P., 2005. CPT tests at CERI broadband seismic stations and ESEE test sites.

Mayne, P.W., 2007. In-situ test calibrations for evaluating soil parameters. Characterization & Engineering Properties of Natural Soils. Taylor & Francis Group, London, 1602-1652.

Mayne, P.W., Peuchen, J., 2013. Unit weight trends with con resistance in soft to firm clays. Geotechnical and Geophysical Site Characterization 4. Taylor & Francis Group, London, 903-910.

Miller, R. D., J. Xia, C. B. Park, and J. M. Ivanov, 1999. Multichannel analysis of surface waves to map bedrock: The Leading Edge, 18, 1392-1396.

Moon, S. W., and Ku, T., 2016. "Empirical estimation of soil unit weight and undrained shear strength from shear wave velocity measurements." Geotechnical and Geophysical Site Characterisation 5, Australian Geomechanics Society.

National Academies of Sciences, Engineering, and Medicine, 2016. State of the Art and Practice in the Assessment of Earthquake-Induced Soil Liquefaction and Its Consequences. Washington, DC: The National Academies Press. doi: 1017226/23474.

NWIS, 2019. Water Resources of the United States-National Water Information System (NWIS) Mapper, <https://maps.waterdata.usgs.gov/> (Feb. 1, 2019).

Ogweno, L.P., M. Withers, and C.H. Cramer, 2019. Earthquake early warning feasibility study for the New Madrid seismic zone, *Seis. Res. Lett.* **90**, accepted.

Park, C. B., R. D. Miller, N. Ryden, J. Xia, and J. Ivanov, 2005. Combined use of active and passive surface waves, Journal of Environmental and Engineering Geophysics, 10, 323-334.

Parrish, S., and Van Arsdale, R., 2004, Faulting along the southeastern margin of the Reelfoot rift in northwestern Tennessee revealed in deep seismic reflection profiles. Seismological Research Letters, v. 75, p. 782-791.

Petersen, M. D., M. Moschetti, P. Powers, C. Mueller, K. Haller, A. Frankel, Y. Zeng, S. Rezaeian, S. Harmsen, O. Boyed, N. Field, R. Chen, K. Rukstales, N. Luco, R. Wheeler, R. Williams, and A. Olsen, 2014, *The 2014 update of the United States national seismic hazard models*, U.S. Geological Survey, OFR 2014-X1091, 255 p.

Pezeshk, S., C.V. Camp, L. Liu, J.M. Evens, and J. He, 1998. Seismic acceleration coefficients for West Tennessee and expanded scope of work for seismic acceleration coefficients for West Tennessee phase 2 – field investigations, Final Report to Tennessee Dept. of Transportation, 420 pp.

Pryne, D.E., 2012, Stratigraphic and structural history of shallow Mississippi embayment sediments in southeastern Missouri, 68 p.

Pryne, D., Van Arsdale, R., Csontos, R., and Woolery, E., 2013, Northeastern Extension of the New Madrid North Fault-New Madrid Seismic Zone, Central United States. Bulletin of the Seismological Society of America, v. 103, p. 2277-2294.

Purser, J.L., and Van Arsdale, R.B., 1998, Structure of the Lake County Uplift: New Madrid seismic zone. Seismological Society of America Bulletin, v. 88, n. 5, p. 1204-1211.Rix, G. J., 2001. Liquefaction Susceptibility Mapping in Memphis/Shelby County, TN, USGS Award No. 01-HQ-AG-0019.

Rix, G. J., and S. Romero-Hudock, 2006. Liquefaction potential mapping in Memphis and Shelby County, Tennessee, unpublished Rept. To the U.S. Geol. Surv., Denver Colorado, 27 pp.

Romero, S., and G.J. Rix (2001). Regional variations in near surface shear wave velocity in the Greater Memphis area, *Eng. Geol.* **62**, 137-158.

Rosenblad, B.L., 2007. Deep shear wave velocity profiles of Mississippi embayment sediments determined from surface wave measurements, Final Technical Report to the USGS, USGS grant 06HQGR0131, 24 pp.

Schrader, T.P., 2008. Potentiometric surface in the Sparta-Memphis aquifer of the Mississippi embayment, Spring 2007, U.S. Geological Survey Scientific Investigations Map 3014.

Schrader, T.P., 2013. Water levels and water quality in the Sparta-Memphis aquifer (middle Claiborne aquifer) in Arkansas, spring–summer 2009: U.S. Geological Survey Scientific Investigations Report 2013–5100, 53 p., 2 plates,http://pubs.usgs.gov/sir/2013/5100/.

Schuler, Juerg, 2008. Joint inversion of surface waves and refracted P and S-wave. Masters Science Thesis, Eidgenossische Technische Hochschule Zurich, Swiss Federal Institute of Technology Zurich.

Seed, H. B., and Idriss, I. M., 1971. ''Simplified procedure for evaluating soil liquefaction potential.'' J. Geotech. Engrg. Div., ASCE, 97(9), 1249–1273.

Seed, H. B., and Idriss, I. M., 1982. ''Ground motions and soil liquefaction during earthquakes.'' Earthquake Engineering Research Institute Monograph, Oakland, Calif.

Seed, H. B., Idriss, I. A., and Arango, I., 1985. "Closure to 'Evaluation of Liquefaction Potential Using Field Performance Data' by H. Bolton Seed, I. M. Idriss, and Ignacio Arango, (March 1983)." Journal of Geotechnical Engineering, 111(11), 1346–1346.

Seed, H. B., Tokimatsu, K., Harder, L. F., and Chung, R. M., 1985. ''The influence of SPT procedures in soil liquefaction resistance evaluations.'' J. Geotech. Engrg., ASCE, 111(12), 1425–1445.

Seed, H. B., and Idriss, I. M., 1967. "Analysis of liquefaction: Niigata earthquake." Proc., ASCE, 93(SM3), 83-108.

Seed, H. B., and Idriss, I. M., 1971. "Simplified procedure for evaluating soil liquefaction potential." J. Soil Mechanics and Foundations Div., ASCE 97(SM9), 1249–273.

Seed, H. B., and Idriss, I. M., 1982. Ground Motions and Soil Liquefaction During Earthquakes, Earthquake Engineering Research Institute, Oakland, CA, 134 pp.

Seed, H. B., Tokimatsu, K., Harder, L. F. Jr., and Chung, R., 1984. The influence of SPT procedures in soil liquefaction resistance evaluations. Earthquake Engineering Research Center, University of California, Berkeley, Report No. UCB/EERC-84/15, 50 pp.

Toprak, S., and Holzer, T. L., 2003. "Liquefaction potential index: Field assessment." Journal of Geotechnical and Geoenvironmental Engineering, ASCE, 129(4), 315-322.

Van Arsdale, R.B., Purser, J.L., Stephenson, W., and Odum, J., 1998, Faulting along the southern margin of Reelfoot Lake, Tennessee. Seismological Society of America Bulletin, v. 88, n. 1, p. 131-139.

Waldron, B., Larsen, D., Hannigan, R., Csontos, R., Anderson, J., Dowling, C., and Bouldin, J., 2011. Mississippi Embayment Regional Ground-Water Study. Mississippi Embayment Regional Ground Water Study, rep., National Research Management Research Laboratory, Ada, Oklahoma.

Ward, A., 2016, Progress toward Quaternary displacement rates on the Meeman-Shelby fault and Joiner ridge horst, eastern Arkansas. MS thesis, University of Memphis, 446 pp. https://umwa.memphis.edu/etd//

Ward, A., Counts, R., Van Arsdale, R., Larsen, D., and Mahan, S., 2017 Quaternary displacement rates on the Meeman-Shelby fault and Joiner Ridge horst, eastern Arkansas: results from coring Mississippi River alluvium. Seismological Research Letters, v. 88, p. 442-455.

Weathers, T., 2019, Geologic mapping of Lake County, Tennessee, MS thesis, University of Memphis, 120 p.

Wessel, P. and W. H. F. Smith (1991). Free software helps map and display data, *EOS Trans. AGU* **72**, 441.

Woolery, E.W., Z. Wang, N.S. Carpenter, R. Street, and C. Brengman, 2016. The Central United States Seismic Observatory: site characterization, instrumentation, and recordings, *Seis. Res. Lett.* **87**, 215-228.

Woolery, E.W., Whitt, J.W., Van Arsdale, R.B., and Almayahi, A., 2018, Geophysical and Geological Evidence for Quaternary Displacement on the Caborn Fault, Wabash Valley Fault System, Southwestern Indiana. Seismological Research Letters, v. 89, n. 6, p. 2473-2480. doi: 10.1785/0220180220

Youd, T. L., Idriss, I. M., Andrus, R. D., Arango, I., Castro, G., Christian, J. T., Dobry, R., Finn, W. D. L., Harder, L. F., Hynes, M. E., Ishihara, K., Koester, J. P., Liao, S. S. C., Marcuson, W. F., Martin, G. R., Mitchell, J. K., Moriwaki, Y., Power, M. S., Robertson, P. K., Seed, R. B., and Stokoe, K. H., 2001. Liquefaction resistance of soils: summary report from the 1996 NCEER and 1998 NCEER/NSF workshops on evaluation of liquefaction resistance of soils, J. Geotechnical, and Geoenvironmental Eng., ASCE 127(10), 817–33.

Youd, T. L., and Noble, S. K., 1997a. Magnitude scaling factors, Proc., NCEER Workshop on Evaluation of Liquefaction Resistance of Soils, Nat. Ctr. for Earthquake Engrg. Res., State Univ. of New York at Buffalo, 149–165.

Youd, T. L., and Noble, S. K., 1997b. Liquefaction criteria based on statistical and probabilistic analyses, Proc., NCEER Workshop on Evaluation of Liquefaction Resistance of Soils, Nat. Ctr. for Earthquake Engrg. Res., State Univ. of New York at Buffalo, 201–215.

Youd, T. L., and Idriss, I. M., 2001. "Liquefaction Resistance of Soils: Summary Report from the 1996 NCEER and 1998 NCEER/NSF Workshops on Evaluation of Liquefaction Resistance of Soils." Journal of Geotechnical and Geoenvironmental Engineering, 127(4), 297–313.

Youd, T. L., Idriss, I. M., Andrus, R. D., Arango, I., Castro, G., Christian, J. T., Dobry, R., Finn, W. D. L., Harder, L. F., Hynes, M. E., Ishihara, K., Koester, J. P., Liao, S. S. C., Marcuson, W. F., Martin, G. R., Mitchell, J. K., Moriwaki, Y., Power, M. S., Robertson, P. K., Seed, R. B., and Stokoe, K. H., 2003. "Closure to 'Liquefaction Resistance of Soils: Summary Report from the 1996 NCEER and 1998 NCEER/NSF Workshops on Evaluation of Liquefaction Resistance of Soils' by T. L. Youd, I. M. Idriss, Ronald D. Andrus, Ignacio Arango, Gonzalo Castro, John T. Christian, Richardo Dobry, W. D. Liam Finn, Leslie F. Harder Jr., Mary Ellen Hynes, Kenji Ishihara, Joseph P. Koester, Sam S. C. Liao, William F. Marcuson III, Geoffrey R. Martin, James K. Mitchell, Yoshiharu Moriwaki, Maurice S. Power, Peter K. Robertson, Raymond B. Seed, and Kenneth H. Stokoe II." Journal of Geotechnical and Geoenvironmental Engineering, 129(3), 284–286.

Appendices (separate files)

Appendix A. Excel spread sheet of geologic well data used in this study.

Appendix B. Three-dimensional model animation of Figure 5. This model illustrates the stratigraphy of the Quaternary Mississippi River floodplain beneath Shelby County from the ground surface to the top of the Eocene. Colors represent different sediments that are defined in Figure 5. Each sediment layer is presented in Appendix C.

Appendix C. Quaternary sediments at ground surface and in underlying 5-foot intervals in Figure 5. For example the map labeled 10 represents sediments between 6 and 10 feet depth, etc.

Appendix D. Three-dimensional model animation for Lake County. This model illustrates the stratigraphy and structure beneath Lake County from the ground surface to the top of the Paleozoic. Faults are presented as vertical brown planes that extend through the base of the model to the top of the Eocene strata.

Appendix E. Individual results for 14 Lake County MASW measurements.